

**ORAL INSULIN DELIVERY SYSTEM
BASED ON CHITOSAN-COMPLEXED
CARBOXYMETHYLATED *IOTA*-
CARRAGEENAN NANOPARTICLES**

PRATYUSA SAHOO

**FACULTY OF MEDICINE
UNIVERSITY OF MALAYA
KUALA LUMPUR**

2019

**ORAL INSULIN DELIVERY SYSTEM
BASED ON CHITOSAN-COMPLEXED
CARBOXYMETHYLATED *IOTA*-
CARRAGEENAN NANOPARTICLES**

PRATYUSA SAHOO

**THESIS SUBMITTED IN FULFILMENT OF THE
REQUIREMENTS FOR THE DEGREE OF DOCTOR OF
PHILOSOPHY**

**FACULTY OF MEDICINE
UNIVERSITY OF MALAYA
KUALA LUMPUR**

UNIVERSITY OF MALAYA
ORIGINAL LITERARY WORK DECLARATION

Name of Candidate: PRATYUSA SAHOO

Registration/Matric No: MHA120046

Name of Degree: DOCTOR OF PHILOSOPHY

Title of Project Paper/Research Report/Dissertation/Thesis (“this Work”):

ORAL INSULIN DELIVERY SYSTEM BASED ON CHITOSAN-COMPLEXED
CARBOXYMETHYLATED *IOTA*-CARRAGEENAN NANOPARTICLES.

Field of Study: PHARMACY

I do solemnly and sincerely declare that:

- (1) I am the sole author/writer of this Work;
- (2) This Work is original;
- (3) Any use of any work in which copyright exists was done by way of fair dealing and for permitted purposes and any excerpt or extract from, or reference to or reproduction of any copyright work has been disclosed expressly and sufficiently and the title of the Work and its authorship have been acknowledged in this Work;
- (4) I do not have any actual knowledge nor do I ought reasonably to know that the making of this work constitutes an infringement of any copyright work;
- (5) I hereby assign all and every rights in the copyright to this Work to the University of Malaya (“UM”), who henceforth shall be owner of the copyright in this Work and that any reproduction or use in any form or by any means whatsoever is prohibited without the written consent of UM having been first had and obtained;
- (6) I am fully aware that if in the course of making this Work I have infringed any copyright whether intentionally or otherwise, I may be subject to legal action or any other action as may be determined by UM.

Candidate’s Signature

Date:

Subscribed and solemnly declared before,

Witness’s Signature

Date:

Name:

Designation:

ORAL INSULIN DELIVERY SYSTEM BASED ON CHITOSAN-COMPLEXED CARBOXYMETHYLATED *IOTA*-CARRAGEENAN NANOPARTICLES

ABSTRACT

Acidic environment of the stomach, poor permeability across intestinal membrane and the mucin barrier are among the major limitations in oral delivery of peptide drugs such as insulin. Thus, different nanostructures using mucoadhesive and pH responsive polymers have been proposed as carrier systems for oral insulin delivery. This study focused on designing insulin nanoparticles from chitosan (CS) and carboxymethylated *iota*-carrageenan (CMCi), based on response surface methodology together with multivariate spline interpolation (RSM^{MSI}). The resulting optimised nanoparticles gave a zeta potential, mean particle size, loading capacity and entrapment efficiency of 52.5 ± 0.5 mV, 613 ± 41 nm, $10.7 \pm 0.6\%$, and $86.9 \pm 2.6\%$, respectively. The pH responsive CMCi protected insulin in an acidic environment and retained its activity as the sulfate moieties of *iota*-carrageenan interacted with the amino group of insulin *via* ionic interaction, and the mucoadhesive chitosan adhered to the intestinal mucosa in *ex vivo* studies. The release of insulin was low ($4.91 \pm 0.2\%$) in simulated gastric fluid (SGF) and high ($86.64 \pm 2.2\%$) in simulated intestinal fluid (SIF) in a 12-h release study, showing a pH-responsive drug release property. The insulin entrapped in the CS/CMCi nanoparticles retained their bioactivity and was stable in simulated enzymatic environment of the gastrointestinal tract (GIT). The nanoparticles were stable up to 3 months at 4 and -20°C , and up to 7 days at room temperature (25°C). The results of cellular membrane permeability experiments suggested that insulin nanoparticles were transported across Caco-2 cell monolayers mainly *via* the paracellular pathway, as inferred by the transepithelial electrical resistance (TEER) and apparent permeability coefficients (P_{app}) of the nanoparticles (22 times higher than control insulin solution), suggesting that the opening of tight junctions (TJs) was involved. The *in vivo* study using diabetic Sprague Dawley (SD) rats showed a bioavailability of $16.1 \pm 1.6\%$ with an

extended blood glucose lowering effect lasting up to 24–30 h (C_{\max} : 175.1 ± 23.7 mIU/L, T_{\max} : 5 h, AUC: 1789.4 ± 158.6). The results support the effectiveness of chitosan-complexed carboxymethylated *iota*-carrageenan nanoparticles as an oral insulin delivery system for extended glycemic control in basal insulin therapy. Further studies such as cellular uptake of entrapped insulin by confocal laser scanning microscope and site specific intestinal insulin release by an *in vivo* imaging system, are required to explore its precise release mechanism.

Keywords: Nanoparticle, Insulin, Chitosan, Carrageenan, Response surface methodology (RMS)

Universiti Malaysia

*ORAL INSULIN DELIVERY SYSTEM BASED ON CHITOSAN-COMPLEXED
CARBOXYMETHYLATED IOTA-CARRAGEENAN NANOPARTICLES*

ABSTRAK

Persekitaran berasid perut, kebolehtelapan melalui membran usus yang lemah dan penghalang mucin adalah antara batasan utama dalam penghantaran mulut ubat peptida seperti insulin. Oleh itu, struktur-struktur nano yang berlainan yang menggunakan polimer-polimer pelekat muko dan pH responsif telah dicadangkan sebagai sistem-sistem pembawa untuk penghantaran insulin mulut. Kajian ini memberi tumpuan kepada reka bentuk nanopartikel-nanopartikel insulin dari kitosan (CS) dan karbosimetilisasi iota-karagenan (CMCi), berdasarkan metodologi permukaan tindak balas bersama dengan interpolasi splina variat pelbagai (RSM^{MSI}). Hasil nanopartikel-nanopartikel optimal memberi potensi zeta, saiz zarah min, kapasiti muatan dan kecekapan penangkapan 52.5 ± 0.5 mV, 613 ± 41 nm, $10.7 \pm 0.6\%$, dan $86.9 \pm 2.6\%$, masing-masing.

CMCi yang responsif pH telah melindungi insulin dalam persekitaran berasid dan mengekalkan aktivitinya apabila moiety-moiety sulfat iota-karagenan berinteraksi dengan kumpulan amino insulin melalui interaksi ionik dan kitosan pelekat muko melekat pada mukosa usus di dalam pengajian *ex vivo*. Pelepasan insulin adalah rendah ($4.91 \pm 0.24\%$) dalam cecair gastrik simulasi (SGF) dan tinggi ($86.64 \pm 2.2\%$) dalam cecair usus simulasi (SIF) dalam suatu kajian pelepasan 12jam, menunjukkan sifat pelepasan ubat responsif pH. Insulin yang terperangkap dalam nanopartikel-nanopartikel CS/CMCi mengekalkan bioaktiviti mereka dan agak stabil dalam persekitaran enzimatik simulasi bagi saluran gastrousus (GIT). Nanopartikel-nanopartikel stabil sehingga 3 bulan pada penyimpanan 4 dan -20°C dan sehingga 7 hari pada suhu bilik. Keputusan eksperimen-eksperimen kebolehtelapan membran selular mencadangkan bahawa nanopartikel-nanopartikel insulin diangkut melalui sel-sel selapis Caco-2 terutamanya melalui laluan paraselular, seperti yang dirujuk oleh rintangan elektrik transepithelial (TEER) dan pekali kebolehtelapan yang jelas (Papp) bagi nanopartikel-nanopartikel (22 kali ganda lebih

daripada larutan insulin kawalan), mencadangkan bahawa pembukaan persimpangan ketat (TJs) adalah terlibat. Kajian *in vivo* menggunakan tikus Sprague Dawley (SD) diabetik menunjukkan bioavailabiliti 16.1 ± 1.6 dengan suatu kesan penurunan glukosa darah yang berlangsung sehingga 24–30 jam (C_{\max} : 175.1 ± 23.7 mIU/L, T_{\max} : 5 jam, AUC: 1789.4 ± 158.6). Keputusan di atas menyokong keberkesanan nanopartikel-nanopartikel kompleks kitosan karbosimetilisasi iota-karagenan sebagai suatu sistem penghantaran insulin mulut untuk kawalan glisemik berpanjangan dalam terapi asas insulin. Walau bagaimanapun, kajian selanjutnya seperti pengambilan selular bagi insulin terperangkap dengan mikroskop pengimbas laser sefokus dan pelepasan insulin tapak spesifik usus dengan suatu sistem pengimejan *in vivo* adalah perlu untuk mengenalpasti mekanisme pelepasan terperinci.

Katakunci: Nanopartikel, Insulin, Kitosan, Karagenan, Metodologi respon permukaan

ACKNOWLEDGEMENTS

Firstly, I would like to express my sincere appreciation to my supervisors, Prof. Dr. Chung Lip Yong, Dr. Leong Kok Hoong and Dr. Shaik Nyamathulla for their motivation, guidance and immense knowledge. Besides, I am very thankful to Prof. Yoshinori Onuki and Prof. Kozo Takayama for their help in RSM^{MSI} modelling. I would like to thank Assoc. Prof. Dr. Kiew Lik Voon and Dr. Lee Hong Boon for their constructive advice and encouragement throughout this research work. I would like to acknowledge the Head of Department of Pharmacy, Prof. Datin Dr. Zorah Aziz for providing access to laboratories and research facilities. Also, I would like to acknowledge our department support staff – Pn. Rustini Karim, En. Mohd Najib Baharom, En. Abdul Aziz Ismail, Pn. Salbiah Mohd Yusoff, Pn. Mariah Ahmad Kairi, Ganges and others for their assistance and technical support.

I would like to acknowledge and express my sincere gratitude to the Ministry of Higher Education, Malaysia, for financial support throughout this project from the High Impact Research Grants (Grant No. UM.C/625/1/HIR/MOHE/MED/17 and UM.C/625/1/HIR/MOHE/MED/33)

My sincere appreciation also extends to all my fellow lab mates – Seetha, Deepa, Siew Hui, Dr. Geeta, Cindy Ng, Elaine Cheah, Eric Saw, Kiew Siaw Fui, Theeba, Manan Fateh, Abdul Samad and Kong Yong for their support and promptitude to share helpful information.

Last but not the least, I would like to thank my family members for their love and guidance throughout the journey. Most importantly, I wish to thank my loving and supportive husband, Sunil, and my cute little boy, Aniket, for providing never-ending motivation.

TABLE OF CONTENTS

Abstract	iii
Abstrak	v
Acknowledgements	vii
Table of contents	viii
List of figures	xii
List of tables	xvi
List of symbols and abbreviations.....	xv xviii
List of appendices	xxi
CHAPTER 1: INTRODUCTION.....	1
1.1 Overview.....	1
1.2 Aim and objectives	5
CHAPTER 2: LITERATURE REVIEW.....	6
2.1 Diabetes mellitus and its pharmacological treatment	6
2.2 Insulin	7
2.3 Current route of insulin administration: Parenteral route	12
2.4 Alternative needle free routes of insulin administration.....	13
2.4.1 Pulmonary route.....	13
2.4.2 Nasal route	14
2.4.3 Buccal or sublingual route	14
2.4.4 Transdermal route	15
2.4.5 Ocular route	16
2.4.6 Rectal route	16
2.4.7 Oral route	17
2.5 Clinical development of oral insulin.....	23

2.6	Polymeric approach for oral delivery of insulin	25
2.6.1	Carrageenan	27
2.6.2	Chitosan	30
CHAPTER 3: METHODOLOGY		32
3.1	Materials	32
3.2	Preparation and characterisation of carboxymethylated <i>iota</i> -carrageenan (CMCi)	33
3.2.1	Experimental design	33
3.2.2	Characterisation of CMCi	35
3.3	Formulation of chitosan-complexed insulin-loaded carboxymethylated <i>iota</i> - carrageenan nanoparticles	38
3.3.1	Characterisation of CS/CMCi nanoparticles.....	39
3.3.2	Insulin entrapment efficiency and insulin loading.....	40
3.3.3	Insulin release from nanoparticles	41
3.3.4	Degree of swelling and gel fraction	42
3.4	Optimisation of insulin carrier system.....	42
3.5	<i>Ex vivo</i> mucoadhesion study.....	43
3.6	Storage stability of insulin	45
3.7	<i>In vitro</i> stability of insulin against enzymatic degradation.....	46
3.8	<i>In vitro</i> bioactivity of insulin released from CS/CMCi nanoparticles.....	46
3.9	Cell culture and cytotoxicity study	47
3.10	<i>In vitro</i> insulin membrane transport study.....	48
3.10.1	Parallel artificial membrane permeability assay (PAMPA)	48
3.10.2	Transepithelial electrical resistance (TEER) measurement and transport of insulin by Caco-2 cells	49

3.11	<i>In vivo</i> hypoglycemic and bioavailability study	52
CHAPTER 4: RESULTS AND DISCUSSION		54
4.1	Preparation and characterisation of c arboxymethylated iota-carrageenan (CMCi)	54
4.2	Pre-formulation of insulin-entrapped CS/CMCi nanoparticles	63
4.3	Degree of swelling of the CS/CMCi nanoparticles	68
4.4	Optimisation of the independent factors using RSM ^{MSI} modeling for suitable carboxymethylation of <i>iota</i> -carrageenan for the preparation of insulin-entrapped CS/CMCi nanoparticles	73
4.5	Characterisation of optimised insulin-entrapped CS/CMCi nanoparticles.....	81
4.6	<i>In vitro</i> studies of optimised insulin-entrapped CS/CMCi nanoparticles.....	87
4.6.1	Release kinetics, stability of released insulin against enzymatic degradation bioactivity of released insulin from CS/CMCi nanoparticles, storage stability and HPLC method validation	87
4.7	Cytotoxicity study.....	95
4.8	<i>In vitro</i> insulin membrane transport study.....	97
4.8.1	Parallel artificial membrane permeability assay (PAMPA)	97
4.8.2	Transepithelial electrical resistance (TEER) measurement and transport of insulin by Caco-2 cells	99
4.9	<i>In vivo</i> hypoglycemic and bioavailability study	104
CHAPTER 5: CONCLUSION, LACUNAE AND FUTURE WORKS		109
5.1	Conclusion	109
5.2	Lacunae and future works of the study	112
References		114

List of publications and presentations.....	134
Appendix.....	150

Universiti Malaya

LIST OF FIGURES

Figure 1.1: Schematic diagram of various routes of insulin administration (This figure was modified from Shah <i>et al.</i> , 2016).....	2
Figure 2.1: Human insulin structure.	8
Figure 2.2: (A) Dimeric structure of human insulin, (B) Hexameric structure of human insulin with zinc ion (●) at the center (downloaded from Protein data bank (PDB code 3JSD, www.rcsb.org/pdb).	9
Figure 2.3: Desired characteristics of polymeric carriers for oral insulin administration.	26
Figure 2.4: Chemical structure of <i>kappa</i> -, <i>iota</i> - and <i>lambda</i> -carrageenan. G4S is D-galactopyranose-4-sulfate; AG is 3, 6-anhydro- α -D-galactopyranose; AG2S is 3, 6-anhydro- α -D-galactopyranose-2-sulfate; G2S is D-galactopyranose-2-sulfate; G2S, 6S is D-galactopyranose-2, 6-disulfate; n is the number of repeating units.	29
Figure 2.5: Structure of chitosan; n is the number of repeating units.	31
Figure 3.1: Representative diagram of chitosan (CS)-complexed insulin-loaded carboxymethylated <i>iota</i> -carrageenan (CMCi) nanoparticles formation. As depicted in the figure, insulin solution (●) was added to CMCi solution (blue). Then the polyelectrolyte complexation was performed by adding the aforementioned solution to CS (red) solution, which results in nanoparticle suspension..	39
Figure 3.2: (A) The everted intestinal sac method (This figure is modified from Santos <i>et al.</i> , 1999). As depicted in the figure, 5 cm of small intestinal tissue was harvested from a male Sprague–Dawley rat, everted, tied at the ends and filled with phosphate buffer saline with 200 mg/dL of glucose (PBSG). The sac was then incubated for 30 min into a tube containing a known amount of nanoparticles and PBSG. The sac was then removed, the unbound nanoparticles were centrifuged, lyophilised and percentage of mucoadhesion was calculated. (B) Everted small intestinal sac filled with 1.4 mL of PBSG.....	45
Figure 3.3: (A) Millicell [®] ERS-2 epithelial volt-ohm meter with probe (B) Schematic diagram of TEER measurement using Caco-2 cells. As depicted in the diagram, the electrode was immersed in the Millicell [®] -24 culture plate so that the shorter tip was in the donor chamber containing Caco-2 cells and the longer tip was in the receiver chamber. For stable and reproducible results, the electrode was held steady and at a 90° angle to the plate insert.	55
Figure 4.1: Reaction scheme for the carboxymethylation process of <i>iota</i> -carrageenan. AG is 3,6-anhydro- α -D-galactopyranose-2-sulfate; G is β -D-galactopyranose-4-sulfate. R = CH ₂ COOH or H; n = number of repeating units; arrow = possible positions for carboxymethylation.	55

Figure 4.2: (A) ^1H NMR spectrum of native Ci. (B) ^1H NMR spectrum of CMCi (sample I01). (C) ^{13}C NMR spectrum of native Ci. (D) ^{13}C NMR spectrum of CMCi (sample I01). AG is 3,6-anhydro- α -D-galactopyranose-2-sulfate; G is β -D-galactopyranose-4-sulfate; labels H1–6 indicate the proton numbering scheme; labels C1–6 indicate the carbon numbering scheme (refer to Figure 4.1 for the numbering scheme); GH2-S and GH6-S denote the substituted (carboxymethylated) peaks for GH2 and GH6, respectively (arrows); COO^- represents the signal for the $-\text{CH}_2\text{COO}^-$ group (arrow); and CH_2 represents the CH_2 group of the $-\text{CH}_2\text{COO}^-$ unit (arrow). 56

Figure 4.3: Two dimension NMR. Heteronuclear single quantum coherence (HSQC) spectrum of sample I01. AG is 3,6-anhydro- α -D-galactopyranose-2-sulfate; G is β -D-galactopyranose-4-sulfate; labels H1–6 indicate the proton numbering scheme; labels C1–6 indicate the carbon numbering scheme (refer to Figure 4.1 for the numbering scheme); GH2-S and GH6-S denote the substituted (carboxymethylated) peaks for GH2 and GH6, respectively. 57

Figure 4.4: GPC profile of CMCi (sample I01) for molecular weight determination (A) Triple analysis plot (refractive index/viscometer/light scattering) of CMCi (sample I01) (B) Distribution curve of CMCi (sample I01). 62

Figure 4.5: (A) Identification of nanoparticle formation under a microscope. (B) Effect of the chitosan (CS)/carboxymethylated *iota*-carrageenan (CMCi) mass ratio on the +/- charge ratio of each formulation. (C) Effect of the CS/CMCi mass ratio on the nanoparticle size. * represents particle size of formulations showing solution and precipitation. 65

Figure 4.6: Preparation and optimisation of the insulin-entrapped CS/CMCi nanoparticles from 0.1% w/v CMCi and 0.1% w/v CS. (A) Entrapment efficiency of insulin using various ratios of CS and CMCi polymers. (B) Zeta potential of the nanoparticles using various ratios of CS and CMCi polymers. (C) Sizes of the nanoparticles using various ratios of CS and CMCi polymers. (D) Entrapment efficiency of insulin with increasing amounts of insulin (0.5–2 mg). (E) Loading of insulin with increasing amounts of insulin (0.5–2 mg). The results are presented as the mean \pm SD (n = 3). ^aParameters selected for the formulation of nanoparticles for further characterisation and in vitro studies * $p < 0.05$ compared to ‘a’ according to Student’s *t*-test. 67

Figure 4.7: (A) Leave-one-out cross-validation showing the predictive power of the RSM^{MSI} model for the gel fraction and the Korsmeyer-Peppas model parameter *k* in both simulated gastric fluid (SGF) (pH 1.2) and simulated intestinal fluid (SIF) (pH 6.8). (B) Response surface plots showing the influence of volume and concentration of NaOH on swelling, gel fraction and the dissolution parameters (*n* and log *k*) in SGF (pH 1.2) and SIF (pH 6.8). (C) Response surface plots showing the influence of volume of NaOH and amount of ClCH_2COOH (MCA) on swelling, gel fraction and the dissolution parameters (*n* and log *k*) in SGF (pH 1.2) and SIF (pH 6.8). (D) Response surface plots showing the


influence of concentration of NaOH and amount of ClCH₂COOH (MCA) on swelling, gel fraction and the dissolution parameters (*n* and log *k*) in SGF (pH 1.2) and SIF (pH 6.8) (E) Response surface plots showing the influence of concentration of NaOH and reaction temperature on swelling, gel fraction and the dissolution parameters (*n* and log *k*) in SGF (pH 1.2) and SIF (pH 6.8).  Dark blue indicates lowest value, red indicates highest value and ● indicates points below predicted value. Refer to Appendix B for further data to Appendix B for further data.76

Figure 4.8: FTIR spectra of (A) CMCi, (B) CS, (C) insulin, and (D) insulin-entrapped CS/CMCi nanoparticles. 85

Figure 4.9: TEM micrographs of nanoparticles made from (A) native CS/Ci and (B) optimised CS/CMCi, and FESEM micrographs of nanoparticles made from (C) native CS/Ci and (D) optimised CS/CMCi..... 87

Figure 4.10: (A) Release study of insulin from the optimised CS/CMCi nanoparticles and native Ci/CS in SGF (pH 1.2) and SIF (pH) 6.8 at 37°C. The results are presented as mean ± SD (n = 3). (B) Release of insulin from the optimised CS/CMCi nanoparticles in SGF (pH 1.2) and SIF (pH) 6.8 at 37°C with enzymes (SGF with pepsin and SIF with trypsin) and without enzymes. The results are presented as the mean ± SD (n = 3).) (C) Insulin release (%) from the CS/CMCi nanoparticles stored at 25, 4 and -20°C over a period of 90 days compared to nanoparticles prepared at the starting point of experiment. The results are presented as the mean ± SD (n = 3).92

Figure 4.11: (A) Representative human recombinant insulin chromatogram (0.250 mg/mL). (B) Standard curve of human recombinant insulin (0.005–1.00 mg/mL) 93

Figure 4.12: (A) Cell viability (%) of Caco-2 cells (MTS assay). (B) Cell death (%) of Caco-2 cells after incubation with CS/CMCi nanoparticles over a concentration range of 0.5–20 mg/mL for 1, 2 or 3 days(LDH assay). The results are presented as the mean ± SD (n = 6)..... 96

Figure 4.13: Standard curve of Lucifer yellow (0.01–50.00 µg/mL). 98

Figure 4.14: (A) Process of paracellular transport of insulin entrapped CS/CMCi nanoparticles. (B) Representative image of paracellular transport of insulin from insulin entrapped CS/CMCi nanoparticles. 102

Figure 4.15: (A) TEER values of Caco-2 cells after incubation with 1.0 mg of insulin entrapped CS/CMCi nanoparticles and control (insulin solution 0.2 mg/mL) (B) Cumulative amount of insulin permeated through Caco-2 cells after incubation with 1.0 mg of insulin entrapped CS/CMCi nanoparticles and control (insulin solution 0.2 mg/mL). The results are presented as the mean ± SD (n = 3).103

Figure 4.16: (A) (A) Blood glucose levels in diabetic SD rats after subcutaneous or oral administration of various preparations. (B) Serum insulin levels in diabetic SD rats after

subcutaneous or oral administration of various preparations. The results are presented as the mean \pm SD (n = 6). * p < 0.05 compared to empty nanoparticles, empty capsules or oral insulin solution (100 IU/kg). 108

Figure 5.1: Summary of insulin entrapped CS/CMC_i nanoparticles study. 111

Universiti Malaya

LIST OF TABLES

Table 2.1: Action time course of various human insulin formulations.....	11
Table 2.2: Methods employed to enhance permeability in oral insulin delivery.	19
Table 2.3: Recent studies on carrier systems and <i>in vivo</i> models for oral insulin delivery.	22
Table 2.4: Clinical development of oral insulin by pharmaceutical industries.....	24
Table 3.1: The Box-Behnken experimental design used to study the four process factors (the volume and concentration of NaOH (X_1 , X_2), the amount of ClCH ₂ COOH (X_3) and the reaction temperature (X_4)) for the carboxymethylation of <i>iota</i> -carrageenan.....	34
Table 4.1: The partial degree of substitution (DS) of samples (I01–I33) derived from ¹ HNMR.	58
Table 4.2: The molecular weight of samples (I01–I33).....	60
Table 4.3: R ² value for different release kinetics models: zero-order, first-order and Higuchi model.....	66
Table 4.4: Dependent variables obtained from various CS/CMC _i nanoparticles. Dependent variable ((swelling ratio (Y_1), gel fraction (Y_2) of CS/CMC _i , the Korsmeyer- Peppas release model parameters k (Y_3) and n (Y_4) of insulin-entrapped CS/CMC _i nanoparticles in simulated gastric fluid (SGF) (pH 1.2) and swelling ratio (Z_1), gel fraction (Z_2) of CS/CMC _i , the Korsmeyer-Peppas release model parameters k (Z_3) and n (Z_4) of insulin-entrapped CS/CMC _i nanoparticles in simulated intestinal fluid (SIF) (pH 6.8)).	70
Table 4.5: Predicted and experimental values for the dependent variables (degree of swelling (Y_1), gel fraction (Y_2) of CS/CMC _i , and the Korsmeyer-Peppas release model parameters k (Y_3) and n (Y_4) for the entrapped insulin in the CS/CMC _i nanoparticles in simulated gastric fluid (SGF) (pH 1.2), and the degree of swelling (Z_1), gel fraction (Z_2) of CS/CMC _i , and the Korsmeyer-Peppas release model parameters k (Z_3) and n (Z_4) for the entrapped insulin in the CS/CMC _i nanoparticles in simulated intestinal fluid (SIF) (pH 6.8)) along with the percentage error.	75
Table 4.6: Comparative properties of the optimised insulin-loaded nanoparticles formulated with native Ci and CMC _i	83
Table 4.7: HPLC method validation of insulin.	94
Table 4.8: The effective permeability (P_e) (cm/s) values and apparent permeability (P_{app}) coefficient values (cm/s) of the <i>in vitro</i> PAMPA and Caco-2 transport study.	98

Table 4.9: Caco-2 cell monolayer confluency measurement by TEER measurement and lucifer yellow rejection (%) test over a 21-days culture period. 100

Table 4.10: Pharmacokinetic data of insulin in diabetic rats after subcutaneous injection of insulin solution or oral administration of insulin entrapped CS/CMC_i nanoparticles. 107

Universiti Malaya

LIST OF SYMBOLS AND ABBREVIATIONS

%	:	Percentage
°C	:	Degree Celsius
μL	:	Microlitre
μm	:	Micrometre
AG	:	3, 6-anhydro- α -D-galactopyranose
AG2S	:	3, 6-anhydro- α -D-galactopyranose-2-sulfate
ANOVA	:	Analysis of variance
ATCC	:	American Type Culture Collection
AUC	:	Area under curve
BA	:	Relative bioavailability
BBD	:	Box-Behnken design
Cm	:	Centimetre
CMC	:	Carboxymethylcellulose
CMCi	:	Carboxymethylated <i>iota</i> -carrageenan
Ci	:	Native <i>iota</i> -carrageenan
COOH	:	Carboxylic acid
CSII	:	Continuous subcutaneous insulin infusion
Da	:	Dalton
DMEM	:	Dulbecco's modified Eagle's medium
DS	:	Degree of substitution
EE	:	Entrapment efficiency
ELISA	:	Enzyme-linked immunosorbent assay
FBS	:	Fetal bovine serum
FDA	:	United States Food and Drug Administration

FESEM	:	Field emission scanning electron microscope
FITC	:	Fluorescein isothiocyanate
FT-IR	:	Fourier transform infrared
G2S	:	D-galactopyranose-2-sulfate
G4S	:	D-galactopyranose-4-sulfate
G2S, 6S	:	D-galactopyranose-2, 6-disulfate
GIT	:	Gastrointestinal tract
H	:	Hour
HBSS	:	Hank's Balanced Salt Solution
HCl	:	Hydrochloric acid
HSQC	:	Heteronuclear single quantum coherence
HPLC	:	High performance liquid chromatography
HPMC	:	Hydroxypropyl methylcellulose
IU	:	International unit
IVIVC	:	<i>In vitro/in vivo</i> correlation
Kg	:	Kilogram
L	:	Litre
LDH	:	Lactate dehydrogenase
LY	:	Lucifer yellow
M	:	Metre
M	:	Molar
MDI	:	Multiple daily injections
Mg	:	Milligram
min	:	Minute
mIU	:	Milliinternational unit
mL	:	Millilitre

Mm	:	Millimetre
mmol	:	Millimole
Nm	:	Nanometre
NMR	:	Nuclear magnetic resonance
PAMPA	:	Parallel artificial membrane permeability assay
PBSG	:	Phosphate buffer saline with glucose
PDI	:	Polydispersity index
PEG	:	Polyethylene glycol
pH	:	Negative logarithm of the hydrogen ion concentration
Ppm	:	Parts per million
Rpm	:	Rotation per minute
RSM ^{MSI}	:	Response surface methodology together with multivariate spline interpolation
SC	:	Subcutaneous
SD	:	Standard deviation
SGF	:	Simulated gastric fluid
SIF	:	Simulated intestinal fluid
T	:	Temperature
TEER	:	Transepithelial electrical resistance
TEM	:	Transmission electron microscopy
TJ	:	Tight junction
v/v	:	Volume per volume
w/w	:	Weight per weight
WHO	:	World Health Organization

LIST OF APPENDICES

Appendix A: Animal ethics approval letter	146
Appendix B: Detailed response surface plots	147

Universiti Malaya

CHAPTER 1: INTRODUCTION

1.1 Overview

Diabetes is a metabolic disorder characterised by hyperglycemia that currently affects 387 million people worldwide (Ogurtsova *et al.*, 2017), with the majority being type 2-diabetes. It is managed and controlled through insulin and/or oral hypoglycaemic drugs such as metformin, glipizide, repaglinide and rosiglitazone. The present mode of insulin administration through subcutaneous route has several disadvantages like local pain, itching, allergy, hyperinsulinemia, and insulin lipodystrophy around the injection site. Therefore, non-invasive delivery systems like oral, transdermal, pulmonary, intranasal, buccal, ocular and rectal routes have been studied with great interest (Soares *et al.*, 2012; Shah *et al.*, 2016). The recent introduction of inhaled Technosphere[®] insulin Afrezza (Sanofi and MannKind), is ideal for postprandial blood glucose control. However, its use is limited by inhaler device complexity, high price and safety especially in chronic lung disease patients (Richardson & Boss, 2007; Neumiller *et al.*, 2010). On the contrary, oral insulin nanoparticles using chitosan and poly- γ -glutamic acid showed a hypoglycemic effect for 10 h in diabetic rats with a relative bioavailability of $15.1 \pm 0.9\%$ (Sonaje *et al.*, 2009). In recent years, pre-clinical studies on an enteric-coated insulin capsule for type-2 diabetic patients exhibited favourable outcomes (Phillips *et al.*, 2004; Whitelaw *et al.*, 2005; Luzio *et al.*, 2010). Therefore, oral administration is a better alternative route of insulin administration. It is physiologically more effective, as absorption of insulin in the intestine reaches the liver through hepatic portal circulation, which is the prime site of its action, having similar effect to that of pancreas-secreted insulin (Morishita *et al.*, 2006; Rekha & Sharma, 2013). Figure 1.1 depicts the various routes of insulin administration.

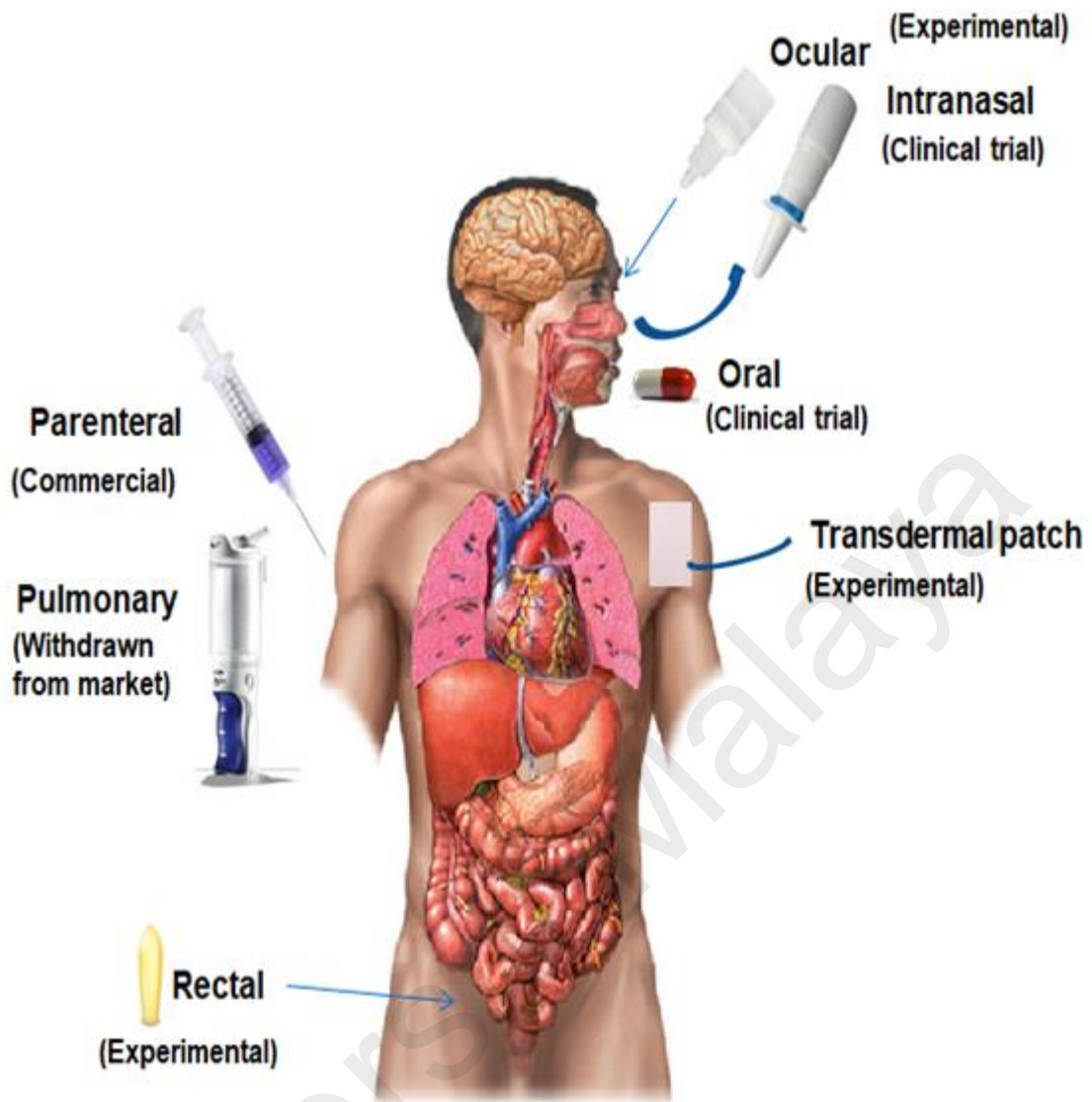


Figure 1.1: Schematic diagram of various routes of insulin administration (This figure was modified from Shah *et al.*, 2016).

Bioavailability of oral insulin is strongly affected by enzymatic degradation in the stomach and intestinal lumen, and poor permeability across the intestinal epithelium (Fonte *et al.*, 2013; Rekha & Sharma, 2013; Lundquist & Artursson, 2016). Recent research have focused on improving bioavailability using nanoparticles as a carrier system that protects insulin against harmful gastric environment, improve drug stability, transcytosis of drugs across the tight intestinal barrier through site specific delivery to the

intestine (Chen *et al.*, 2011b; Pan *et al.*, 2002; Sandri *et al.*, 2010; Han *et al.*, 2012). Few attempts to formulate nanoparticles of insulin have been reported, using various natural polymers as nanocarriers, such as carrageenan (Leong *et al.*, 2011a; Cheng *et al.*, 2015), chitosan (Mukhopadhyay *et al.*, 2012; Mukhopadhyay *et al.*, 2013; Sarmiento *et al.*, 2006b), alginate (Sarmiento *et al.*, 2006a; Sarmiento *et al.*, 2007), and gelatin (Zhao *et al.*, 2012).

One of the major concerns in designing oral insulin systems is poor bioavailability. To improve bioavailability, insulin must be protected from degradation by stomach acid (pH 1–3) and proteolytic enzymes. It is then released in a more neutral intestinal environment (pH 7) for absorption into the systemic circulation to be effective. This pH responsive behaviour can be imparted to a polymer through carboxymethylation process (Frag & Mohamed, 2013; Hu *et al.*, 2015). A recent research shows that the attachment of pH sensitive groups such as –COOH group to carrageenan helps in site-specific release of insulin (Leong *et al.*, 2011a). The incorporation of carboxymethylated *kappa*-carrageenan in the encapsulation of insulin protects insulin from the acidic stomach environment and prolongs the glycemic effect. These results from the interaction of the sulfate moieties of the carrageenan with the amino acid groups of insulin *via* ionic bonding (Leong *et al.*, 2011b).

Entrapment of insulin in mucoadhesive chitosan nanoparticles is found to improve intestinal permeability of insulin (Rubeaan *et al.*, 2016). Evidence shows enhanced permeation of insulin entrapped in thiolated trimethyl chitosan nanoparticles (Yin *et al.*, 2009), multilayered nanoparticles of alginate, dextran sulfate, poloxamer, chitosan and albumin (Woitiski *et al.*, 2010), lauryl succinyl chitosan nanoparticles (Rekha & Sharma, 2009). Moreover, chitosan has been shown to open intercellular tight junctions (TJs),

facilitating paracellular permeability of hydrophilic macromolecules (Ma & Lim, 2003; Jin *et al.*, 2016).

In contrast to previous research that used carboxymethylated *kappa*-carrageenan microparticles with a diameter of 1273 μm , the current study utilised *iota*-carrageenan as an intestine-targeted insulin carrier. Insulin-entrapped lectin-functionalized microparticles of *kappa*-carrageenan conferred an overall bioavailability of 12.8–14.8% compared to subcutaneous route in rats (Leong *et al.*, 2011b). This study sought to improve the delivery of insulin by entrapping insulin in chitosan-complexed carboxymethylated *iota*-carrageenan nanoparticles. The advantage of these nano sized particles is that they possess a higher surface-to-volume ratio than other microparticles (Leong *et al.*, 2011b). The additional sulfate groups in carboxymethylated *iota*-carrageenan are hypothesized to enhance its interaction with amino groups of insulin and may improve insulin stability and entrapment (Leong *et al.*, 2011b). Chitosan serves as a complexation agent and imparts mucoadhesive properties to the nanoparticles. It facilitates the transient opening of the TJs of the intestinal mucosa to assist the transportation of macromolecules across the intestinal barrier into systemic circulation. This is supported by its ability to form nanoparticles by polyelectrolyte complexation method to entrap peptide-based drugs (Grenha *et al.*, 2010; Rodrigues *et al.*, 2012; Rodrigues *et al.*, 2015). This uses procedures that avoid degradation, avoiding deleterious organic solvents or elevated mechanical forces. Hence, this method has great potential for safe protein drug entrapment.

1.2 Aim and objectives

The main aim of the study is to formulate, optimise and characterise an improved oral insulin delivery system using chitosan complexed carboxymethylated *iota*-carrageenan and investigate its *in vitro* and *in vivo* insulin delivery efficacy. The specific objectives are as follows:

- 1) To develop and characterise a pH sensitive (carboxymethylated) *iota*-carrageenan with the aid of a modelling tool, dataNESIA[®] software.
- 2) To prepare, characterise and evaluate the *ex vivo* mucoadhesiveness of insulin entrapped chitosan complexed carboxymethylated *iota*-carrageenan nanoparticles.
- 3) To determine the *in vitro* insulin release kinetics and active and passive transport of insulin in nanoparticles using parallel artificial membrane permeability assay (PAMPA) and Caco-2 cells.
- 4) To investigate the cytotoxicity of prepared nanoparticles on Caco-2 cells.
- 5) To determine *in vivo* bioavailability of insulin nanoparticles in streptozocin induced type-1 diabetic Sprague Dawley rats.

CHAPTER 2: LITERATURE REVIEW

2.1. Diabetes mellitus and its pharmacological treatment

Diabetes mellitus is a group of metabolic disorders characterised by hyperglycemia, resulting from defects in insulin secretion or resistance, and/or altered metabolism of lipids, carbohydrates and proteins. International Diabetes Federation (IDF) projected that one in every 11 adults worldwide suffer from diabetes and the diabetic population is predicted to increase from 415 million in 2015 to 642 million by 2040 (Ogurtsova *et al.*, 2017). The word diabetes comes from the Greek word meaning passing through, a reference to increase urination (polyuria). Mellitus is a Latin word meaning honey, a reference to excess glucose in the urine of diabetic patients. Normal fasting blood glucose in healthy adults is around 70–100 mg/dL. Prolonged failure to maintain normal blood glucose levels causes diabetes. Diabetes increases the risk of macrovascular diseases such as cardiovascular disease, coronary artery disease, stroke and others. The primary microvascular complications of diabetes include damage to the eyes, kidneys and nerves (Amini & Parvaresh, 2009). Generally, diabetes can be classified into type 1, type 2 and gestational diabetes. Type 1 diabetes is characterised by the inability of the pancreas to produce enough insulin and hence daily administration of insulin is required. Type 2 diabetes is characterised by hyperglycemia, insulin resistance and the body's ineffective use of insulin. Gestational diabetes is associated with hyperglycemia that happens during pregnancy (Jain & Saraf, 2010; Chen *et al.*, 2011a; Xie *et al.*, 2014; Ogurtsova *et al.*, 2017; Zaccardi *et al.*, 2016).

Basically, the pharmacological treatment options for diabetes include antihyperglycemic agents and insulin. Oral antihyperglycemic agents include sulphonylureas (tolbutamide, glipizide, glimepiride and others), biguanides (phenformin and metformin), thiazolidinediones (rosiglitazone and pioglitazone), α -glucosidase

inhibitors (acarbose and miglitol) and dipeptidyl peptidase 4 inhibitors (sitagliptin, vildagliptin and others) (Jain & Saraf, 2010; Wu *et al.*, 2014). Injected antihyperglycemic agents include glucagon-like peptide 1 agonists (dulaglutide, exenatide and others) and amylinomimetic (pramlintide) (Dipiro *et al.*, 2011; Chaplin & Bain, 2016).

Antihyperglycemic agents are only used to treat type 2 diabetes (Dipiro *et al.*, 2011) and not recommended for gestational diabetes unless the benefits outweigh the risks (Cosson *et al.*, 2017). The first line agent for type 1 (McGibbon *et al.*, 2013) and gestational diabetes is insulin (Cosson *et al.*, 2017; Thompson *et al.*, 2013). Insulin is also the first line treatment for hyperglycemia in hospitalized diabetic patients (Houlden *et al.*, 2013). In type 2 diabetic patients, insulin is given when the dose of oral antihyperglycemic agents have been optimised but the blood glucose level and HbA1c value of the diabetic patients are still above normal levels (Ministry of Health, Malaysia, 2009; Ogurtsova *et al.*, 2017). Hence, insulin plays an important role in the management of all types of diabetes.

2.2. Insulin

The discovery of insulin for the treatment of diabetes goes back to the 20th century. In 1901, Eugene Opie discovered that diabetes was an outcome of the destruction of the Islets of Langerhans. In 1916, Nicolae Paulescu reported that pancreatic extract lowered blood glucose levels in diabetic dogs. In 1921, Banting and Best, working in the laboratory of Prof. John Macleod, made a breakthrough in the discovery of insulin. They isolated insulin from pancreatic extracts and tested it on diabetic dogs and successfully cured hyperglycemia (Quianzon & Cheikh, 2012).

Insulin is a polypeptide hormone, made up of 51 amino acids (AAs) with a molecular weight of 5808 Da. It is secreted in the β -cells of pancreas and consists of two chains, A-chain 21 AAs and B-chain 30 AAs. Three disulphide links exist between the cysteine groups, two at position A7 with B7 and A20 with B19 (inter-chains A and B) and one at A6 with A11 (intra-chain of A) (Figure 2.1). These links stabilize the tertiary structure of the insulin. Insulin is more stable as crystalline hexamers. It consists of six insulin molecules with two zinc ions at the centre (Figure 2.2). Bonds with zinc ions improve the stability of the insulin hexamers (Manoharan & Singh, 2015). However, these are biologically inert and must be made broken down into its monomeric form to be biologically active (De Meyts, 2004).

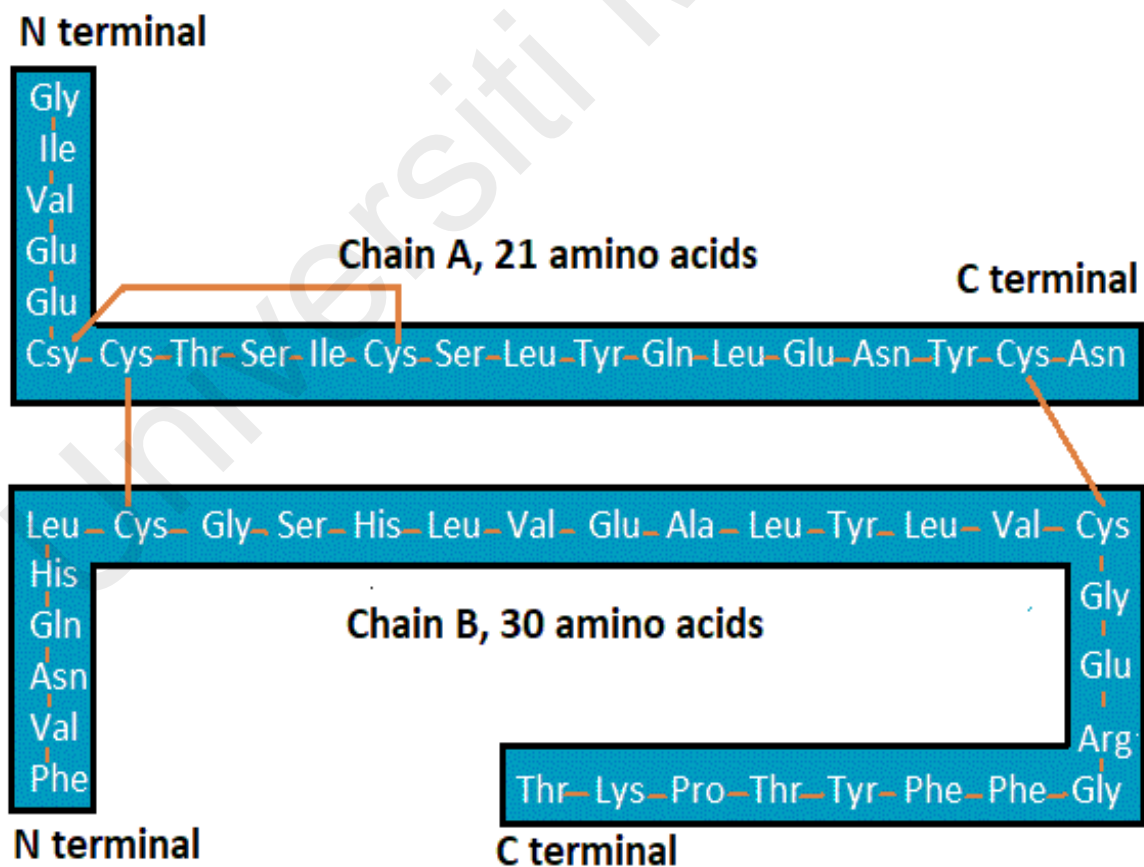


Figure 2.1: Human insulin structure.

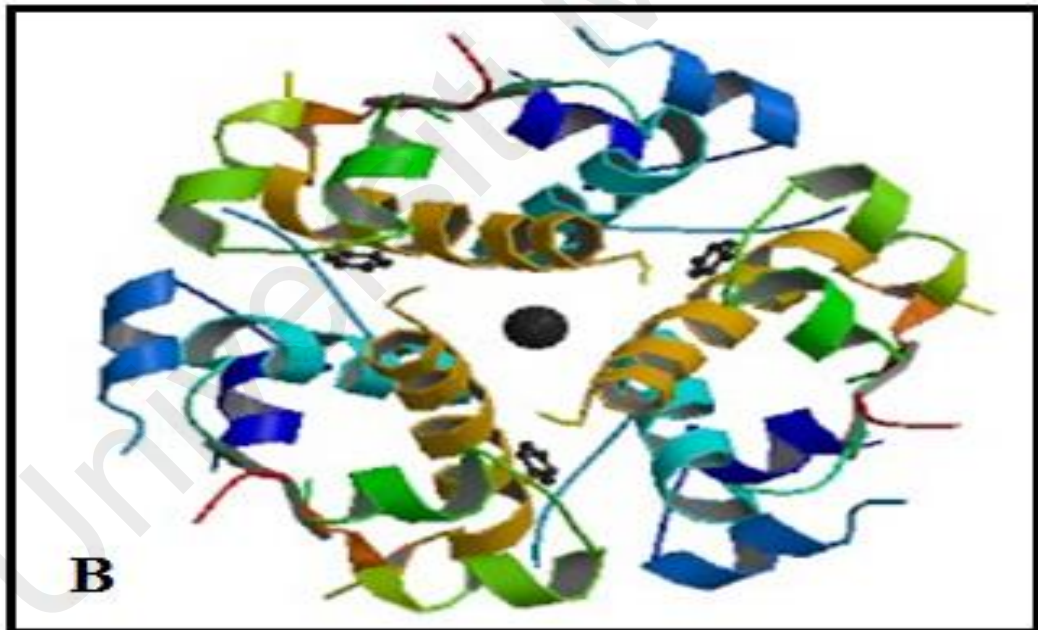
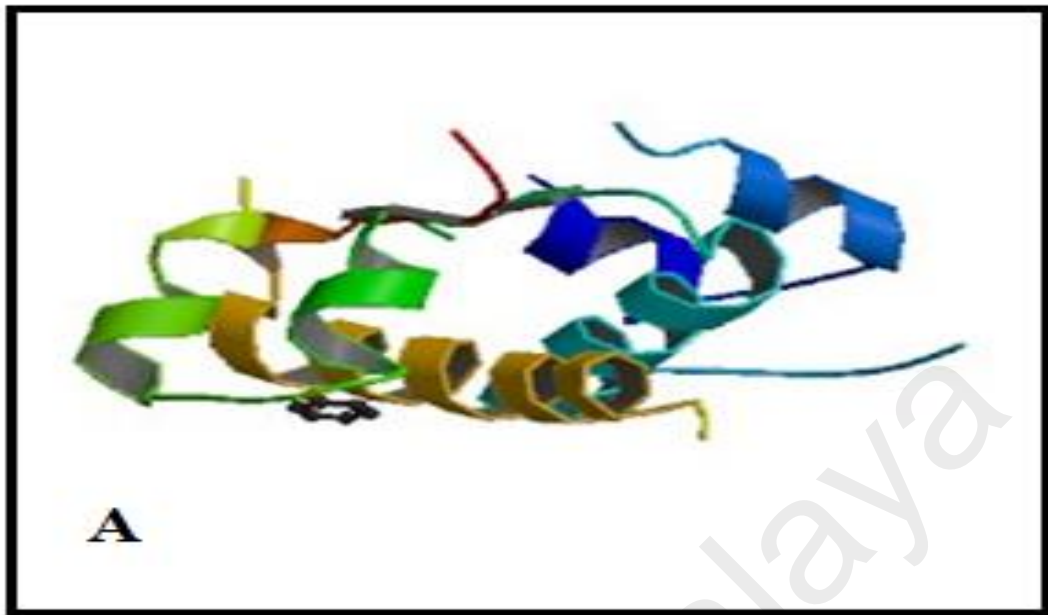


Figure 2.2: (A) Dimeric structure of human insulin, (B) Hexameric structure of human insulin with zinc ion (●) at the centre (downloaded from Protein data bank (PDB code 3JSD, www.rcsb.org/pdb).

Advances in recombinant DNA technology help in the generation of human insulin. Human insulin is available in two forms depending on the duration of action, such as short acting i.e. regular insulin and intermediate acting i.e. Neutral Protamine Hagedorn [NPH] (McGibbon *et al.*, 2013). Further advancement in protein engineering produced insulin analogues, with modified AAs and improved pharmacokinetic properties. These are categorised into rapid-acting insulin analogues i.e. insulin aspart, insulin glulisine and insulin lispro and long-acting insulin analogues i.e. ultralente, insulin detemir and insulin glargine (McGibbon *et al.*, 2013). Table 2.1 shows the action time course of various human insulin formulations.

The roles of insulin and its analogues in humans are:

- To enable glucose transportation across cell membranes.
- To convert excess glucose into glycogen in both liver and muscle for storage.
- To allow conversion of excess glucose to fat.
- To prevent the breakdown of protein for generating energy for the body (De Meyts, 2004).

In normal physiology plasma glucose reflects the balance between: (i) the release of glucose into the circulation by either absorption from the intestine or the breakdown of stored glycogen in the liver and (ii) the uptake and metabolism of blood glucose by peripheral tissues. In diabetics, normal glucose metabolism is flawed, and patients require insulin to retain normal glucose level. The current administration of insulin is through parenteral route (subcutaneous injection), as the physical and chemical properties of insulin are affected when delivered *via* non-parenteral route.

Table 2.1: Action time course of various human insulin formulations.

Insulin formulations	Onset of action	Peak action	Duration of action
<u>Short-acting Insulin</u>			
Regular Insulin	30–60 min	2–4 h	6–8 h
<u>Intermediate-acting Insulin</u>			
Neutral protamine	1–3 h	5–7 h	13–16 h
Hagedorn (NPH)			
Semilente	5–7 h	5–7 h	12–16 h
Lente	1–3 h	4–8 h	13–18 h
<u>Rapid-acting Insulin</u>			
Insulin lispro	5–15 min	1–3 h	4–6 h
Insulin aspart	5–15 min	40–50 min	4–6 h
Insulin glulisine	5–15 min	1–2 h	3–4 h
<u>Long-acting Insulin</u>			
Ultralente	2–4 h	8–14 h	16–20 h
Insulin glargine	1–2 h	Peakless	24 h
Insulin detemer	3–4 h	4–6 h	20 h
<u>Pre-mix Insulin</u>			
Insulin lispro protamine/lispro (75/25)	15 min	30 min–1 h	13–16 h
Insulin aspart protamine/ aspart (70/30)	5–15 min	2–5 h	10–16 h

Adapted from Gradel *et al.*, 2018, McGibbon *et al.*, 2013

2.3. Current route of insulin administration: Parenteral route

In the early 20th century insulin was administered via intramuscular injection. Researchers found that subcutaneous route was as effective as intramuscular route with less pain. Initially, needles and syringes were used for subcutaneous injections. However, it had some disadvantages like local pain, itching, allergy, hyperinsulinemia, and insulin lipodystrophy around the injection site. Therefore, other delivery devices were developed, including insulin pens and insulin pumps (Shah *et al.*, 2016).

Insulin pen (NovoPen) was first launched by Novo Nordisk A/S, Bassvaerd, Denmark in 1985 (Luijf & DeVries, 2010). Presently, different insulin pens such as HumaPen[®] Memoir[™], SoloStar[®], FlexPen[®], NovoPen[®], KwikPen[®], OptiClik[™] are marketed. Recently, NovoPen Echo[®] was designed for children and half-unit increment (0.5 U of insulin) dosing with a simple memory function (Hyllested-Winge *et al.*, 2016). Insulin pens are more convenient than syringes and needles due to their portability, smaller needle size, less pain, ease of handling and self-injection capabilities (Luijf & DeVries, 2010).

Reports have showed that continuous subcutaneous insulin infusion (CSII) using insulin pump is superior to multiple daily injections (MDI) (Farrar *et al.*, 2016). The insulin pump is a battery-operated insulin reservoir, connected to a catheter with a needle and a computerised chip that helps to regulate insulin delivery (e.g., Velosulin[®]BR). The pump supplies a constant slow rate of insulin to fulfill the basal insulin requirement as well as the administration of a higher dose to meet meal time requirements. However, patients must monitor their blood sugar and regulate the amount of insulin infusion. Furthermore, patients must check the catheter for blockage, which leads to diabetic ketoacidosis (Saboo & Talaviya, 2012). Cost is also another downside of insulin pumps (Skyler, 2010).

Although parenteral route is currently the predominant mode of insulin administration, it has various disadvantages such as local pain, itching, hypersensitivity, localized drug saturation and insulin lipodystrophy surrounding the injection site (Shah *et al.*, 2016). Hence, researchers have explored other needle free modes of insulin administration which include pulmonary, transdermal, intranasal, buccal, rectal and oral routes.

2.4 Alternative needle free routes of insulin administration

2.4.1 Pulmonary route

The available thin alveolar epithelium for absorption, high vascularisation and good ability for drug interchange are distinct characteristics of the lung that can assist the absorption of peptides and proteins *via* the pulmonary route (Yu & Chien, 1997; Henkin, 2010). The lack of first-pass metabolism and reduced enzymatic degradation are other advantages of inhaled insulin (Agu *et al.*, 2001; Henkin, 2010). The first inhaled insulin developed was ‘Exubera[®]’ jointly formulated by Pfizer, Sanofi-Aventis and Nektar Therapeutics, which acquired market consent in 2006 but was withdrawn in 2007 due to low cost-effectiveness and poor patient compliance (Bailey & Barnett, 2007). Other developments such as ‘AIR’ by Eli Lilly and Alkermes, Technosphere[®] Insulin System under MannKind Corporation, ProMaxx[®] developed by Baxter Healthcare, ‘AERx[®]’ Insulin Diabetes Management System (AERx[®] iDMS) under Novo Nordisk and Aradigm Corporation and ‘AeroDose[™]’ by Aerogen. However, these products were withdrawn due to high cost and compromised long term safety, except for Technosphere[®] that received FDA approval in 2014 (Kugler *et al.*, 2015).

2.4.2 Nasal route

Apart from pulmonary route, nasal delivery of insulin is also a potential route due to easy access, good vascularisation, lack of first pass metabolism and availability of large surface (150 cm²) for absorption (Duan & Mao, 2010). However, this route is limited due to mucociliary clearance, enzymatic degradation and absorption barrier (mucus layer) (Illum, 2003). To enhance the absorption of drugs, various enhancers have been studied such as bile salts (sodium glycocholate, taurodihydrofusidate and deoxycholate), surfactants (sodium lauryl sulfate, saponin, polyoxyethylene-9-lauryl ether), phospholipids (didecanoyl-phosphatidylcholine and lysophosphatidylcholine), chelating agents (ethylenediaminetetraacetic acid, salicylates), enzyme inhibitors (bestatin, amastatin), cell penetrating peptides (penetratin, octaarginine) and cyclodextrins (Khafagy *et al.*, 2007; Duan & Mao, 2010).

Development of nasal insulin by the pharmaceutical industry has been limited. CPEX pharmaceuticals applied the enhancer, CPE-215 together with recombinant human insulin to develop a liquid emulsion nasal spray (Nasulin™). The formulation reached peak level of insulin within 10–20 min and lasts up to 2 h and has a relative bioavailability of 15–20% relative to subcutaneous insulin injection (Leary *et al.*, 2008).

2.4.3 Buccal or sublingual route

Buccal or sublingual route attracted the interest of researchers due to its convenience, large surface area (100–200 cm²), reduced proteolytic interaction and better vascularisation for absorption of drugs. Moreover, it bypasses the liver and directly enters the systemic circulation through the internal jugular vein (Heinemann & Jacques, 2009). However, constant flow of saliva and multilayered oral epithelium are barriers to the

absorption of insulin (Bernstein, 2008). Various attempts, like absorption enhancers, protease inhibitors, bioadhesive delivery systems, modified insulin lipophilicity have been employed for effective buccal insulin absorption. However, these methods yielded variable glucose control with poor efficacy (Heinemann & Jacques, 2009).

‘OralLyn™’ is the only US FDA approved (conditionally) buccal insulin formulation, developed by Genex Biotechnology Corporation (Canada), based on RapidMist®, the company’s proprietary formulation and device design (Heinemann & Jacques, 2009). Pharmacokinetics of ‘OralLyn™’ showed a quick blood glucose lowering in 5 min, peak concentration at around 30 min and lasts for 2 h (Fennell, 2009). This buccal insulin formulation can be a substitute to subcutaneous injection, but further research on its variability, effectiveness and safety is needed (Bernstein, 2008).

2.4.4. Transdermal route

The transdermal route is favorable for insulin administration because of its ease of access and large surface area (1–2 m²). However, the permeability of insulin is restricted by the skin's outermost layer, the stratum corneum (Khafagy *et al.*, 2007; Prausnitz & Langer, 2008). Other methods have been investigated to overcome this difficulty via iontophoresis (Kanikkannan, 2002), sonophoresis (Amin *et al.*, 2008; Rao & Nanda, 2009), microdermal ablation (Andrews *et al.*, 2011), electroporation (Charoo *et al.*, 2010) and transferosome (Malakar *et al.*, 2012). Nguyen *et al.*, (2014) developed an insulin loaded conductive polymer nanotube in a transdermal patch, with controlled release of insulin over 24 h. Another study combining iontophoresis with liposomes decreased the blood glucose level gradually in type-1 diabetic rats up to 24 h (Kajimoto *et al.*, 2011).

Studies on transdermal route for insulin administration are at an advanced stage, with further clinical and safety studies underway.

2.4.5. Ocular route

The ocular route is feasible for protein and peptide deliveries as it avoids the liver and directly enters the systemic circulation (Xuan *et al.*, 2005). However, local discomfort and low bioavailability due to the lachrymal drainage are its main drawbacks. Various emulsificants such as saponin, Brij-78, BL-9, dodecylmaltoside and fucidic acid are used to enhance the absorption of insulin but these emulsificants are dangerous to the eyes at increased concentration (Lassmann-Vague & Raccach, 2006). To overcome the problem, an insulin loaded absorbable gelatine sponge, Gelfoam[®] was developed. Lee & Yalkowsky (1999) investigated the efficacy of Gelfoam[®] discs in rabbits and concluded that it can reduce blood glucose level up to 80%.

2.4.6. Rectal route

There have been few studies on insulin delivery systems *via* the rectum. However, absorption of insulin has been poor, variable and requires the addition of enhancers into suppositories or gels to improve absorption (Khafagy *et al.*, 2007). Various enhancers (sodium taurocholate, deoxycholic acid, polycarbophil) were tested in animal models (Hosny, 1999). However, the results showed various local reactions and variability (Sayani & Chien, 1996). Hence this route remains challenging to deliver insulin for managing diabetes (Khafagy *et al.*, 2007).

2.4.7. Oral route

Delivering insulin *via* the oral route is favoured over other routes due to its convenience and ability to mimic natural insulin secretion. Insulin is directly delivered to the GIT and reaches the liver through hepatic portal circulation, which is the prime site of action, thus producing a similar effect to pancreas-secreted insulin (Morishita *et al.*, 2006; Rekha & Sharma, 2013). However, its effectiveness remains limited due to its low bioavailability. This is caused by proteolysis of insulin in the acidic GIT, poor permeability *via* the intestinal membrane, the mucin barrier and the high molecular weight of insulin, limits its oral absorption (Wong *et al.*, 2016; Alai *et al.*, 2015).

The above problems can be overcome by using permeation enhancers, enzyme inhibitors, mucoadhesive polymers, and particulate carrier system (Table 2.2). Several permeation enhancers have been studied to enhance the permeability of insulin across the intestinal lining, including bile salts, fatty acids, surfactants, salicylates, chelators, zonular occludent toxin and thiolated polymers. They improve the permeability by transiently opening the TJs for the movement of insulin across the mucus barrier (Park *et al.*, 2011). However, long term use of such enhancers allows undesirable toxins to enter the circulation along with insulin when the TJs are opened (Goldberg & Gomez-Orellana, 2003; Khafagy *et al.*, 2007).

Along with the mucin barrier, proteolytic enzymes across the GIT also hampers protein absorption. To overcome this, various enzyme inhibitors such as aprotinin, leupeptin, FK-448, soybean trypsin inhibitors, sodium cholate, camostat mesilate, chromostatin, chicken ovomucoids, duck ovomucoids and bacitracin have been used (Wong *et al.*, 2016). However, their long-term use at high concentrations can impact the absorption of other proteins (Agarwal *et al.*, 2000; Khafagy *et al.*, 2007).

An improvement in oral insulin formulations is to use mucoadhesive polymers as they have pH responsive swelling behaviour and can adhere to the mucus layer to enhance insulin gradient across the intestine for absorption (Shaikh *et al.*, 2011; Banerjee *et al.*, 2016). The pH-responsiveness protects insulin in the stomach and releases it in the intestine in a controlled manner. For example, poly(methacrylic acid) (PMAA) complexed with poly(ethylene glycol) (PEG), represented as P(MAA-g-EG), shows high degree of complexation at low pH of the stomach and swells at higher pH in the small intestine (Ichikawa & Peppas, 2003; Sharpe *et al.*, 2014; Liu *et al.*, 2017). In another study, mucoadhesive polymer was conjugated with an enzyme inhibitor, protects insulin along with site specific release (Bernkop-Schnürch, 1998; Marschütz & Bernkop-Schnürch, 2000).

Universiti Malaysia

Table 2.2: Methods employed to enhance permeability in oral insulin delivery.

Approaches	Examples	Advantages	Limitations
Permeation enhancers	Bile salts, fatty acids, surfactants, salicylates, chelators, zonular occludents toxin and thiolated polymers	Improves permeation (Aungst, 2000; Lee <i>et al.</i> , 2005)	Access of both drugs and toxins to systemic circulation and local damage to the intestinal wall (Swenson <i>et al.</i> , 1994; Goldberg & Gomez-Orellana, 2003)
Enzyme inhibitors	Aprotinin, leupeptin, FK-448, soybean trypsin inhibitors, sodium cholate, camostat mesilate, chromostatin, chicken ovomucoids, duck ovomucoids and bacitracine	Protection against proteolytic enzymes present in stomach and intestine (Marschütz <i>et al.</i> , 2000)	Enzyme deficiency and side effects (Park <i>et al.</i> , 2011)
Mucoadhesive polymers	Chitosan, lectin, PLGA, thiolated polymer and alginate	Site specific permeation and enhanced membrane permeation (Peppas, 2004; Rekha & Sharma, 2009)	Premature clearing due to natural mucus shedding in intestine (Park <i>et al.</i> , 2011)
Particulate carrier system	Emulsions	Protection against proteolytic enzymes and chemical degradation (Toorisaka <i>et al.</i> , 2003)	Stability issues upon long-term storage (Toorisaka <i>et al.</i> , 2005)
	Microspheres	Protection against acidic environment of the stomach (Leong <i>et al.</i> , 2011a)	Insulin stability issues during formulation and storage (Park <i>et al.</i> , 2011)
	Nanoparticles	Protection against proteolytic enzymes (Fonte <i>et al.</i> , 2015)	Possibility of particle agglomeration (Morishita & Peppas, 2006)
	Liposomes	Protection against proteolytic enzymes (Niu <i>et al.</i> , 2011)	Low stability (Degim <i>et al.</i> , 2004)

Further enhancement in bioavailability is achieved using particulate carrier systems like emulsions, liposomes, microparticles and nanoparticles, which protects it from the harmful gastric environment and prevent enzymatic degradation. These carrier systems are also formulated for controlled and site-specific release in the intestine. Emulsions developed by mixing insulin with oil and surfactant, protects it from degradation and enhances its permeability across the intestinal wall (Toorisaka *et al.*, 2003). Nevertheless, hypoglycaemia and stability issues are the primary downsides for such systems (Toorisaka *et al.*, 2005). Stability issues may be overcome via dry emulsions, using techniques like spray drying, lyophilisation or evaporation (Dollo *et al.*, 2003; Takeuchi *et al.*, 1992).

Liposome carrier system protects insulin from enzymatic degradation, thereby enhancing its bioavailability. Oral sodium taurocholate-insulin liposomes notably decreased blood sugar level and exhibited better IVIVC in Caco-2 model (Degim *et al.*, 2004). Niu *et al.*, (2011) used sodium glycocholate to formulate insulin liposomes to protect against enzymatic degradation. Agrawal *et al.*, (2014) formulated folic acid functionalized poly(acrylic acid) and (allyl amine) hydrochloride coated insulin liposomes, which demonstrated around 20% bioavailability compared to subcutaneous insulin.

Among particulate carrier systems, microparticles formulated from synthetic or natural polymers have captured great interest recently (Sinha & Trehan, 2003; Srivastava *et al.*, 2016). Leong *et al.* (2011a) developed a pH-responsive and intestine-specific lectin coated carboxymethylated *kappa*-carrageenan microparticles containing insulin, with bioavailability of around 15% in diabetic rats. These pH-responsive microparticles prevent the release of insulin in acidic environment of the stomach. However, it swells and releases insulin at the intestinal basic pH level. In another study, insulin entrapped

bacterial cellulose-g-poly(acrylic acid) microparticles, offered protection from proteolytic enzymes (up to 60%) with better hypoglycemic effect (Ahmad *et al.*, 2016).

Recently, nanoparticles are being investigated as an alternative for oral insulin delivery. The nanoparticulate drug delivery system protects the drug from gastrointestinal environment, modulates drug release properties such as delayed or prolonged and biological behaviours such as bioadhesion, targeting or improved cellular uptake. Moreover, the submicron particle size i.e. from 10 to 1000 nm and the large surface area improves the absorption of nanoparticles compared to other larger carrier systems (Rieux *et al.*, 2006). One of the significant addition in the field of nanoparticulate systems is the use of acrylate polymers. For example, nanospheres of methacrylic acid complexed with PEG and acrylic acid complexed with PEG, through precipitation, offer high degree of complexation at low stomach pH and swell at higher pH in the small intestine to release insulin efficiently (Foss *et al.*, 2004). The nanoparticles formulated using mucoadhesive polymers adhere to the mucus lining of the GIT longer, which results in increased bioavailability of protein drugs (Banerjee *et al.*, 2016). Mukhopadhyay *et al.*, (2013) developed chitosan complexed insulin nanoparticles without using any organic solvents in the process. These nanoparticles showed 33% blood glucose reduction at 4 h post-administration in diabetic mice and lasted up to 8 h. In another study, lecithin-insulin complex was mixed with chitosan solution to produce nanoparticles with prolonged glycemic control of 12 h (Liu *et al.*, 2016b). In another study (Ansari *et al.*, 2016), glyceryltrimyristate, soy lecithin and polyvinyl alcohol nanoparticles (insulin 30 IU/kg) exhibited relative bioavailability of 8.26% compared to subcutaneous insulin injection (2 IU/kg), which showed a relative bioavailability of 1.7%.

Table 2.3 highlights some of the recent advances in oral insulin delivery. The list is confined to those with available bioavailability data.

Table 2.3: Recent studies on carrier systems and selected *in vivo* models for oral insulin delivery.

Carrier system	<i>In vivo</i> models	Dose; BA (%)	Reference
Insulin entrapped alginate and chitosan coated nanoemulsion	Diabetic male Goto-Kakizaki rats	25 IU/kg; 8.19	Li <i>et al.</i> , 2013b
Lectin-conjugated insulin liposomes	Healthy Sprague Dawley rats	50 IU/kg; 9.12	Zhang <i>et al.</i> , 2005
Bile salt incorporated insulin liposomes	Diabetic male Wistar rats	20 IU/kg; 11.0	Niu <i>et al.</i> , 2012
Poly(ester amide) combined insulin microspheres	Diabetic male Wistar rats	50 IU/kg; 5.89	He <i>et al.</i> , 2013
Insulin loaded biotin-grafted 1, 2-distearoyl-sn-glycero-3-phosphatidyl ethanolamine liposomes	Gene-knocked out diabetic (SLAC/GK) rats	20 IU/kg; 8.23	Zhang <i>et al.</i> , 2014
Insulin contained lectin-conjugated solid lipid nanoparticles	Healthy Sprague Dawley rats	50 IU/kg; 7.11	Zhang <i>et al.</i> , 2006
Insulin loaded multilayered nanoparticles	Diabetic male Wistar rats	50 IU/kg; 13.2	Woitiski <i>et al.</i> , 2010
Insulin loaded poly- γ -glutamic acid complexed chitosan nanoparticles	Diabetic male Wistar rats	30 IU/kg; 15.1	Sonaje <i>et al.</i> , 2009
Insulin contained polyester (poly(- ϵ -caprolactone)) and Eudragit [®] RS nanoparticles formulated by multiple emulsion method	Diabetic male Wistar rats	50 IU/kg; 13.21	Damgé <i>et al.</i> , 2007
Insulin entrapped alginate and chitosan coated nanoemulsion	Diabetic male Goto-Kakizaki rats	25 IU/kg; 8.19	Li <i>et al.</i> , 2013b
Amphiphilic cyclodextrin-based insulin nanoparticles	Healthy male Wistar rats	50 IU/kg; 5.5	Presas <i>et al.</i> , 2018
Intestinal absorption of insulin in self-emulsifying drug delivery systems	Healthy Sprague Dawley rats	72 IU/kg; 0.1	Liu <i>et al.</i> , 2019

BA (%) represents relative bioavailability of oral insulin compared with subcutaneous insulin injection

2.5. Clinical development of oral insulin

Oral delivery of insulin is still in the developmental phase. A list of pharmaceutical companies that successfully conducted clinical trial stages of oral insulin delivery is provided in Table 2.4.

Universiti Malaya

Table 2.4: Clinical development of oral insulin by pharmaceutical companies.

Companies	Brand Name	Preparation	Clinical development
Access Pharmaceuticals, Inc (USA)	CobOral™ Insulin	Nanoparticles	Preclinical
Aphios Corporation (USA)	APH-0907	Nanospheres	Preclinical
Biocon/Bristol-Myers Squibb (India)	IN-105	Conjugated insulin	II
Diabetology Ltd (UK)	Capsulin™	Capsule	II
Diasome Pharmaceuticals, Inc (USA)	HDV-Insulin	Liposomes	III
Emisphere Technologies, Inc (USA)	Eligen® Insulin	Tablet	II
Jordanian Pharmaceutical Manufacturing Co (Jordan)	JPM Oral Insulin	Nanoparticles	I
Novo Nordisk A/S (Denmark)	NN1954	Tablet	I
Oramed, Inc (Israel)	ORMD-0801	Capsule	II b
Oshadi Drug Administration Ltd (Israel)	Oshadi Icp	Nanoparticles	II
NOD Pharmaceuticals, Inc (USA)	Nodlin	Nanoparticles	II
Transgene Biotek Ltd (India)	TBL1002OI	Nanoparticles	Preclinical
Apollo Life Science (India)	Oraldel	Tablet	I b

Adapted from Zijlstra *et al.*, 2014, "Oramed completes patient," 2019.

2.6. Polymeric approach for oral delivery of insulin

Over the past few decades, researchers have focused on polymeric carriers including both synthetic and natural polymers for oral delivery of insulin. Figure 2.3 represents characteristics of polymeric carriers for oral insulin administration. These polymers help to stabilise and control the release of insulin, leading to improved bioavailability (Fonte *et al.*, 2015). Hydrogel polymers like carrageenan, chitosan, polymethacrylic acid, eudragit, lectin and poly(acrylic acid) protect insulin from acid degradation during gastrointestinal tract transit via swelling and deswelling in response to the pH (Chaturvedi *et al.*, 2013). Furthermore, mucoadhesiveness of some of the hydrogel polymers like chitosan, lectin and poly(acrylic acid) helps in paracellular transport of insulin by opening the TJs, hence improving biological activity (Woitiski *et al.*, 2011; Luo *et al.*, 2016). Cytotoxicity is a major concern in designing polymeric nanoparticles. Polymeric carriers should improve bioavailability without being toxic to cells (Grabowski *et al.*, 2013; Chaubey *et al.*, 2018). Polymers like, carrageenan and chitosan are extensively studied due to their ease of chemical alterations and propitious biological properties (Hamidi *et al.*, 2008; Luo *et al.*, 2016).

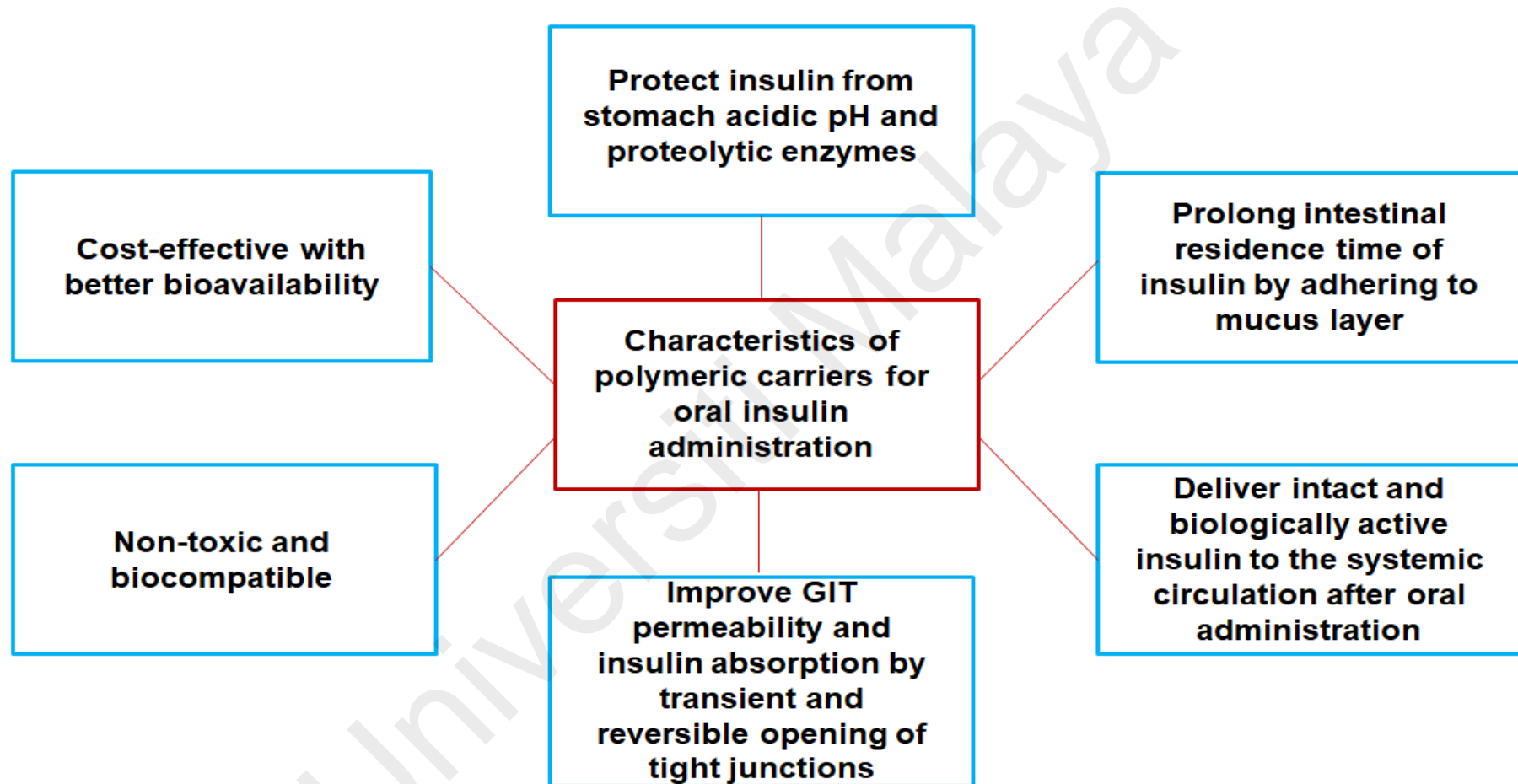


Figure 2.3: Desired characteristics of polymeric carriers for oral insulin administration

2.6.1. Carrageenan

Carrageenans are sulfated anionic polysaccharides obtained from red seaweed of the *Rhodophyceae* family. *Eucheme cottonii* and *E. spinosum* are the main species of *Rhodophyceae* for commercial production of carrageenan. Basically, these are polymers with high molecular weight and comprised of repeating units of galactopyranose and 3, 6-anhydrogalactopyranoses joined by α -1, 3 and β -1, 4-glycosidic linkages. There are three main types of carrageenans depending on the number and position of ester sulfate groups, namely *kappa*, *iota* and *lambda* carrageenan. *Kappa*-carrageenan consists of D-galactopyranose-4-sulfate and 3,6-anhydro- α -D-galactopyranose; *iota*-carrageenan consists of β -D-galactopyranose-4-sulfate and 3,6-anhydro- α -D-galactopyranose-2-sulfate and *lambda*-carrageenan contains D-galactopyranose-2-sulfate and β -D-galactopyranose-2,6-disulfate (Figure 2.4) (Prajapati *et al.*, 2014). *Kappa*- and *iota*-carrageenans easily form hydrogels with association with necessary cations such as potassium, sodium or calcium. The amount and location of the sulfated ester groups and the variety of cations determine the strength of gel formation (Prajapati *et al.*, 2014).

Carrageenans are being investigated as a carrier for oral protein and peptide. Carrageenans encapsulate peptide drugs effectively as there is an ionic interaction between the sulfate groups present in the carrageenan and the amino groups present in the peptide drug. Moreover, *iota*-carrageenan has the added advantage of two sulfate groups present in the molecular structure, which intensify its interaction with the amino groups of the insulin molecules, hence improve the insulin stability and entrapment (Nadvorny *et al.*, 2018). Leong *et al.*, (2011b) reported microparticles of carboxymethylated *kappa*-carrageenan used in oral insulin delivery. The carboxymethylated *kappa*-carrageenan produces a pH sensitive site-specific release of insulin, which can prevent premature release and degradation in the stomach. Tomoda *et al.*, (2009), prepared carrageenan microspheres of

allopurinol and local anaesthetic agents for the treatment of oral mucositis. The dispersing and membrane forming property of carrageenan microspheres uniformly cover the inner surface of oral cavity to prevent and treat oral mucositis. Sankalia *et al.*, (2006) reported the improvement in stability of alpha-amylase entrapped in cross linked *kappa*-carrageenan. *Kappa*-carrageenan beads protected the alpha-amylase and improved its duration and pattern of dissolution and enzyme loading capacity.

Universiti Malaya

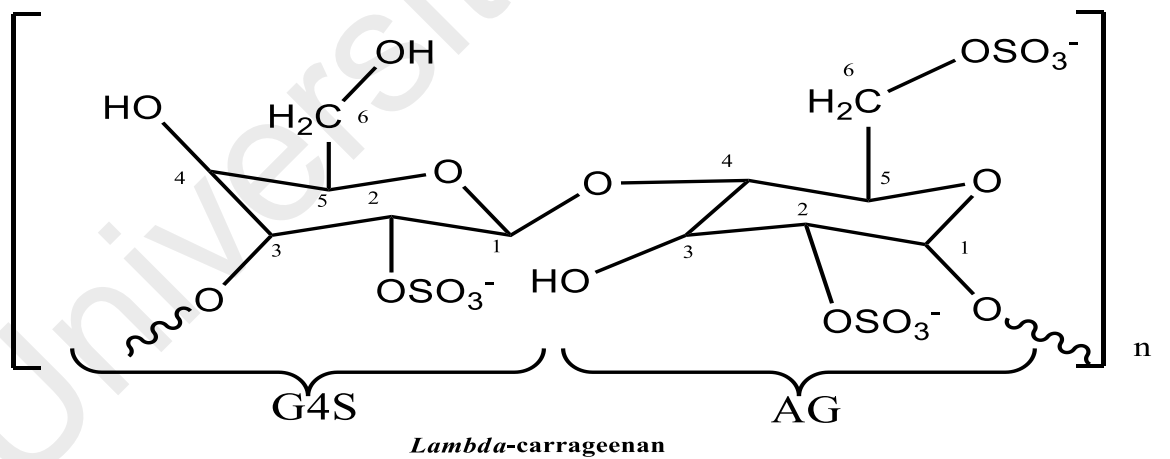
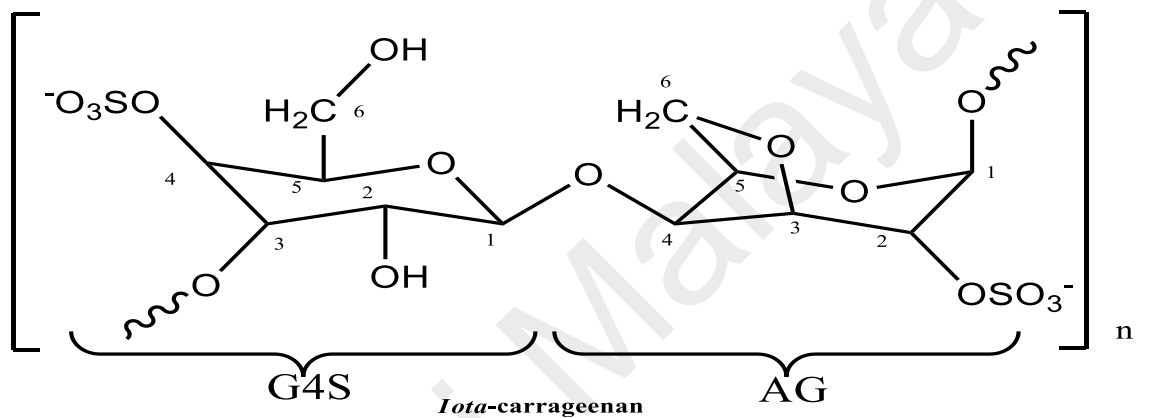
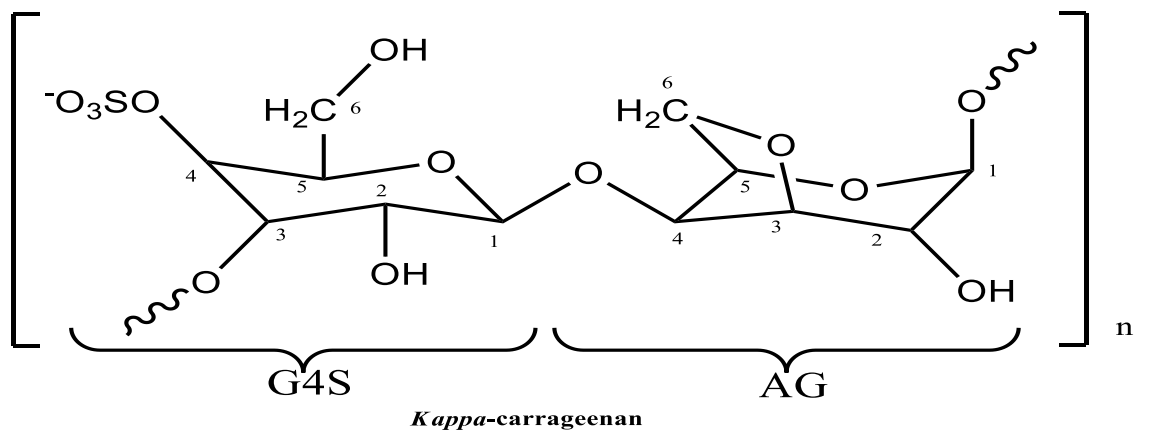


Figure 2.4: Chemical structure of *kappa*-, *iota*- and *lambda*-carrageenan. G4S is D-galactopyranose-4-sulfate; AG is 3, 6-anhydro- α -D-galactopyranose; AG2S is 3, 6-anhydro- α -D-galactopyranose-2-sulfate; G2S is D-galactopyranose-2-sulfate; G2S, 6S is D-galactopyranose-2, 6-disulfate; n is the number of repeating units.

2.6.2. Chitosan

Chitosan is a cationic polymer obtained from deacetylated chitin. It originates mainly from exoskeletons of crustaceans, insects, and cell walls of fungi. Chitosan comprises of repeating units of β -(1-4)-linked D-glucosamine and N-acetyl-D-glucosamine units (Figure 2.5). It is an ideal candidate for controlled release, nanoparticle and hydrogel formulations (Bhattarai *et al.*, 2010).

The mucoadhesive property of chitosan is ideal for protein drug delivery as it enhances the absorption of protein by retaining close contact and prolonging the time of the formulation stays in the intestine (Dudhani & Kosaraju, 2010). The hydrogen bond between the amino groups of positively charged chitosan and carboxyl groups of negatively charged intestinal mucosa results in an adhesive effect (Jin *et al.*, 2016). Moreover, chitosan transiently opens the TJs of the intestinal epithelial cells and allows paracellular absorption of insulin *via* the intestinal lining (Vllasaliu *et al.*, 2010). Liu *et al.*, (2016a) reported that N-trimethyl chitosan chloride coated poly (lactide-co-glycolide)–monomethoxy-poly (polyethylene glycol) nanoparticles helps transient and reversible opening of TJs between Caco-2 cells and helps insulin permeation through Caco-2 cells. Pan *et al.*, (2002) reported that chitosan nanoparticles have better intestinal insulin absorption with 14.9 % relative bioavailability compared to subcutaneous injection. In another study, insulin entrapped chitosan coated alginate nanoparticles exhibited better mucoadhesion and internalization of insulin in rat ileum (Sarmiento *et al.*, 2007). Diop *et al.*, (2015) formulated insulin loaded chitosan nanoparticles using freeze-drying and crosslinking techniques. These nanoparticles showed better stability in GIT and improved cellular uptake with reduced blood glucose level.

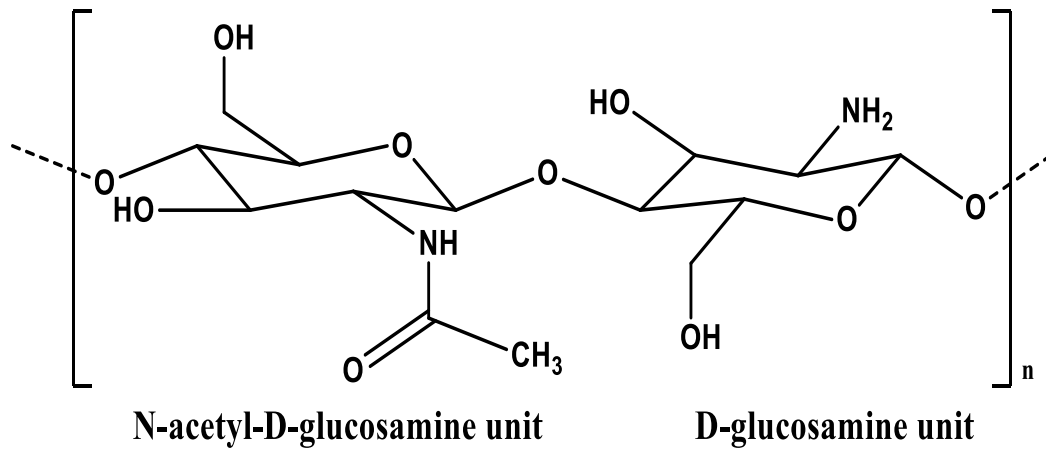


Figure 2.5: Structure of chitosan; n is the number of repeating units.

Universiti Malaysia

CHAPTER 3: METHODOLOGY

3.1 Materials

Iota-carrageenan (batch no.: 405301) was acquired from Marine Science Co. Ltd. (Tokyo, Japan). Sodium hydroxide, monochloroacetic acid, potassium dihydrogen phosphate, sodium chloride, hydrochloric acid, ortho-phosphoric acid, acetic acid, dipotassium hydrogen phosphate, acetonitrile, sodium sulfate, and deuterium oxide were purchased from Merck (Darmstadt, Germany). 2-Propanol and ethanol were obtained from Fisher Scientific UK Ltd. (Loughborough, Leicestershire, UK). Chitosan (low molecular weight, 50–190 kDa; deacetylation $\geq 75.0\%$; batch no.: SLBG5615V), human recombinant insulin (≥ 27.5 IU/mg), pepsin, trypsin, lucifer yellow, streptozocin were purchased from Sigma-Aldrich Co. (St. Louis, MO, USA). Gentamycin (50 $\mu\text{g/mL}$), amphotericin B, Dulbecco's modified Eagle's medium (DMEM), Hank's balanced salt solution (HBSS) and 100 mM of non-essential amino acid were obtained from Invitrogen Corporation (Carlsbad, CA, USA). Human insulin ELISA kit was purchased from Mercodia AB (Uppsala, Sweden), lactate dehydrogenase (LDH) assay kit was supplied by Roche (Mannheim, Germany) and [3-(4,5-dimethylthiazol-2-yl)-5-(3-carboxymethoxyphenyl)-2-(4-sulfophenyl)-2H-tetrazolium, inner salt] (MTS) assay kit was from Promega (Madison, WI, USA).

3.2 Preparation and characterisation of carboxymethylated *iota*-carrageenan (CMCi)

3.2.1. Experimental design

A Box-Behnken design (BBD) with four independent factors and three dependent variables was used to optimise the carboxymethylation of *iota*-carrageenan. The four factors included the volume of NaOH (X_1), the concentration of NaOH (X_2), the amount of ClCH₂COOH (X_3) and the reaction temperature (X_4), which generated 33 different experimental runs listed as I01 to I33 (Table 3.1). The dependent variables included the degree of swelling of insulin-free CS/CMCi nanoparticles in SGF (pH 1.2) (Y_1), the gel fraction of insulin free CS/CMCi nanoparticles in SGF (pH 1.2) (Y_2) and the release of entrapped insulin (Korsmeyer-Peppas model (Eq. 3.1) parameters k (Y_3) and n (Y_4) for the CS/CMCi nanoparticles in SGF (pH 1.2). The same parameters were investigated for the nanoparticles in SIF (pH 6.8), including Z_1 : the degree of swelling of insulin-free CS/CMCi nanoparticles; Z_2 : the gel fraction of insulin-free CS/CMCi nanoparticles; Z_3 : parameter k and Z_4 : parameter n . SGF and SIF were prepared according to the British Pharmacopeia (BP 2013). Both independent factors and dependent variables were simultaneously optimised to obtain the optimal formula.

$$\frac{M_t}{M_\infty} = kt^n \quad (\text{Eq. 3.1})$$

Where, M_t/M_∞ is the fraction of insulin released at time t , k is the structural/geometric constant for a particular system, and n is the release exponent representing the release mechanism. Statistical data analyses were performed using Student's paired t-tests, where $p < 0.05$ was deemed statistically significant.

The synthesis of CMCi was carried out using a modified version of a previously described method (Leong *et al.*, 2011a). Firstly, *iota*-carrageenan (5.0 g) was suspended in

2-propanol (100mL) and then a specified amount and concentration of NaOH (1mL in 15min) was added to it and stirred continuously at room temperature (25 °C), as shown in Table 3.1. Varying amount of ClCH₂COOH (Table 3.1) were added and the mixtures were heated to the specified temperature (Table 3.1) with continuous stirring for 4 h. Then, CMCi was vacuum filtered and washed three times alternately with ethanol-water (4:1) and ethanol, and finally dried at 70 °C for 12 h in an oven, powdered and kept in an air tight desiccator.

Table 3.1: The Box-Behnken experimental design used to study the four process factors (the volume and concentration of NaOH (X₁, X₂), the amount of ClCH₂COOH (X₃) and the reaction temperature (X₄)) for the carboxymethylation of *iota*-carrageenan.

Sample code	X ₁ (mL)	X ₂ (N)	X ₃ (g)	X ₄ (°C)
I01	6	4	2.25	50
I02	6	4	4.55	50
I03	6	4	3.40	40
I04	6	4	3.40	60
I05	6	12	6.80	50
I06	6	12	13.60	50
I07	6	12	10.20	40
I08	6	12	10.20	60
I09	6	8	4.55	40
I10	6	8	9.05	60
I11	6	8	4.55	60
I12	6	8	9.05	40
I13	4	4	2.25	50
I14	4	12	6.80	50
I15	4	8	3.05	50
I16	4	8	6.03	50

Table 3.1, continued

Sample code	X ₁ (mL)	X ₂ (N)	X ₃ (g)	X ₄ (°C)
I17	4	8	4.55	40
I18	4	8	4.55	60
I20	8	12	13.60	50
I21	8	8	6.03	50
I22	8	8	12.10	50
I23	8	8	9.05	40
I24	8	8	9.05	60
I25	6	8	6.80	50
I26	6	8	6.80	50
I27	6	8	6.80	50
I28	6	8	4.55	50
I29	6	8	9.05	50
I30	6	8	6.80	40
I31	6	8	6.80	60
I32	4	8	4.55	50
I33	8	8	9.05	50

3.2.2. Characterisation of CMCi

The CMCi samples were synthesised as mentioned in section 3.2.1. After the synthesis, the samples were characterised for degree of substitution by NMR, molecular weight and amount of sulfate content. For the NMR analysis, the samples were purified by dialysis using a Spectra/Por cellulose ester dialysis membrane (molecular weight cut off of 500 Da, Cole-Palmer, Vernon Hills, IL, USA) against ultrapure water for 24 h, with the water changed twice, and the samples were then lyophilised overnight at -40°C. After lyophilisation, the samples were re-dissolved in 20 mL of D₂O and sonicated 4 times for 2 h each (CX400 sonicator, Sonics and Materials Incorporation, Newtown, CT,

USA; 19 mm tip, power 400 W, frequency 20 kHz) in melting ice. Then, the samples were lyophilised at -40°C overnight for the second time.

The degree of substitution (DS) from the carboxymethyl groups was estimated using a modified version of a previously reported NMR procedure (Leong *et al.*, 2011a). The lyophilised native *iota*-carrageenan (Ci) and modified *iota*-carrageenan (30 mg) were dissolved in D₂O and transferred into individual 5 mm NMR tubes. The ¹H NMR spectra were recorded on a nuclear magnetic resonance spectrometer (ECA 400, JEOL Inc., Peabody, MA, USA) operated at 400 MHz. A total of 128 scans were taken at 25 °C using a 45° pulse with a relaxation delay of 5 s and an acquisition time of 2.21 sec. The ¹³C NMR spectra were recorded at 400 MHz collected at 28,200 scans with a relaxation delay of 2 s and an acquisition time of 1.05 sec. ¹H/¹H COSY spectra were obtained using 66 scans with an acquisition time of 0.17 sec and ¹H/¹³C HSQC were obtained using 32 scans with an acquisition time of 0.14 sec. 2,2-dimethyl-2-silapentane-3,3,4,4,5,5-d₆-5-sulphonate (DSS) was used as the internal standard and the pH adjusted by adding 20 mM of Na₂HPO₄.

The chemical shifts (δ) of both ¹H and ¹³C NMR were corrected relative to the internal standard ($\delta = 0.000$ ppm) according to IUPAC recommendations. The DS was determined by the integration of ¹H NMR peaks between 3.5–5.3 ppm, as per Eq. 3.2 (Leong *et al.*, 2011a; Heinze *et al.*, 2001). This is based on the hydroxyl groups at C-2 and C-6 substitutions of the β -D galactopyranose-4-sulfate unit (G).

$$X_a = \frac{A(\text{proton(s) of the carboxymethylated } i\text{-carrageenan at position O-}a)}{A(\text{proton(s) of the carboxymethylated } i\text{-carrageenan at position O-}a) + A(\text{proton(s) of the non-carboxymethylated } i\text{-carrageenan at position O-}a)} \quad (\text{Eq. 3.2})$$

$$\text{DS} = \sum X_a$$

Where, A is the peak area, O is the oxygen atom at position a (a = positions of C-2 and C-6 of β -D-galactopyranose-4-sulfate unit (G), and X_a is the partial DS.

The molecular weight of *iota*-carrageenan was measured using an Agilent 1260 Infinity Multiple Detector Suite (refractive index-viscometer-light scattering) GPC/SEC system (Santa Clara, CA, USA) with two coupled Waters Ultrahydrogel Linear columns (7.8 mm \times 300 mm, Waters Co., Milford, MA, USA). The mobile phase comprised of 0.1 M lithium nitrate. The flow rate was 0.6 mL/min and 100 μ L of sample was injected into the GPC/SEC system at a concentration of 2 mg/mL. A standard solution of polyethylene oxide (200 k Da) at 2 mg/mL was used to calibrate the system.

The amount of sulfate in *iota*-carrageenan was measured using ion chromatography and expressed as percent weight (% w/w) by ALS TECHNICHEM (M) Sdn Bhd. Selangor, Malaysia (Leong *et al.*, 2011b). The *iota*-carrageenan (1 mg) was hydrolysed in an incubator using 2 M trifluoroacetic acid (1 mL) for an hour at 120 $^{\circ}$ C. The product was diluted with ultrapure water (2 mL) and centrifuged at 5,000 rpm. Then, 50 μ L of supernatant was analysed using an ICS 1600 ion chromatography system equipped with a conductivity detector (Dionex Corporation, Sunnyvale, California, USA) and Waters IC-Pak Anion (4.6 \times 150 mm) column. The composition of the mobile phase was borate-gluconate buffer (pH 8.5), which consisted of 3.5 mM boric acid, 0.80 mM tetraborate, 0.80 mM gluconate, 0.25% v/v glycerine and 10% v/v acetonitrile with a flow rate of 2 mL/min. The sulfate content was expressed as percent weight (% w/w).

3.3. Formulation of chitosan-complexed insulin-loaded carboxymethylated *iota*-carrageenan nanoparticles

Chitosan (CS)-complexed insulin-loaded carboxymethylated *iota*-carrageenan (CMCi) nanoparticles were prepared using a polyelectrolyte complexation method (Grenha *et al.*, 2010). CS was dissolved in 1% w/v acetic acid, stirred at 500 rpm for 12 h at room temperature. *Iota*-carrageenan was dissolved in 0.1 M phosphate buffer of pH 8, stirred at 500 rpm for 1 h at 60°C in a water bath and 30 min at room temperature. The nanoparticles were formulated using various concentrations of CS (0.1 and 0.2% w/v in 1% acetic acid) and CMCi (0.1, 0.2, and 0.3% w/v in 0.1 M phosphate buffer pH 8). Insulin (0.5–2 mg) was dissolved in 100 µL of 0.01 M hydrochloric acid (Jin *et al.*, 2012). Then, the solution was added immediately to the prepared CMCi solution and neutralised. Next, complexation with the prepared CS solution was performed via drop-wise addition while stirring at 500 rpm at room temperature for 30 min to yield nanoparticles of different mass ratios of CS to CMCi (0.5:1, 1:1, 1.5:1, 2:1, 2.5:1, 3:1, 4:1 and 5:1). The resulting total volume of nanoparticle suspension containing both *iota*-carrageenan and CS was 15 mL. Then, the nanoparticles were centrifuged for 30 min at $16,000 \times g$ at 15°C with a top layer of 10 µL glycerol, and the recovered nanoparticles were resuspended in 200 µL of purified water. Finally, the insulin-loaded nanoparticles were lyophilised for 24 h. Figure 3.1 is a schematic diagram that depicts CS/CMCi nanoparticles formation.

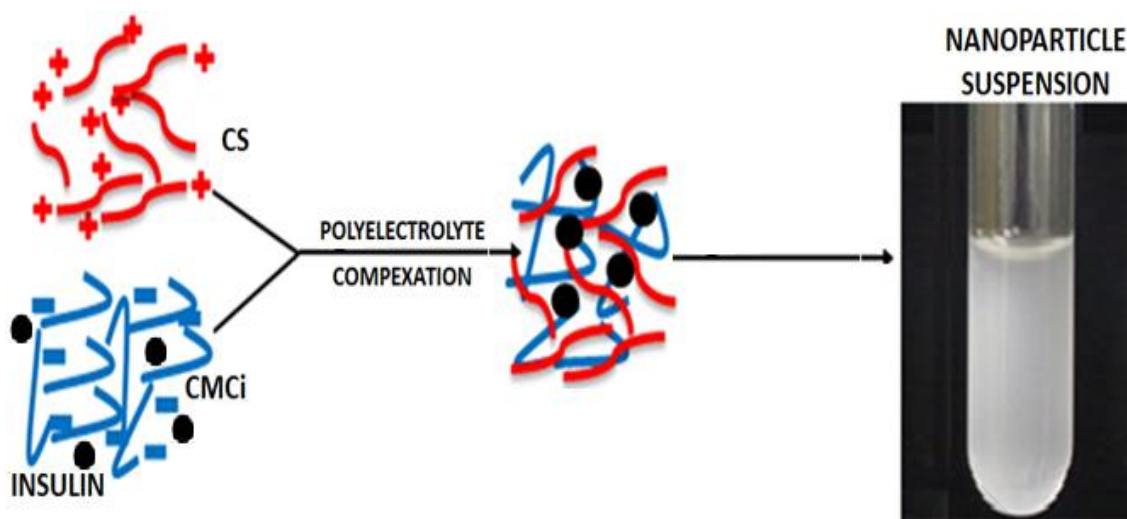


Figure 3.1: Representative diagram of chitosan (CS)-complexed insulin-loaded carboxymethylated *iota*-carrageenan (CMCi) nanoparticles formation. As depicted in the figure, insulin solution (●) was added to CMCi solution (blue). Then the polyelectrolyte complexation was performed by adding the aforementioned solution to CS (red) solution, which results in nanoparticle suspension.

3.3.1. Characterisation of CS/CMCi nanoparticles

The zeta potential, particle size and polydispersity index (PDI) of the nanoparticles were analysed based on the dynamic light scattering principle using a Nano ZSP Zetasizer (Malvern, Wochestershire, UK) at a constant temperature of 25°C. The freshly prepared samples of nanoparticular suspensions were diluted to the appropriate concentration (100 µg/mL) with ultrapure water and placed in electrophoretic cells for analysis (n = 3) (Rodrigues *et al.*, 2012).

The morphological examination of CS/CMCi nanoparticles was conducted using transmission electron microscopy (TEM) (Leo Libra120, Carl Zeiss, Oberkochen, Germany). The samples, along with 2% w/v phosphotungstic acid, were deposited on copper grids with Formvar® films for TEM observation. The surface characteristics of the nanoparticles were determined using a field emission scanning electron microscope (FESEM) (Quanta FEG 650, FEI, Hillsboro, OR, USA). The nanoparticles were positioned

on a stub and covered with a thin layer of gold for the FESEM observations under high vacuum.

The interaction between the components of the CS/CMCi nanoparticles was analysed using Fourier transform infrared (FT-IR) spectroscopy (PerkinElmer, Waltham, MA, USA). CMCi, CS, insulin and CS/CMCi nanoparticles were triturated separately with KBr and pressed into discs for analysis. The FT-IR spectra were recorded in transmittance mode with a resolution of 4 cm^{-1} in a scanning region of $4000\text{--}400\text{ cm}^{-1}$ for 32 scans per sample at room temperature.

3.3.2. Insulin entrapment efficiency and insulin loading

To estimate the entrapment efficiency and insulin loading, dry nanoparticles (15 mg) were incubated in 10 mL of SIF (pH 6.8) for 2 h shaken at 100 rpm in an orbital shaker (Grant OLS 200, Cambridge, UK). The tube was vortexed 6 times for 5 min each. SIF (pH 6.8) was used to facilitate greater deprotonation of the carboxyl groups of CMCi, leading to more extensive swelling of the polymer and higher insulin release. Then, the mixture was centrifuged at $16,000 \times g$ for 30 min at 15°C (Reis *et al.*, 2008). The insulin content in the supernatant was measured by HPLC according to a method described previously (Leong *et al.*, 2011b). Aliquots of samples (50 μL) were injected into Chomolith Performance RP-18 columns (4.6 mm \times 100 mm, Merck, Darmstadt, Germany) attached to the Waters millennium v3.02 system with a PDA detector (Waters Co., Milford, MA, USA), managed with Waters Empower software and the area under curve (AUC) was monitored at 214 nm. The mobile phase consisted of a mixture of acetonitrile and 0.2 M sodium sulfate (23.5:76.5) (pH 2.3 adjusted with orthophosphoric acid) with a flow rate of 1 mL/min. A standard solution of human insulin (0.005-1.000 mg/mL) was used to

construct a standard curve. The encapsulation efficiency (EE) and the drug loading (DL) capacity are calculated as per Eq. 3.3 and 3.4 respectively

$$EE = \frac{(\text{Total insulin added (mg)} - \text{Free insulin in supernatant (mg)})}{\text{Total insulin added (mg)}} \times 100\% \quad (\text{Eq. 3.3})$$

$$DL = \frac{(\text{Total insulin added (mg)} - \text{Free insulin in supernatant (mg)})}{\text{Polymer weight (mg)}} \times 100\% \quad (\text{Eq. 3.4})$$

The HPLC method was validated with limit of quantification (3 µg/mL) and three quality control concentrations (low 5 µg/mL, medium 100 µg/mL and high 750 µg/mL). Its precision is determined by measuring the coefficient of variance (CV) and accuracy for both interday and intraday in triplicates.

3.3.3. Insulin release from nanoparticles

The *in vitro* release study was carried out according to methods described previously (Reis *et al.*, 2008; Leong *et al.*, 2011b). The simulated gastric fluid (SGF) (pH 1.2) and simulated intestinal fluid (SIF) (pH 6.8) were prepared according to British Pharmacopeia 2010. A more highly acidic pH was used for both SGF (pH 1.2) and SIF (pH 6.8) to correlate with the fasted state *in vivo* study in section 3.11 (Klein, 2010). Briefly, nanoparticles (15 mg) were dispersed in 10 mL of SGF (pH 1.2) at 37°C up to 2 h while stirring at a rate of 100 rpm in an orbital shaker (Grant OLS 200, Cambridge, UK). Then, 500 µL aliquots were taken at scheduled time intervals (0, 0.5, 1, 1.5 and 2 h) and replaced with fresh SGF (pH 1.2) of the same temperature (37°C). After 2 h, the nanoparticles were transferred into 10 mL of SIF (pH 6.8) at 37°C stirred at 100 rpm. Aliquots of 500 µL were

taken at scheduled time intervals (0, 1, 2, 4, 6, 8 and 10 h) and replaced with fresh SIF (pH 6.8) up to 10 h. Then, the sample was analysed by HPLC and the insulin content calculated using the standard curve, as described in section 3.3.2.

3.3.4. Degree of swelling and gel fraction

Degree of swelling and gel fraction studies were performed using to a previously described method, with minor modifications (Leong *et al.*, 2011a). Briefly, 50 mg (W_I) of insulin free CS/CMC_i nanoparticles were immersed in 50 mL of SGF (pH 1.2) or SIF (pH 6.8) at room temperature and allowed to swell. After 2 h the nanoparticles were removed, excess surface solution was removed and weighed (W_S). Then, the gelled nanoparticles were lyophilised for 48 h and weighed again (W_D). The results are calculated as per Eq. 3.5 and 3.6 (Onuki *et al.*, 2008; Lin & Metters, 2006).

$$\text{Degree of swelling} = \frac{W_S}{W_D} \quad (\text{Eq. 3.5})$$

$$\text{Percent gel fraction} = \frac{W_D}{W_I} \times 100 \quad (\text{Eq. 3.6})$$

Where, W_S is the weight of the swollen nanoparticles, W_D is the weight of the dried nanoparticles and W_I is the initial weight of the nanoparticles.

3.4. Optimisation of the insulin carrier system

The response surface methodology together with multivariate spline interpolation (RSM^{MSI}) approaches were used to investigate the correlation between the independent factors and dependent variables using the dataNESIA[®] version 3.0 software package (Yamatake Corp., Tokyo, Japan).

3.5. *Ex vivo* mucoadhesion study

The *ex vivo* mucoadhesive property of CS/CMC_i nanoparticles was determined by everted sac method (Santos *et al.*, 1999; Alam *et al.*, 2012). Two fasted male Sprague–Dawley rats (6–7 weeks, 210–290 g) were used, and small intestinal tissues were cut and washed with cold phosphate buffer saline containing 200 mg/dL of glucose (PBSG, pH 7.2) (Animal Ethics approval number: 20150407/PHARM/R/CLY). Then, 5 cm sections of intestine were cut and everted over a glass rod. One end of the everted intestine was tied with a suture and the other end of the everted intestine was tied after filling it with 1.4 mL of PBSG (Figure 3.2 A and B). Then the sac was incubated in 6 mL of PBSG containing 50 mg of CS/CMC_i nanoparticles at 37°C up to 30 min stirred at 100 rpm. The sac was removed from PBSG after 30 min. Then, the PBSG with unbound nanoparticles were centrifuged at 5000 rpm for 30 min, the supernatant discarded, and the remaining nanoparticles were lyophilised. The percentage of mucoadhesion is calculated as per the following equation.

$$\text{Percent mucoadhesion} = \frac{W_I - W_F}{W_I} \times 100 \quad (\text{Eq. 3.7})$$

Where, W_I and W_F are the weight of nanoparticles before and after incubation respectively.

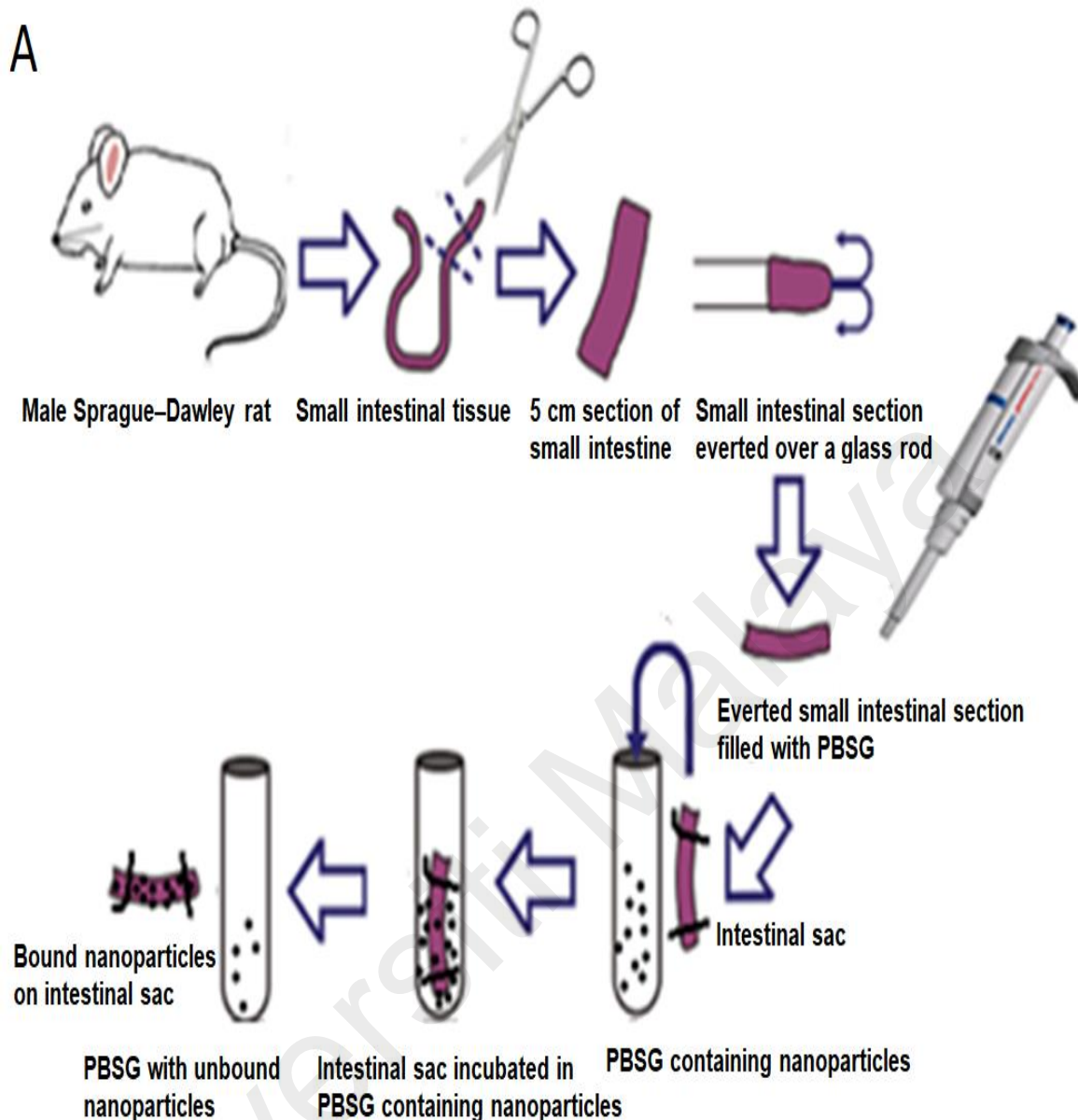


Figure 3.2: (A) The everted intestinal sac method (This figure is modified from Santos *et al.*, 1999). As depicted in the figure, 5 cm of small intestinal tissue was harvested from a male Sprague–Dawley rat, everted, tied at the ends and filled with phosphate buffer saline with 200 mg/dL of glucose (PBSG). The sac was then incubated for 30 min into a tube containing a 50 mg of nanoparticles and PBSG. The sac was then removed, the unbound nanoparticles were centrifuged, lyophilised and percentage of mucoadhesion was calculated. (B) Everted small intestinal sac filled with 1.4 mL of PBSG.



3.6. Storage stability of insulin

The storage stability of insulin-entrapped CS/CMC_i nanoparticles was determined using an earlier method (Vimalavathini & Gitanjali, 2009). Freeze dried nanoparticles were placed in amber glass vials and stored at 25°C (room temperature), 4 and -20°C in the dark for 90 days. Samples were collected periodically throughout a 90-day period (day 1, 5, 7, 14, 30, 45, 60, 75 and 90), and the drug release against storage time was determined by HPLC analysis, as described in section 3.3.2. For control, pure insulin solution (1mg/mL) was stored at room temperature for 7 days and the insulin concentration (mg/mL) was quantified using HPLC.

3.7. *In vitro* stability of insulin against enzymatic degradation

The *in vitro* stability of insulin against enzymatic degradation is used to evaluate the protective action of CS/CMC_i nanoparticles from GIT enzymes. Briefly, nanoparticles (15 mg) were mixed in 10 mL of SGF containing pepsin (pH 1.2) at 37°C up to 2 h stirred at 100 rpm. Then, 500 µL aliquots were taken at scheduled time intervals (0.0, 0.5, 1.0, 1.5 and 2 h) and the enzymatic degradation was stopped by adding 500 µL of 0.1M NaOH. After 2 h, the nanoparticles were mixed in 10 mL of SIF containing trypsin (pH 6.8) at 37°C stirred at 100 rpm up to 10 h. Aliquots of 500 µL were taken at scheduled time intervals (0, 1, 2, 4, 6, 8 and 10 h) and 500 µL of 0.1M HCl was added to stop the enzymatic degradation (Niu *et al.*, 2011; Lopes *et al.*, 2016). Then, the samples were analyzed by HPLC and the insulin content is calculated using the standard curve, as described in section 3.3.2.

3.8. *In vitro* bioactivity of insulin released from CS/CMC_i nanoparticles

Nanoparticulate formulation can be a good medium to ensure insulin's bioactivity is intact following entrapment. To evaluate the bioactivity of entrapped insulin in CS/CMC_i nanoparticles, the final time interval (12 h) sample of *in vitro* insulin release study without enzymes (section 3.3.3) is chosen and the insulin content is determined using ELISA (Merckodia AB, Uppsala, Sweden) kit. This is a solid phase two-site enzyme immunoassay based on the sandwich method, in which two monoclonal antibodies are subjected to distinct antigenic determinants on the insulin molecule, following the manufacturer's protocol. Briefly, 25 µL of samples were added to a 96 well ELISA microplate followed by addition of peroxidase-labelled anti-insulin antibodies. Then the microplates were incubated for 1 h at room temperature on a plate shaker (700 rpm). Then the reaction solutions were discarded and washed with washing buffer 5 times to remove unbound

antibodies. 200 μL of 3,3',5,5'-tetramethylbenzidine (TMB) was added to each well and incubated for 15 min at room temperature. Then, 50 μL of stop solution was added to stop the reaction. Finally, the absorbance of the ELISA plate was measured at 450 nm using a microplate reader and calculated from an insulin standard concentration curve obtained from the same kit.

3.9. Cell culture and cytotoxicity study

Caco-2 (Human colorectal carcinoma cell) (passage no.: 50–60) was used to evaluate the cytotoxicity of the CS/CMCi nanoparticles. Caco-2 cells were cultured in DMEM (Dulbecco's modified Eagle medium) supplemented with 10% foetal bovine serum (FBS), 1% non-essential amino acids, 50 $\mu\text{g}/\text{mL}$ gentamycine, 2.5 $\mu\text{g}/\text{mL}$ amphotericine B and 1 mM L-glutamine in 5% CO_2 at 37°C with controlled humidity.

The cytotoxicity of the nanoparticles was evaluated by determining both viability (MTS assay) and cell death (LDH assay) according to an earlier method (Leong *et al.*, 2011b). Briefly, the cells were seeded at a density of 5×10^4 (MTS assay) or 2.5×10^4 (LDH assay) cells per well in a 96 well plate in 5% CO_2 at 37°C with controlled humidity for 24 h. After 24 h, the media was discarded and replaced with media containing nanoparticles, with concentration ranging from 0.5–20.0 mg/mL (0.5, 1.25, 2.5, 5, 10, 20 mg/mL) and incubated for 1–3 days. 5-flourouracil (0.005–500 $\mu\text{g}/\text{mL}$) and Triton-X (1% v/v) were used as positive controls. Cytotoxicity was determined by MTS and LDH assay as per manufacturer's protocol and the cell viability and cell death were calculated as per Eq. 3.8 and 3.9 respectively.

$$\text{Percent cell viability} = \frac{A_T}{A_C} \times 100\% \quad (\text{Eq. 3.8})$$

Where, A_T is the absorbance after treatment with test nanoparticles and A_C is the absorbance for negative control.

$$\text{Percent cell death} = \frac{A_T - A_S}{A_{T-X} - A_S} \times 100\% \quad (\text{Eq. 3.9})$$

Where, A_T is the absorbance after treatment with test nanoparticles and A_S is the absorbance without treatment and A_{T-X} is the absorbance after treated with Triton-X.

3.10. *In vitro* insulin membrane transport study

3.10.1. Parallel artificial membrane permeability assay (PAMPA)

The passive transport study of insulin entrapped CS/CMC_i nanoparticles is evaluated using a parallel artificial membrane assay (PAMPA) assay with modification (Righeschi *et al.*, 2016). The transport was collated with lucifer yellow, a membrane integrity marker. Firstly, 5 μL of 1% (w/v) lecithin in *n*-dodecane solution was pipetted into the donor plate of multiscreen filter plates (MultiScreen-IP, PVDF membrane, 0.45 μm pore, Darmstadt, Germany). Then, 300 μg of CS/CMC_i nanoparticles and control (pure insulin 100 $\mu\text{g}/\text{mL}$) were added to the donor compartment and 200 μL of PBS were added to the acceptor compartment. Then, the acceptor compartment was placed over the donor compartment to form a sandwich and incubated at room temperature. At scheduled time intervals (0.0, 0.5, 1.0, 2.0, 3.0, 4.0, 6.0, 8.0, 10.0 and 12.0 h) 100 μL of samples were pipetted from both the acceptor and donor compartments and analyzed by HPLC for its insulin content as described in section 3.3.2. Lucifer yellow is analyzed by fluorescence (Tecan Infinite M200

PRO, Männedorf, Switzerland) at an excitation/emission wavelength of 485/535 nm. The effective permeability (Pe) (cm/s) is calculated as per the following equation.

$$Pe \text{ (cm/s)} = \frac{-\ln[1-C_A(t)/C_e]}{A \times \left(\frac{1}{V_D} + \frac{1}{V_A}\right)} \quad (\text{Eq. 3.10})$$

$$\text{Where } C_e = \frac{C_D(t) \times V_D + C_A(t) \times V_A}{V_D + V_A}$$

Where, $C_A(t)$ is the sample concentration in the acceptor compartment at time t , $C_D(t)$ is the sample concentration in the donor compartment at time t , V_D is the donor compartment volume (ml), V_A is the acceptor compartment volume (ml), A is the membrane surface area (cm^2), t is the incubation time (s) and C_e is the equilibrium concentration.

3.10.2. Transepithelial electrical resistance (TEER) measurement and transport of insulin by Caco-2 cells

The active transport of insulin in CS/CMCi nanoparticles are evaluated using Caco-2 cells (passage no.:50–60). The experiment using a previously described method with modifications (Niu *et al.*, 2014). The cells were seeded on a polycarbonate filter membrane (0.4 μm pores, 0.7 cm^2 active membrane area) microplate (Millicell[®]-24, Darmstadt, Germany) at a density of 6×10^4 cells per well in DMEM media as discussed in section 3.9. The confluence of Caco-2 cell monolayer was observed by transepithelial electrical resistance (TEER) (value $\geq 600 \Omega \text{ cm}^2$) measurement and lucifer yellow rejection (%) test over a 21-day culture period. The TEER was measured with a Millicell[®] ERS-2 epithelial volt-ohm meter (Darmstadt, Germany) as per Figure 3.3 (A). Figure 3.3 (B) is a schematic diagram that depicts the TEER measurement. The TEER value is calculated as per the following equation.

$$\text{TEER } (\Omega \text{ cm}^2) = (T_{w/c} - T_{w/o/c}) \times A \quad (\text{Eq. 3.11})$$

Where, $T_{w/c}$ is the TEER value with cells, $T_{w/o/c}$ is the TEER value without cells and A is the active membrane area (cm^2).

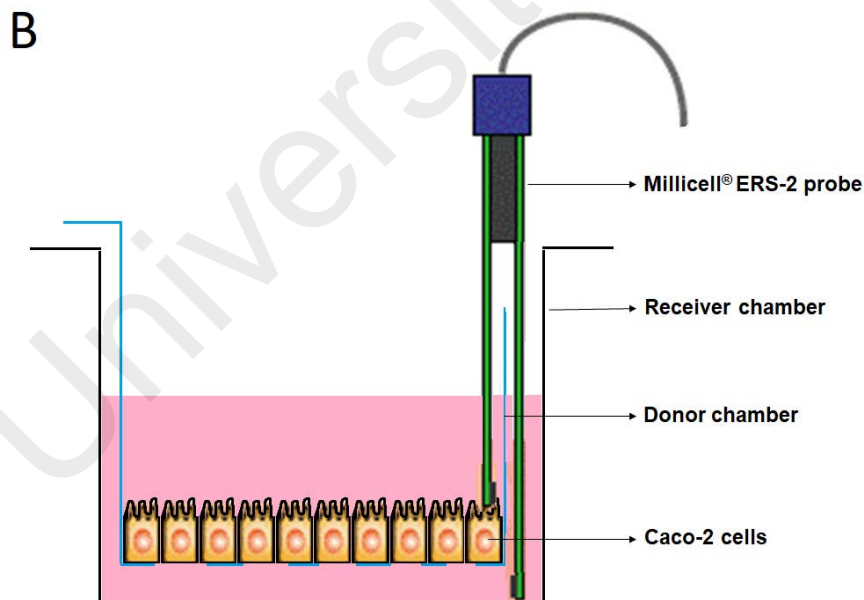
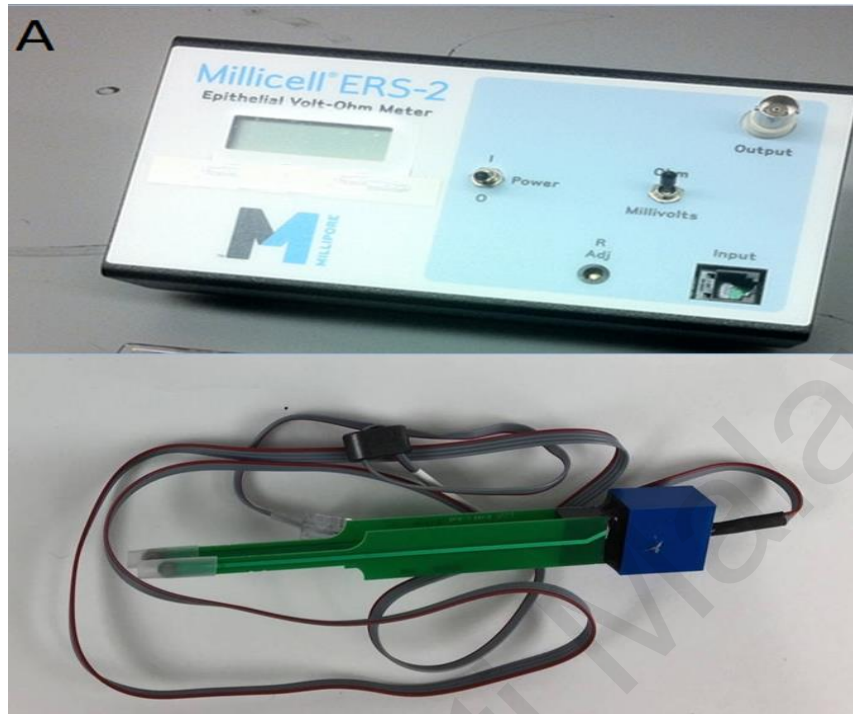


Figure 3.3: (A) Millicell[®] ERS-2 epithelial volt-ohm meter with probe (B) Schematic diagram of TEER measurement using Caco-2 cells. As depicted in the diagram, the electrode was immersed in the Millicell[®]-24 culture plate so that the shorter tip was in the donor chamber containing Caco-2 cells and the longer tip was in the receiver chamber. For stable and reproducible results, the electrode was held steady and at a 90° angle to the plate insert.

After 21 days, the lucifer yellow rejection test was performed. Briefly, the cells were washed twice with PBS (pH 7.4) and 100 μL of lucifer yellow solution (2 $\mu\text{g}/\text{mL}$) was added to the donor chamber and the receiver chamber was filled with 600 μL of transport medium (HBSS supplemented with 10 mM D-glucose and 10 mM HEPES, pH 7.4). At scheduled time intervals (0.0, 0.5, 1.0, 2.0, 3.0, 4.0, 6.0, 8.0, 10.0 and 12.0 h), 200 μL of samples were pipetted from the basolateral chamber and analyzed by fluorescence (Tecan Infinite M200 PRO, Männedorf, Switzerland) at an excitation/emission wavelength of 485/535 nm. The lucifer yellow rejection (%) is calculated as per the following equation.

$$\text{Lucifer yellow rejection (\%)} = [1 - (\text{LY}_{\text{C bl}} / \text{LY}_{\text{C 0}})] \times 100 \quad (\text{Eq. 3.12})$$

Where, $\text{LY}_{\text{C bl}}$ is the concentration of lucifer yellow in receiver chamber and $\text{LY}_{\text{C 0}}$ is the initial concentration of lucifer yellow.

For the transport study, insulin solution was used as control. First, the confluent Caco-2 cell monolayers grown in Millicell[®]-24 plates were washed thrice with PBS (pH 7.4) and equilibrated with transport medium (HBSS supplemented with 10 mM D-glucose and 10 mM HEPES, pH 7.4) for 15 min. Then, the transport medium in the donor chamber was replaced with 1.0 mg of insulin entrapped CS/CMC_i nanoparticles or control (insulin solution in transport medium at a concentration of 0.2 mg/mL). At scheduled time intervals (0.0, 0.5, 1.0, 2.0, 3.0, 4.0, 6.0, 8.0, 10.0 and 12.0 h) 100 μL of samples were pipetted from the receiver chamber and analyzed using ELISA and the insulin content was calculated, as described in section 3.8. The change in TEER values was measured with a Millicell[®] ERS-2 epithelial volt-ohm meter (Darmstadt, Germany) at the same scheduled time intervals. The apparent permeability (P_{app}) coefficient values (cm/s) are calculated as per the following equation.

$$P_{app} \text{ (cm/s)} = \left(\frac{dQ}{dt}\right) \times \left(\frac{1}{AC_0}\right) \quad (\text{Eq. 3.13})$$

Where, dQ/dt is the steady-state flux (ng/min), A is the membrane surface area (cm^2), and C_0 is the initial insulin concentration in the donor chamber (ng/mL).

3.11. *In vivo* hypoglycemic and bioavailability study

Male Sprague–Dawley rats (6–7 weeks, 210–290 g), from Animal Experimental Unit, UM, housed at $20 \pm 2^\circ\text{C}$ and 30–70% relative humidity with a 12-h light–dark cycle were used in this study. The experimental protocol was approved by the institutional animal care and use committee (FOM IACUC), UM with ethics reference number: 20150407/PHARM/R/CLY.

The study was performed using an earlier method with minor modifications (Leong *et al.*, 2011b). The experiments used 56 rats, divided into seven groups. The rats were induced with type 1 diabetes by intraperitoneal injections of streptozocin at a dose of 65 mg/kg body weight in 0.1 M sodium citrate buffer (pH 4.5). After one week, rats with fasted blood glucose ≥ 16 mmol/L were included for *in vivo* evaluation. The diabetic rats were fasted 6 h prior and throughout the experiments with water *ad libitum*. Group 1, 2 and 3 animals received CS/CMCi nanoparticles entrapped insulin (packed in size 9, Qualicaps[®] capsule, Shionogi Qualicaps Co., Ltd., Nara, Japan, hard gelatin capsules) orally, at a dose of 25, 50 and 100 IU/kg by gavage needle. Group 4 animals received 2 IU/kg insulin solution as positive control (subcutaneous injection). Group 5 animals received 100 IU/kg insulin solution orally as insulin control. Group 6 animals received empty CS/CMCi nanoparticles packed in capsules orally as negative control. Group 7 animals received empty capsules without nanoparticles orally as capsule control. Blood samples (40 μL) were collected from tail veins at scheduled time intervals (0, 1, 3, 5, 7, 9, 12, 24 and 36 h) and the hypoglycemic effect was determined as % difference relative to the initial value by Accu-Check active

blood glucose meter (Roche, Mannheim, Germany). Serum was separated by centrifugation of blood sample at 5000 rpm at 4°C for 10 min and the serum insulin was quantified using ELISA as described in section 3.7. Pharmacokinetic data (C_{max} , T_{max} , AUC, and BA (%)) were estimated from the serum insulin versus time graph. The relative bioavailability (BA %) is calculated as per the following equation:

$$BA (\%) = \left[\frac{AUC_{oral} \times DOSE_{sc}}{AUC_{sc} \times DOSE_{oral}} \right] \times 100 \quad (\text{Eq. 3.14})$$

Where, AUC is the total area under the curve of serum insulin concentration, DOSE is the different doses of oral administration of insulin entrapped CS/CMC_i nanoparticles and subcutaneous administration of insulin solution, oral represents oral administration and sc represents subcutaneous administration. The results were expressed as mean \pm SD (n = 6) and statistical significant difference was evaluated by a one-way ANOVA at $p < 0.05$.

CHAPTER 4: RESULTS AND DISCUSSION

4.1. Preparation and characterzation of carboxymethylated *iota*-carrageenan (CMCi)

To formulate insulin-entrapped CS/CMCi nanoparticles suitable for oral delivery, the nanoparticles must protect the entrapped insulin from degradation by stomach acid (pH 1–3) and enzymes (Sgorla *et al.*, 2018). The contents are released in a more neutral intestinal region (pH 7) for absorption into the systemic circulation to exert its biological effect. This pH-responsive behavior can be imparted on *iota*-carrageenan through carboxymethylation. Briefly the mechanism of carboxymethylation involves a strong base, NaOH that deprotonates the R-OH groups in *iota*-carrageenan, producing alkoxides (R-O⁻) which, upon reaction with ClCH₂COOH, form carboxymethyl groups (CH₂COOH) (Leong *et al.*, 2011a). The overall reaction is shown in Figure 4.1. Thus, pH responsiveness depends on various independent factors.

The study adopted the Box-Behnken design (BBD) to produce 33 experimental runs of carboxymethylated *iota*-carrageenan, listed as I01 to I33 as per Table 3.1 to obtain the dependent variables for RSM^{MSI} optimization. These experimental runs were randomly generated to avoid systematic bias using the four independent factors described earlier. This approach is expected to reduce trial and error and improve the success rate of optimising the formulation.

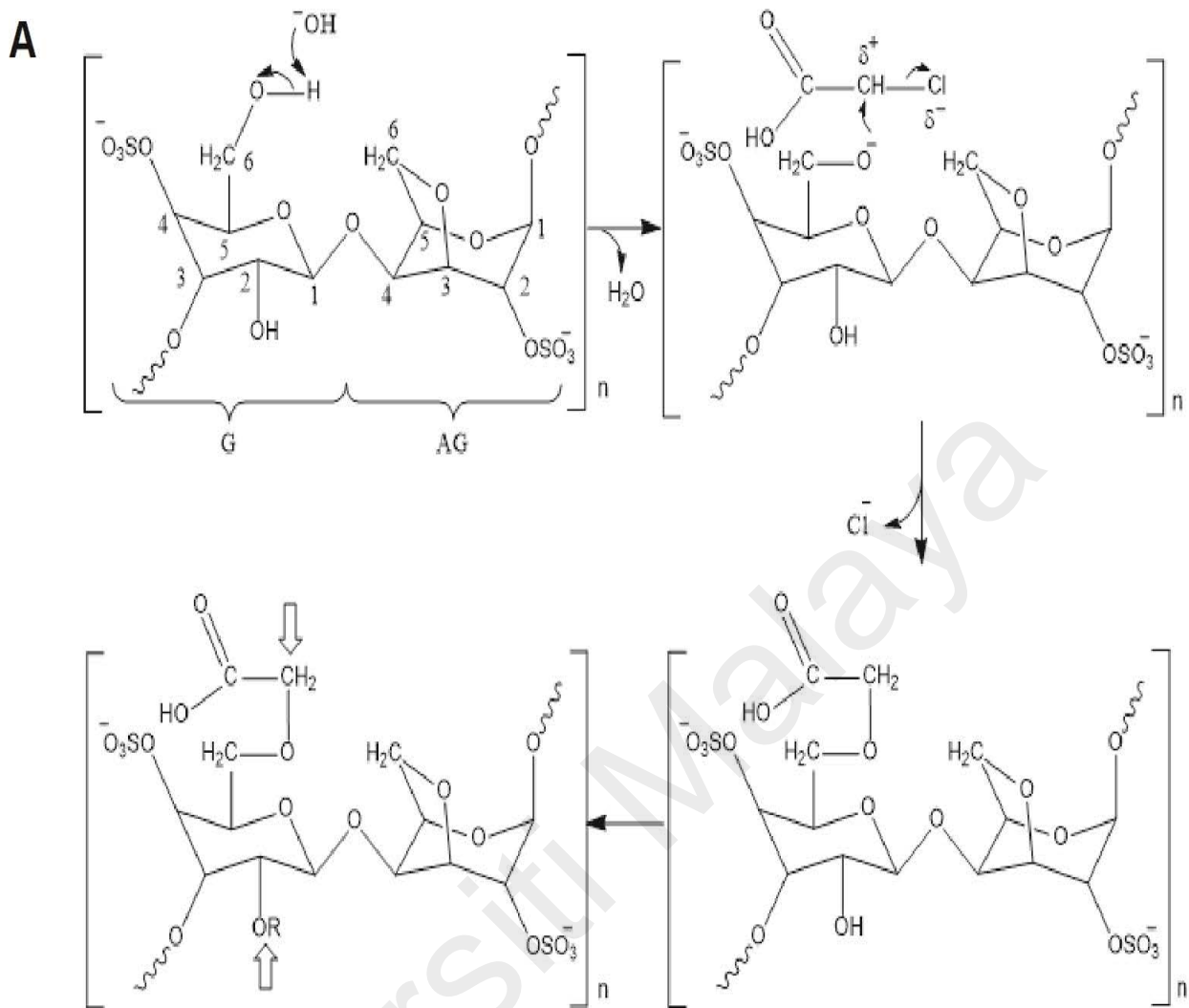


Figure 4.1: Reaction scheme for the carboxymethylation process on *iota*-carrageenan. AG is 3,6-anhydro- α -D-galactopyranose-2-sulfate; G is β -D-galactopyranose-4-sulfate. R = CH_2COOH or H; n = number of repeating units; arrow = possible positions for carboxymethylation.

Prior to DS determination, assignment of signals in both the ^1H and ^{13}C NMR spectra (Figure 4.2) of the *iota*-carrageenan samples were performed by referring to previous published spectra and confirmed by $^1\text{H}/^{13}\text{C}$ HSQC (Figure 4.3) (Campo *et al.*, 2009; van de Velde & Rollema, 2006).

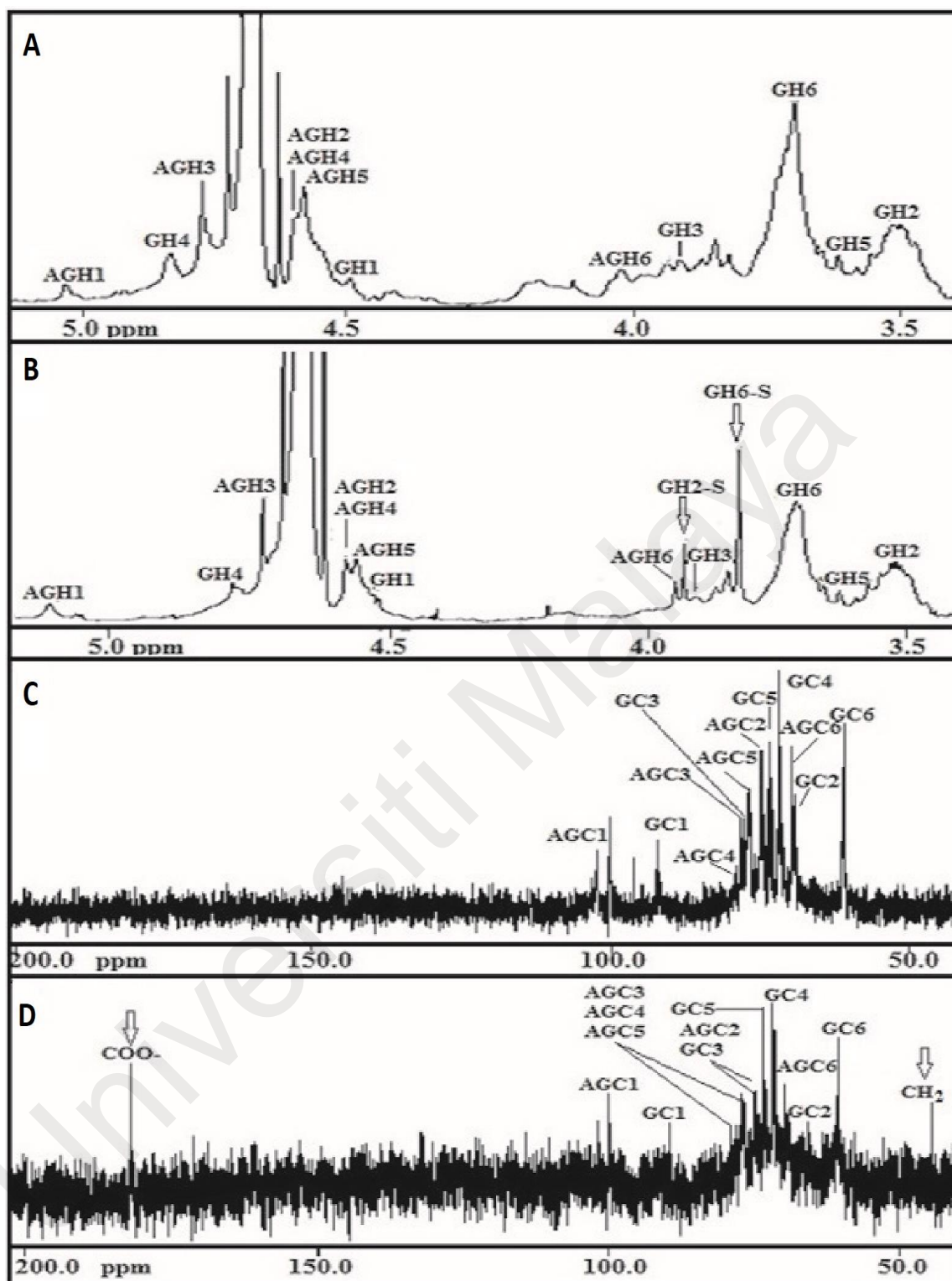


Figure 4.2: (A) ^1H NMR spectrum of native Ci. (B) ^1H NMR spectrum of CMCi (sample I01). (C) ^{13}C NMR spectrum of native Ci. (D) ^{13}C NMR spectrum of CMCi (sample I01). AG is 3,6-anhydro- α -D-galactopyranose-2-sulfate; G is β -D-galactopyranose-4-sulfate; labels H1–6 indicate the proton numbering scheme; labels C1–6 indicate the carbon numbering scheme (refer to Figure 4.1 for the numbering scheme); GH2-S and GH6-S denote the substituted (carboxymethylated) peaks for GH2 and GH6, respectively (arrows); COO^- represents the signal for the $-\text{CH}_2\text{COO}^-$ group (arrow); and CH_2 represents the CH_2 group of the $-\text{CH}_2\text{COO}^-$ unit (arrow).

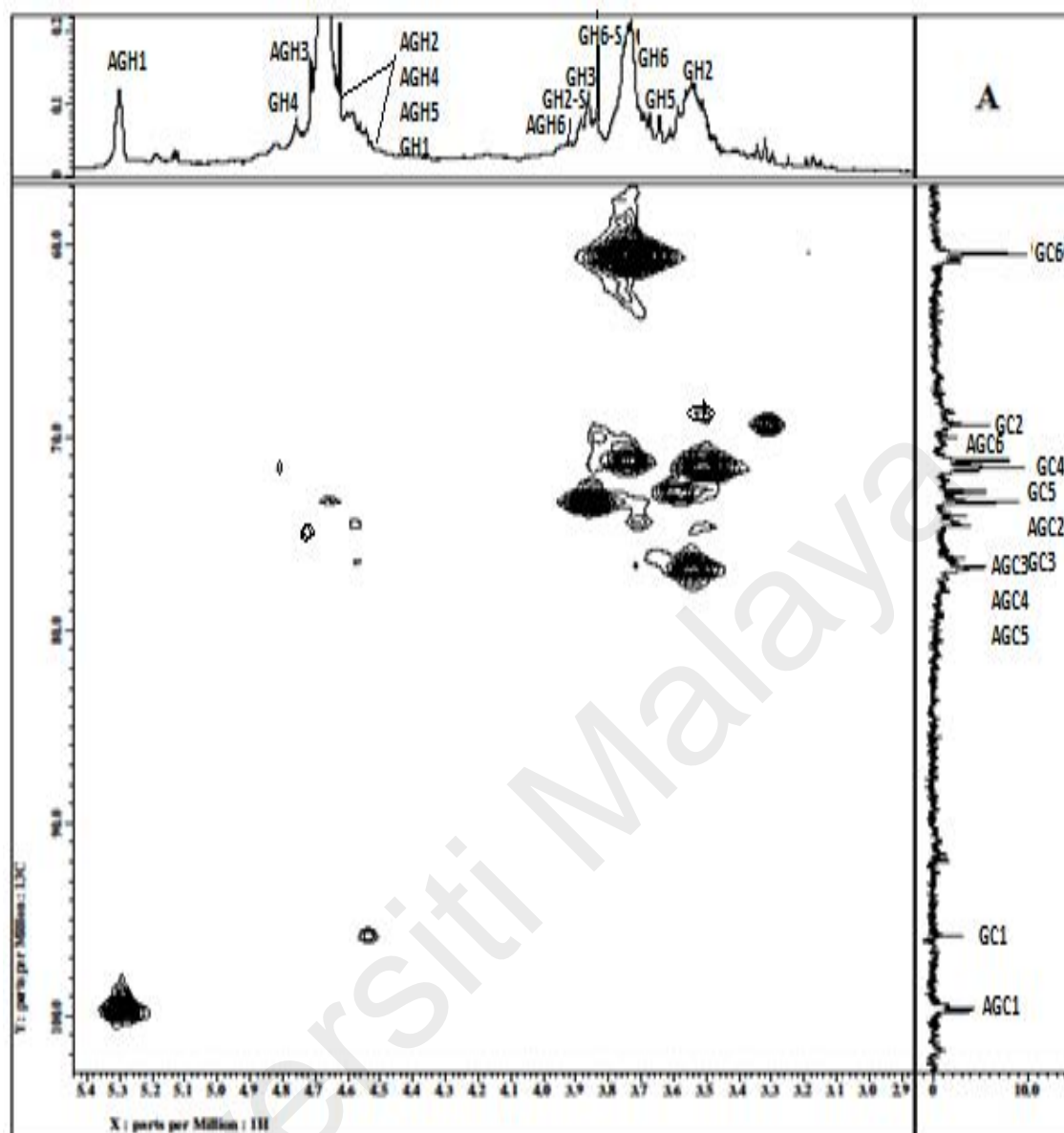


Figure 4.3: Two dimensions NMR. Heteronuclear single quantum coherence (HSQC) spectrum of sample I01. AG is 3,6-anhydro- α -D-galactopyranose-2-sulfate; G is β -D-galactopyranose-4-sulfate; labels H1–6 indicate the proton numbering scheme; labels C1–6 indicate the carbon numbering scheme (refer to Figure 4.1 for the numbering scheme); GH2-S and GH6-S denote the substituted (carboxymethylated) peaks for GH2 and GH6, respectively.

The ^1H NMR spectra of the native Ci and CMCi (sample I01, DS = 0.1782) are presented in Figure 4.2(A) and Figure 4.2(B), respectively. The additional signals at $\delta = 3.82$ and 3.93 correspond to the methylene hydrogens bonded to C-6 and C-2 of the β -D-galactopyranose-4-sulfate unit (G unit), respectively, and indicate carboxymethylation. The DS was calculated from the assigned ^1H NMR spectra as per Eq. 3.2 (Table 4.1) (Leong

et al., 2011a). Previous reports established that ^1H NMR spectra provided reliable data with comparable precision to that of HPLC, acid-base titration or mass spectrometer (MS)-based methods (Elomaa *et al.*, 2004; Petzold *et al.*, 2006; Wende *et al.*, 2016).

Further corroboration of carboxymethylation was provided by comparing the ^{13}C NMR spectra obtained for native Ci (Figure 4.2(C)) and carboxymethyl *iota*-carrageenan (sample I01) (Figure 4.2(D)). The ^{13}C NMR spectrum of carboxymethyl *iota*-carrageenan exhibited an additional signal at $\delta = 181.91$ ppm characteristic of the carbonyl of the carboxylate group (COO^-) (Leong *et al.*, 2011a; Fan *et al.*, 2011). In addition, the occurrence of a signal at 44.43 ppm provided evidence for the methylene group in the carboxymethyl unit. The appearance of a single peak was probably due to the weak intensity of the signals in the ^{13}C NMR.

Table 4.1: The partial degree of substitution (DS) of samples (I01–I33) derived from $^1\text{HNMR}$.

Sample code	G-2	G-6	Total DS
I01	0.0606	0.1176	0.1782
I02	0.0041	0.0154	0.0195
I03	0.0000	0.0089	0.0089
I04	0.0370	0.0144	0.0514
I05	0.0909	0.1296	0.2205
I06	0.0378	0.0117	0.0495
I07	0.0000	0.0134	0.0134
I08	0.1111	0.0093	0.1204
I09	0.0155	0.0392	0.0547
I10	0.0000	0.0144	0.0144
I11	0.0874	0.0121	0.0995
I12	0.0474	0.0186	0.0660

Table 4.1, continued

Sample code	G-2	G-6	Total DS
I13	0.0248	0.0602	0.0850
I14	0.0412	0.0821	0.1233
I15	0.0756	0.0095	0.0851
I16	0.0314	0.0322	0.0636
I17	0.0191	0.0300	0.0491
I18	0.0266	0.0312	0.0578
I19	0.0107	0.0157	0.0264
I20	0.1667	0.0087	0.1754
I21	0.0057	0.0112	0.0169
I22	0.0000	0.0166	0.0166
I23	0.0027	0.0121	0.0148
I24	0.0000	0.0142	0.0142
I25	0.0286	0.0153	0.0439
I26	0.0272	0.0170	0.0442
I27	0.0294	0.0134	0.0428
I28	0.0198	0.0406	0.0604
I29	0.0252	0.0195	0.0447
I30	0.0328	0.0131	0.0459
I31	0.0169	0.0293	0.0462
I32	0.0106	0.0371	0.0477
I33	0.0000	0.0090	0.0090

DS is the degree of carboxymethylation of the hydroxyl groups at C-2 and C-6 of the β -D-galactopyranose-4-sulfate unit (G-units in the *iota*-carrageenan samples as determined by ¹H NMR according to Eq. (3.2).

Table 4.2: The molecular weight of samples (I01–I33)

Sample code	M_w (kDa)	M_n (kDa)	MW _{PDI}
I01	545	512	1.046
I02	489	468	1.045
I03	366	345	1.061
I04	487	458	1.063
I05	527	500	1.054
I06	304	289	1.052
I07	269	249	1.080
I08	395	369	1.070
I09	360	348	1.034
I10	212	203	1.044
I11	343	331	1.036
I12	380	369	1.030
I13	209	200	1.045
I14	392	383	1.023
I15	468	459	1.020
I16	514	501	1.026
I17	298	279	1.068
I18	328	319	1.028
I19	391	379	1.032
I20	520	511	1.018
I21	285	278	1.025
I22	469	453	1.035
I23	499	487	1.025
I24	467	453	1.031
I25	228	218	1.046
I26	258	247	1.049
I27	364	354	1.028
I28	270	258	1.046
I29	388	379	1.024
I30	300	289	1.038
I31	206	200	1.030

Table 4.2, continued

Sample code	M_w (kDa)	M_n (kDa)	MW _{PDI}
I32	284	272	1.044
I33	242	230	1.052

M_w is the weight-average molecular weight, M_n is the number-average molecular weight and MW_{PDI} is molecular weight distribution in term of polydispersity. $MW_{PDI} = M_w / M_n$

The weight average molecular weight, number average molecular weight and molecular weight distribution in term of polydispersity of 33 modified CMCi (I01–I33) are shown in Table 4.2. GPC triple analysis profiles for the molecular weight estimation of sample I01 are shown in Figure 4.4. Most of the observed CMCi had slightly lower molecular weight compared to the native *iota*-carrageenan (522 ± 15 kDa). This may be due to the depolymerization of the native *iota*-carrageenan during carboxymethylation. Investigation of polymer molecular weight and swelling of polymer have been of interests for many years. Erdogan *et al.*, (2002) conducted swelling studies on different molecular weight anthracene labeled poly(methyl methacrylate) polymer. It was found that, high molecular weight polymers untangled easily, which led to higher degree of swelling. Higher degree of swelling helps to dissolve the polymer used in designing a carrier (Miller-Chou & Koenig, 2003). Hence, the dissolution rate is influenced by the molecular weight of the polymer and its chain disentanglement property (Parsonage. *et al.*, 1987).

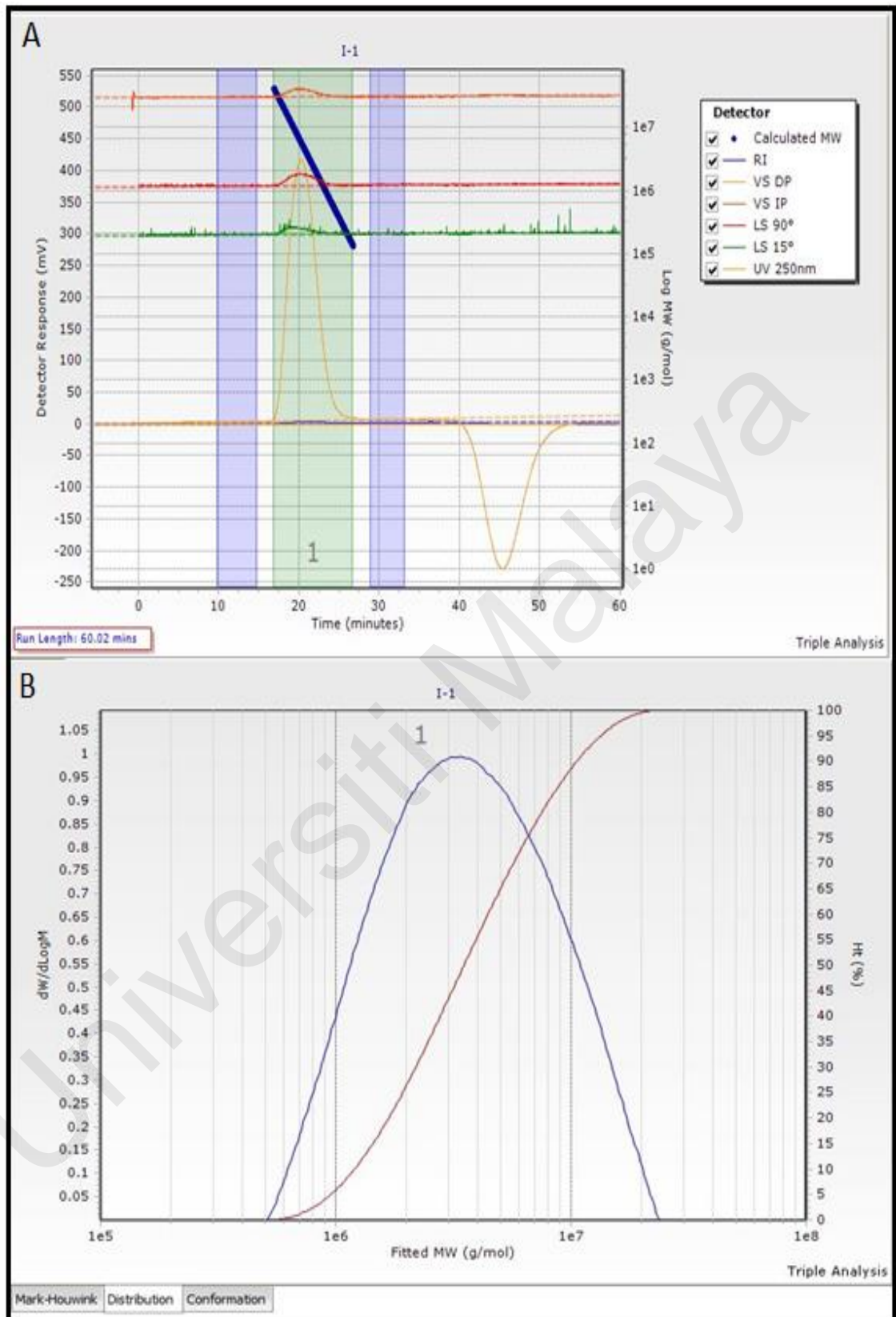


Figure 4.4: GPC profile of carboxymethylated *iota*-carrageenan (CMCi) (sample I01) for molecular weight determination (A) Triple analysis plot (refractive index/viscometer/light scattering) of CMCi (sample I01) (B) Distribution curve of CMCi (sample I01).

4.2. Pre-formulation of insulin-entrapped CS/CMCi nanoparticles

To optimise the ratio of CMCi to CS, the study selected CMCi (I01) with the second highest degree of carboxymethylation (total DS of 0.1782, as it showed better insulin release in the preliminary study compared to I05 with a total DS of 0.2205) to estimate the amount of CS required to complex with CMCi to form nanoparticles. The difference in insulin release between the samples with the highest and second highest DS may be due to the substitution of carboxymethylated groups at the GC-2 and GC-6 positions in the repeating *iota*-carrageenan structures as per Figure 4.1. Substitution at GC-6 in sample I01 was almost double the GC-2 position, whereas it was less pronounced in sample I05. Therefore, it can be inferred that carboxymethylation at position GC-6 is better at controlling insulin release. Variations in the positions of substitution may influence the formation of hydrogen bonds between the –COOH groups, which subsequently affects the release of insulin from the nanoparticles.

The nanoparticles were formulated by a mild polyelectrolyte complexation method, which avoided deleterious organic solvents or harsh mechanical force (Grenha *et al.*, 2010). The formulations were observed under a microscope and classified into solutions, precipitations and nanoparticles as per Figure 4.5(A). The positive to negative (+/–) charge ratios for the various formulations were calculated based on a previous study (Rodrigues *et al.*, 2012). Briefly, CS has one positive charge per deacetylated monomer, and its degree of deacetylation is $\geq 75\%$. Thus, it has a mean value of 0.8 with an average monomeric molecular weight of 169 g/mol (Ma *et al.*, 2008; Rodrigues *et al.*, 2012). CMCi has a molecular weight of 568 g/mol with two negative charges per disaccharide monomer. The +/- charge ratio was calculated by converting the mass of each polymers in every formulation into moles of charge.

The formulation with a +/- charge ratio below 1 (mass ratio 0.5:1, CS 0.1% w/v and CMCi 0.1% w/v) resulted in a solution as per Figure 4.5(B). The observed solution is attributed to the excess of CMCi SO_4^{2-} groups, which neutralized the positive charges of NH_2 groups in CS (Rodrigues *et al.*, 2012). Conversely, the formulations with +/- charge ratios of approximately 5 or more (e.g., a mass ratio 5:1, CS 0.2% w/v and CMCi 0.3% w/v, +/- charge ratio of 14.4) formed precipitates. The observed precipitation can be attributed to insufficient CMCi negative charges (SO_4^{2-}) to balance the amino groups (positive charges) from CS, which led to precipitation (Fernández-Urrusuno *et al.*, 1999). Although the formulations with higher concentrations of CS (0.2% w/v) and CMCi (0.2 and 0.3% w/v) formed nanoparticles, the mean particle size was larger than those formulated with concentrations of 0.1% w/v CS and 0.1% w/v CMCi (excluding the mass ratios of 3:1, 4:1 and 5:1) as per Figure 4.5(C). Hence, formulations with concentrations of 0.1% w/v CS and 0.1% w/v CMCi (mass ratios of 1:1, 1.5:1, 2:1, and 2.5:1) were used to prepare insulin-loaded nanoparticles for further optimisation.

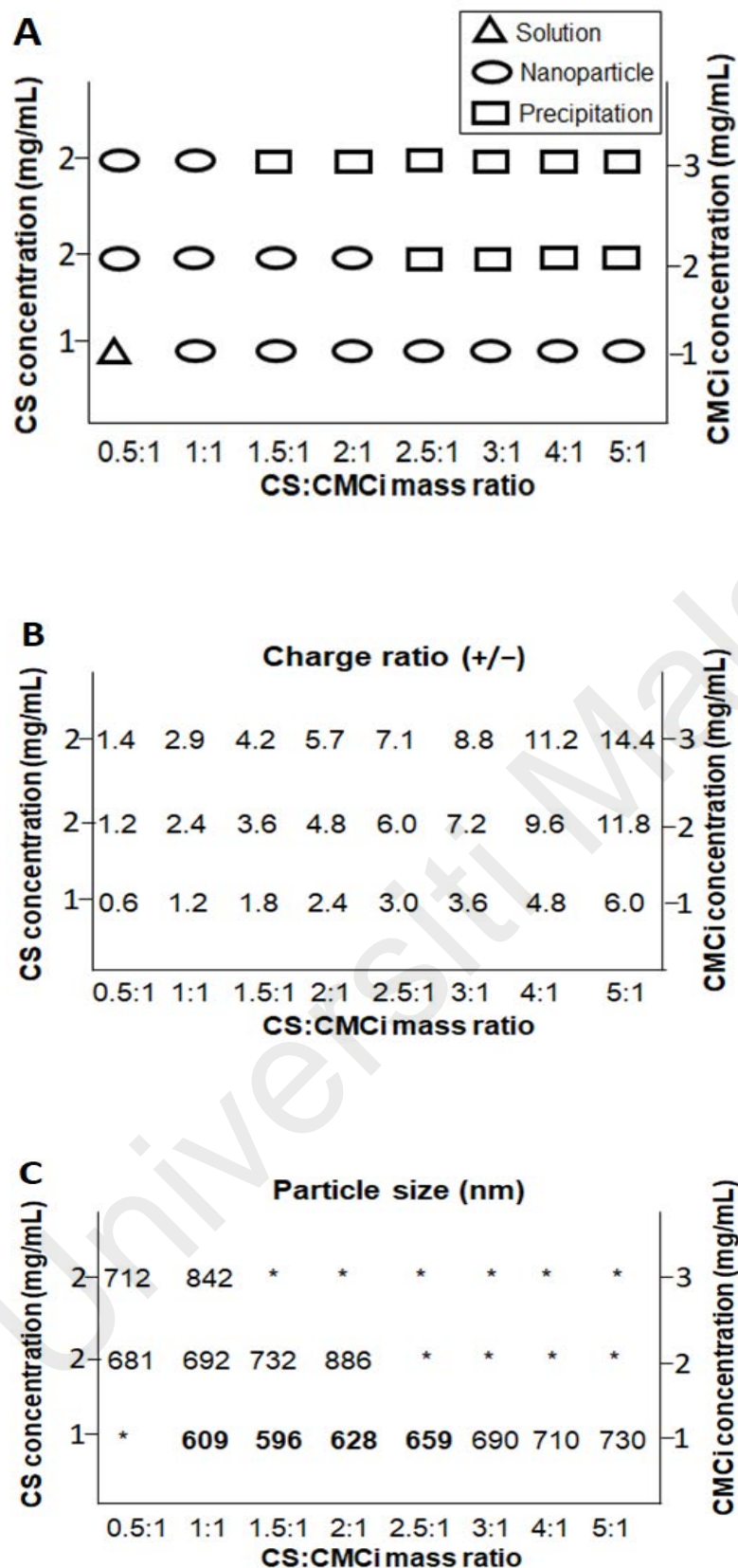


Figure 4.5: (A) Identification of nanoparticle formation under a microscope. (B) Effect of the chitosan (CS)/carboxymethylated *iota*-carrageenan (CMCi) mass ratio on the +/- charge ratio of each formulation. (C) Effect of the CS/CMCi mass ratio on the nanoparticle size. * represents particle size of formulations showing solution and precipitation.

Further optimisation of the formulation was performed by evaluating the insulin entrapment efficiency, zeta potential and particle size. The formulation ratio of 1.5:1 showed better entrapment efficiency than other formulation ratios as per Figure 4.6(A). The zeta potential was greater than +50 mV, indicating better nanoparticles stability as per Figure 4.6(B) (Heurtault *et al.*, 2003). The positive zeta potential was due to higher concentration of chitosan in the nanoparticles. The formulation ratio of 1.5:1 showed size of 597 ± 15 nm with a poly dispersity index of 0.3 ± 0.01 as per Figure 4.6(C). Similar results have been observed in other chitosan/carrageenan nanoparticle formulations, which furnished stable nanoparticles with better drug entrapment (Grenha *et al.*, 2010; Cody *et al.*, 2012). Furthermore, release kinetics parameters of various kinetic models, such as zero-order, first-order and Higuchi models, were analysed (Table 4.3), and the optimal weight ratio of CS to CMCi was found to be 1.5:1 based on the R^2 value. The insulin loading of the nanoparticles was evaluated by using different amounts of insulin (0.5–2 mg). The entrapment efficiency and insulin-loading capacity dropped when 1.5 mg of insulin was used, indicating the amount of insulin exceeded the capacity of nanoparticles. Hence, 1 mg was selected as the optimal amount of insulin with an entrapment efficiency of $86.4 \pm 2.0\%$ as per Figure 4.6(D) and an insulin-loading capacity of $8.9 \pm 0.2\%$ as per Figure 4.6(E).

Table 4.3: R^2 value for different release kinetics models: zero-order, first-order and Higuchi model.

Polymer ratio CS/CMCi	R^2 value for release kinetics of different models		
	Zero Order	First Order	Higuchi Model
1:1	0.865 ± 0.009	0.830 ± 0.009	0.802 ± 0.002
1.5:1	0.925 ± 0.004	0.964 ± 0.003	0.866 ± 0.007
2:1	0.902 ± 0.007	0.923 ± 0.004	0.811 ± 0.007
2.5:1	0.921 ± 0.004	0.948 ± 0.002	0.844 ± 0.001

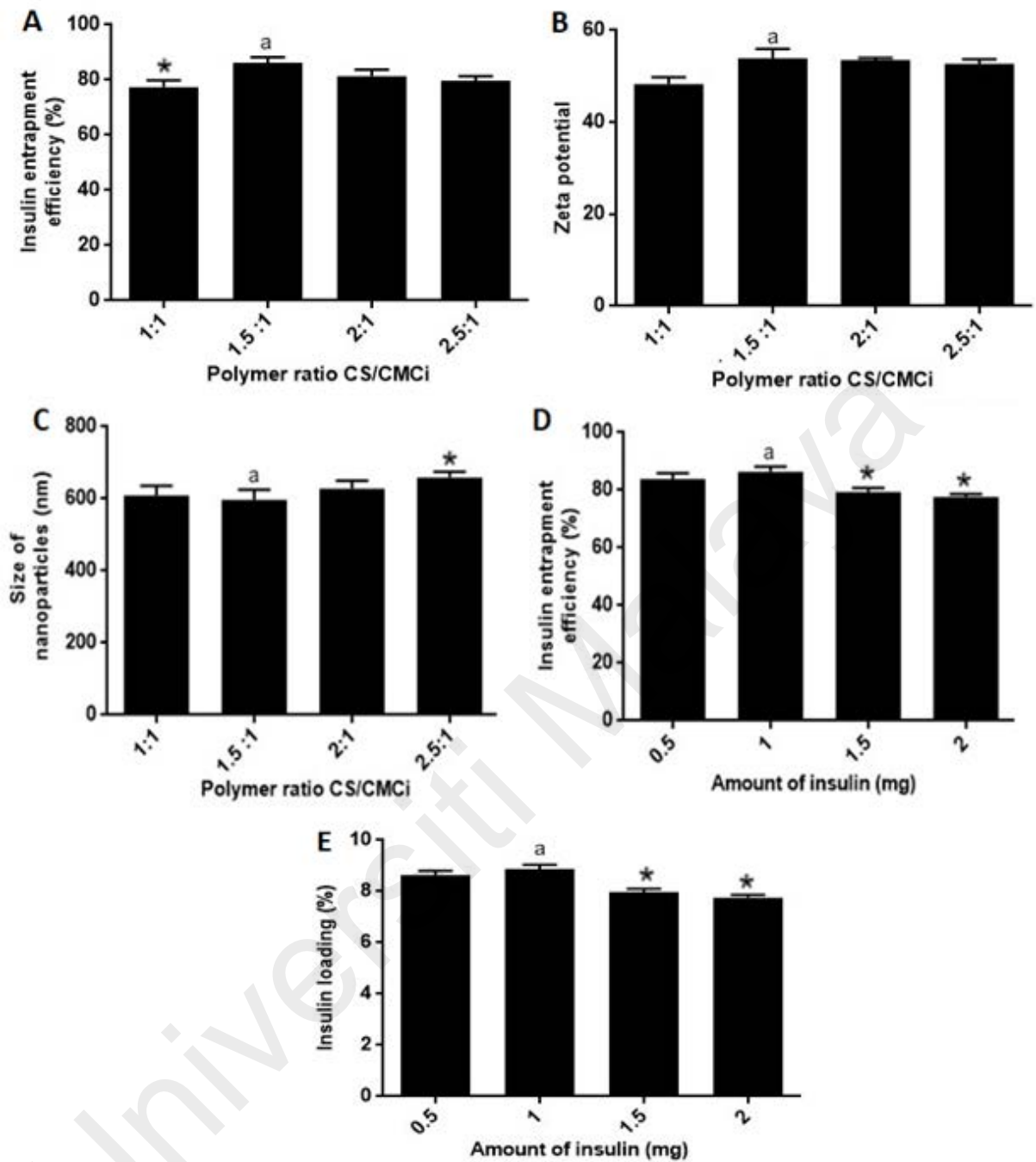


Figure 4.6: Preparation and optimisation of the insulin-entrapped chitosan (CS)/carboxymethylated *iota*-carrageenan (CMCi) nanoparticles from 0.1% w/v CMCi and 0.1% w/v CS. (A) Entrapment efficiency of insulin corresponding to various ratios of CS and CMCi polymers. (B) Zeta potential of the nanoparticles corresponding to various ratios of CS and CMCi polymers. (C) Size of the nanoparticles corresponding to various ratios of CS and CMCi polymers. (D) Entrapment efficiency of insulin with increasing amounts of insulin (0.5–2 mg). (E) Loading of insulin with increasing amounts of insulin (0.5–2 mg). The results are presented as mean \pm SD ($n = 3$). ^aParameters selected in formulating nanoparticles for further characterisation and *in vitro* studies. * $p < 0.05$ compared to ‘a’ according to Student’s *t*-test

4.3. Degree of swelling of CS/CMC_i nanoparticles

Swelling study is very essential for polymeric drug delivery system, as it has a significant impact on the release pattern of a drug. The CS/CMC_i (I01–I33) nanoparticles displayed a pH-dependent swelling (Table 4.4). Most of the nanoparticles showed a lower degree of swelling than CS/native Ci nanoparticles (7.04) in SGF media (pH 1.2) ($p < 0.05$). However, in SIF (pH 6.8), most of the nanoparticles had higher degree of swelling than CS/native Ci nanoparticles (6.87) ($p < 0.05$). At a lower pH (pH 1.2), the degree of swelling decreased due to protonation of the carboxylic acid groups, which led to the formation of hydrogen bonds. At a higher pH (pH 6.8), the degree of swelling increased due to deprotonation, which led to electrostatic repulsion between the carboxylate units. The degree of swelling was measured at fixed time point as the nanoparticles lyophilised in order to get the dry weight as it is account for dissolution and hence, drug release.

The drug release study using SGF (pH 1.2) and SIF (pH 6.8), which was described in section 4.6.1, revealed that the cumulative amount of insulin released in in SGF was $4.91 \pm 0.24\%$ and in SIF was $86.64 \pm 2.20\%$. CS/CMC_i nanoparticles in SGF was both diffusion- and swelling-controlled, while in SIF, it was swelling-controlled. This result suggests formation of strong hydrogen bonds between polymers which restrict the swelling, hence low release of insulin in SGF. However, the electrostatic repulsion between the carboxylate units facilitate the degree of swelling, hence higher amount of insulin release in SIF. Thus, the swelling ability of polymeric drug delivery system is a fundamental property that influence both the diffusion and release of drug. Different polymers having carboxylic acid groups, such as poly(methacrylic acid-co-acrylamide), have shown similar swelling behavior (Gupta & Shivakumar, 2012). Zhang *et al.*, (2016) formulated pH responsive carboxymethyl chitosan functionalized acrylic acid grafted insulin hydrogels, which showed only 16.3% release in SGF while 93% release in SIF. In another study, BSA loaded

alginate and methoxy poly(ethylene glycol) grafted carboxymethyl chitosan hydrogels showed similar pH responsive drug release (Yang *et al.*, 2013).

Universiti Malaya

Table 4.4: Dependent variables obtained from various CS/CMCi nanoparticles. Dependent variable ((swelling ratio (Y_1), gel fraction (Y_2) of CS/CMCi, the Korsmeyer-Peppas release model parameters k (Y_3) and n (Y_4) of insulin-entrapped CS/CMCi nanoparticles in simulated gastric fluid (SGF) (pH 1.2) and swelling ratio (Z_1), gel fraction (Z_2) of CS/CMCi, the Korsmeyer-Peppas release model parameters k (Z_3) and n (Z_4) of insulin-entrapped CS/CMCi nanoparticles in simulated intestinal fluid (SIF) (pH 6.8)).

Sample code	Y1	Y2	Y3	Y4	Z1	Z2	Z3	Z4
I01	5.24 ± 0.31	89.95 ± 1.32	0.22 ± 0.02	0.62 ± 0.03	7.06 ± 0.39	95.46 ± 2.01	0.98 ± 0.04	0.81 ± 0.04
I02	8.84 ± 0.39	86.23 ± 1.21	0.19 ± 0.02	0.65 ± 0.04	9.03 ± 0.40	95.94 ± 2.04	0.89 ± 0.03	0.89 ± 0.03
I03	5.09 ± 0.27	89.80 ± 2.37	0.21 ± 0.03	0.65 ± 0.03	5.12 ± 0.36	92.48 ± 3.01	0.90 ± 0.01	0.82 ± 0.04
I04	8.07 ± 0.51	89.30 ± 3.19	0.21 ± 0.01	0.63 ± 0.05	9.94 ± 0.93	91.21 ± 4.71	0.97 ± 0.01	0.86 ± 0.01
I05	7.51 ± 0.47	98.19 ± 4.02	0.20 ± 0.03	0.62 ± 0.06	7.97 ± 0.62	99.85 ± 5.01	1.10 ± 0.03	0.86 ± 0.02
I06	7.33 ± 0.56	92.79 ± 5.11	0.20 ± 0.02	0.63 ± 0.01	8.85 ± 0.80	96.27 ± 4.95	0.97 ± 0.04	0.87 ± 0.03
I07	6.36 ± 0.60	87.99 ± 2.93	0.21 ± 0.01	0.64 ± 0.03	7.51 ± 0.25	89.44 ± 5.01	1.04 ± 0.05	0.71 ± 0.04
I08	7.72 ± 0.32	86.96 ± 3.32	0.21 ± 0.02	0.63 ± 0.04	8.21 ± 0.64	88.76 ± 3.01	0.99 ± 0.06	0.81 ± 0.04
I09	5.90 ± 0.49	85.20 ± 4.36	0.20 ± 0.01	0.63 ± 0.08	6.58 ± 0.34	89.21 ± 3.85	0.99 ± 0.02	0.85 ± 0.04
I10	5.81 ± 0.71	84.28 ± 3.52	0.24 ± 0.01	0.66 ± 0.03	6.93 ± 0.52	88.72 ± 2.91	1.00 ± 0.04	0.74 ± 0.07
I11	6.18 ± 0.83	93.36 ± 5.32	0.23 ± 0.03	0.64 ± 0.05	7.91 ± 0.60	94.26 ± 5.05	1.03 ± 0.06	0.86 ± 0.05
I12	4.42 ± 0.29	88.20 ± 4.42	0.20 ± 0.04	0.63 ± 0.04	6.20 ± 0.30	90.11 ± 4.93	1.01 ± 0.04	0.86 ± 0.05
I13	5.60 ± 0.53	84.50 ± 2.53	0.21 ± 0.03	0.63 ± 0.06	6.26 ± 0.32	87.97 ± 4.05	1.06 ± 0.05	0.81 ± 0.03
I14	4.48 ± 0.28	84.24 ± 5.01	0.22 ± 0.04	0.63 ± 0.08	5.93 ± 0.50	87.78 ± 5.56	1.04 ± 0.02	0.81 ± 0.05

Table 4.4, continued

Sample code	Y1	Y2	Y3	Y4	Z1	Z2	Z3	Z4
I15	5.76 \pm 0.52	85.30 \pm 4.46	0.21 \pm 0.01	0.63 \pm 0.05	6.04 \pm 0.31	87.89 \pm 5.65	1.07 \pm 0.05	0.81 \pm 0.05
I16	5.31 \pm 0.52	83.56 \pm 2.61	0.20 \pm 0.01	0.63 \pm 0.04	7.81 \pm 0.43	93.18 \pm 3.02	1.09 \pm 0.02	0.75 \pm 0.03
I17	4.61 \pm 0.31	91.64 \pm 4.39	0.21 \pm 0.02	0.64 \pm 0.05	6.00 \pm 0.51	93.32 \pm 4.50	1.05 \pm 0.03	0.77 \pm 0.02
I18	6.70 \pm 0.80	86.06 \pm 5.30	0.20 \pm 0.02	0.64 \pm 0.08	6.93 \pm 0.73	90.50 \pm 5.54	1.03 \pm 0.03	0.82 \pm 0.02
I19	6.17 \pm 0.59	86.21 \pm 4.76	0.20 \pm 0.03	0.65 \pm 0.09	6.22 \pm 0.51	87.71 \pm 2.39	0.93 \pm 0.04	0.85 \pm 0.01
I20	6.08 \pm 0.74	88.82 \pm 5.36	0.18 \pm 0.02	0.43 \pm 0.04	7.59 \pm 0.29	91.08 \pm 5.38	1.23 \pm 0.02	0.82 \pm 0.04
I21	6.10 \pm 0.83	82.53 \pm 5.73	0.20 \pm 0.03	0.65 \pm 0.05	6.56 \pm 0.40	84.91 \pm 5.67	0.88 \pm 0.05	0.90 \pm 0.05
I22	7.35 \pm 0.79	83.63 \pm 4.11	0.24 \pm 0.04	0.66 \pm 0.04	7.40 \pm 0.47	85.22 \pm 4.08	0.85 \pm 0.04	0.91 \pm 0.04
I23	7.52 \pm 0.41	84.67 \pm 5.25	0.27 \pm 0.06	0.67 \pm 0.01	7.69 \pm 0.40	91.98 \pm 5.67	0.82 \pm 0.06	0.93 \pm 0.05
I24	7.42 \pm 0.50	84.88 \pm 2.62	0.29 \pm 0.05	0.68 \pm 0.07	7.81 \pm 0.78	91.95 \pm 5.01	0.95 \pm 0.04	0.80 \pm 0.05
I25	6.28 \pm 0.48	85.33 \pm 3.42	0.25 \pm 0.05	0.65 \pm 0.03	6.87 \pm 0.67	92.11 \pm 2.61	1.04 \pm 0.02	0.75 \pm 0.04
I26	5.60 \pm 0.39	86.01 \pm 2.76	0.22 \pm 0.03	0.64 \pm 0.03	5.66 \pm 0.49	91.69 \pm 4.87	1.03 \pm 0.01	0.76 \pm 0.03
I27	6.51 \pm 0.52	85.02 \pm 4.73	0.28 \pm 0.05	0.67 \pm 0.04	6.94 \pm 0.67	92.94 \pm 3.67	1.01 \pm 0.05	0.77 \pm 0.02
I28	5.84 \pm 0.59	87.13 \pm 1.76	0.23 \pm 0.03	0.64 \pm 0.05	6.70 \pm 0.59	92.38 \pm 5.56	1.02 \pm 0.06	0.79 \pm 0.05
I29	4.94 \pm 0.39	87.88 \pm 6.62	0.22 \pm 0.02	0.64 \pm 0.06	4.81 \pm 0.45	91.65 \pm 2.31	1.05 \pm 0.04	0.73 \pm 0.06
I30	5.13 \pm 0.72	87.80 \pm 2.76	0.21 \pm 0.03	0.63 \pm 0.01	5.88 \pm 0.45	91.76 \pm 4.01	1.06 \pm 0.03	0.74 \pm 0.03

Table 4.4, continued

Sample code	Y1	Y2	Y3	Y4	Z1	Z2	Z3	Z4
I31	5.07.±.0.48	88.88.±.6.45	0.21.±.0.04	0.64.±.0.03	5.31.±.0.47	92.98.±.5.74	1.07.±.0.03	0.74.±.0.02
I32	5.17.±.0.38	85.38.±.4.87	0.21.±.0.01	0.64.±.0.04	5.43.±.0.34	93.03.±.4.57	0.99.±.0.02	0.76.±.0.05
I33	5.80.±.0.51	82.98.±.2.41	0.21.±.0.03	0.65.±.0.04	5.40.±.0.49	83.70.±.2.40	1.03.±.0.04	0.83.±.0.04

The observed values presented in mean ± SD; n = 3

4.4. Optimisation of independent factors using RSM^{MSI} modeling for carboxymethylation of *iota*-carrageenan in the preparation of insulin-entrapped CS/CMCi nanoparticles

The correlation between independent factors and dependent variables was investigated using the RSM^{MSI} technique. The data of the modified *iota*-carrageenan (I01–I33) shown in Table 3.1 and Table 4.4 were fitted into the RSM^{MSI} model using dataNESIA[®] version 3.0 software for a simultaneous optimisation study (Takayama *et al.*, 2004). Figure 4.7(A) shows the actual and estimated dependent variables using leave-one-out cross-validation. The *r* values for the gel fraction and Korsmeyer-Peppas model parameter *k* (in both SGF and SIF) were high enough to suggest that the RSM^{MSI} model had a high predictive power as per Figure 4.6(A). In Figure 4.7(B, C, D, E), the independent factors had a significant impact on the release profiles of insulin in SGF (pH 1.2). A similar impact was noted in SIF (pH 6.8) as per Figure 4.7(B, C, D, E). Refer to Appendix B for further response surface plots.

The most important aspect of RSM^{MSI} model is its ability to predict the optimum independent factors together with its corresponding dependent variables (Table 4.5). The predicted optimum independent factors for the carboxymethylation process were 7.04 mL of 9.89 N NaOH solution, 3.93 g of ClCH₂COOH (MCA) and a reaction temperature of 50.93°C. The nanoparticles were then prepared using these parameters, and the dependent variables were investigated in triplicates. The differences in predicted and experimental values were insignificant (Student's paired t-test ($p > 0.05$)) and the % error was found to be within limits ($< \pm 10\%$), suggesting the reliability of RSM^{MSI} prediction (Gupta & Shivakumar, 2012).

The prepared CMCi based on the RSM^{MSI} optimum independent factors showed a total DS of 0.1749 with 0.0638 at the GC-2 position and 0.1111 at the GC-6 position as per

Figure 4.1(A), which suggested that, in total, 17.5% of the GC-2 and GC-6 positions were substituted with carboxymethylated groups. The higher substitution at the GC-6 position is likely due to its accessibility and the optimum independent factors recommended by the RSM^{MSI} model that agreed with the observation in the pre-formulation study (section 4.2) for a better insulin release control. The estimated molecular weight was 466 ± 12 kDa, which was slightly lower than the value of 522 ± 15 kDa for native Ci. This suggested minimal depolymerisation of the native carrageenan during carboxymethylation despite the presence of a strong base (10 N NaOH) and a higher temperature (51°C). The sulfate content before and after carboxymethylation remained similar, with values of $28.08 \pm 0.9\%$ and $27.82 \pm 0.7\%$, respectively. The presence of sulfate groups is important, as they are expected to interact with the amino side chains of insulin and may promote insulin stabilisation (Leong *et al.*, 2011b).

Table 4.5: Predicted and experimental values for the dependent variables (degree of swelling (Y_1), gel fraction (Y_2) of CS/CMCi, and the Korsmeyer-Peppas release model parameters k (Y_3) and n (Y_4) for the entrapped insulin in the CS/CMCi nanoparticles in simulated gastric fluid (SGF) (pH 1.2), and the degree of swelling (Z_1), gel fraction (Z_2) of CS/CMCi, and the Korsmeyer-Peppas release model parameters k (Z_3) and n (Z_4) for the entrapped insulin in the CS/CMCi nanoparticles in simulated intestinal fluid (SIF) (pH 6.8)) along with the percentage error.

Dependent Variable	Predicted value from RSM^{MSI}	Experimental value^a	Percentage error (%)^b
Y_1	6.430	6.361 ± 0.152	-1.07
Y_2	91.354	91.228 ± 1.226	-1.07
Y_3	0.211	0.214 ± 0.009	1.56
Y_4	0.623	0.630 ± 0.003	1.12
Z_1	7.400	7.313 ± 0.255	-1.18
Z_2	92.348	92.414 ± 0.529	0.07
Z_3	0.997	1.083 ± 0.017	8.64
Z_4	0.896	0.853 ± 0.010	-4.83

a: The observed values presented in mean \pm SD; n = 3.

b: Percentage error calculated as (predicted value–observed value) /predicted value \times 100%.

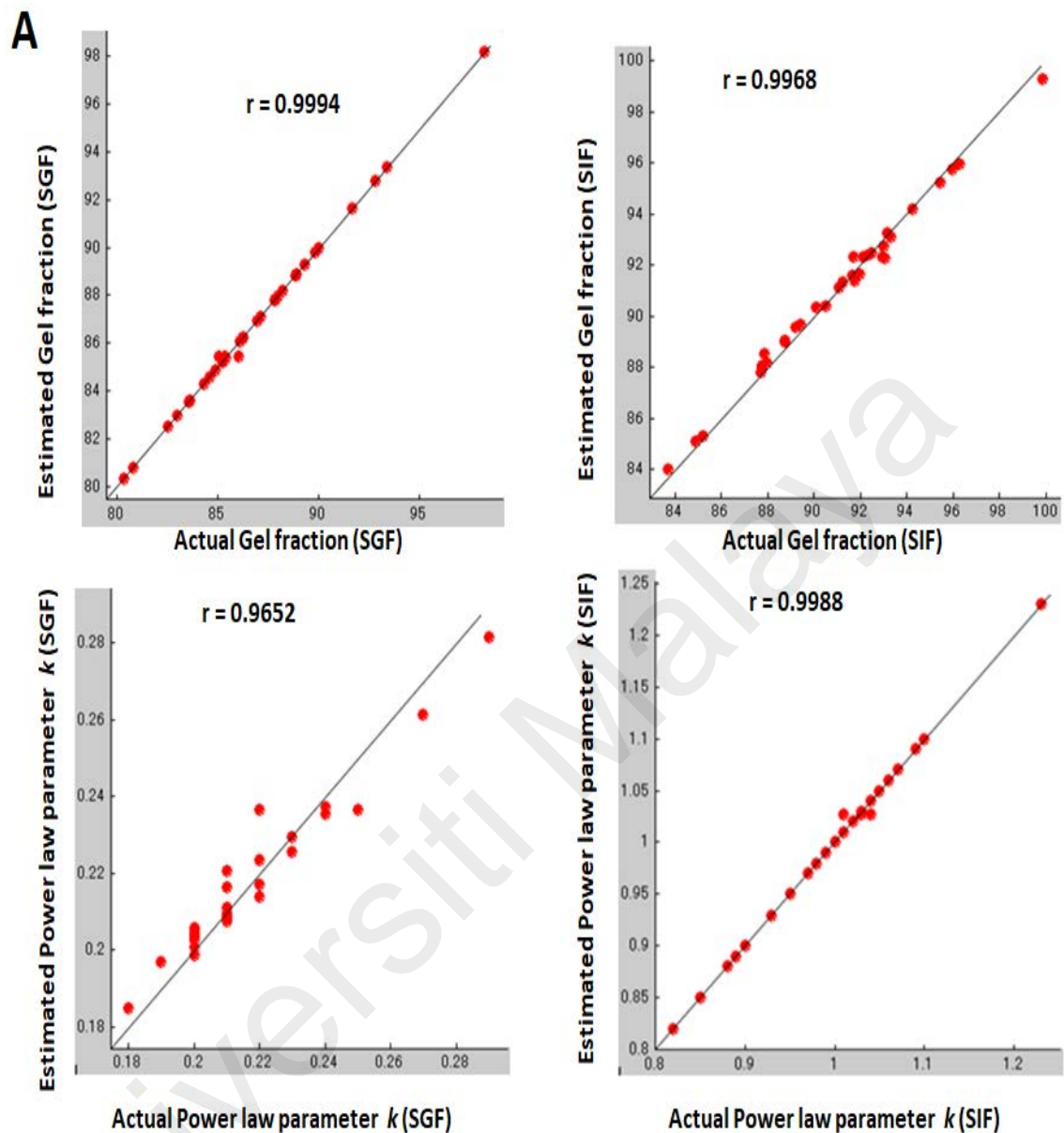



Figure 4.7: (A) Leave-one-out cross-validation showing the predictive power of the RSM^{MSI} model for the gel fraction and the Korsmeyer-Peppas model parameter k in both simulated gastric fluid (SGF) (pH 1.2) and simulated intestinal fluid (SIF) (pH 6.8). (B) Response surface plots showing the influence of volume and concentration of NaOH on swelling, gel fraction and the dissolution parameters (n and $\log k$) in SGF (pH 1.2) and SIF (pH 6.8). (C) Response surface plots showing the influence of volume of NaOH and amount of ClCH₂COOH (MCA) on swelling, gel fraction and the dissolution parameters (n and $\log k$) in SGF (pH 1.2) and SIF (pH 6.8). (D) Response surface plots showing the influence of concentration of NaOH and amount of ClCH₂COOH (MCA) on swelling, gel fraction and the dissolution parameters (n and $\log k$) in SGF (pH 1.2) and SIF (pH 6.8) (E) Response surface plots showing the influence of concentration of NaOH and reaction temperature on swelling, gel fraction and the dissolution parameters (n and $\log k$) in SGF (pH 1.2) and SIF (pH 6.8).  Dark blue indicates lowest value, red indicates highest value and \bullet indicates points below predicted value. Refer to Appendix B for further data.

Figure 4.7, continued

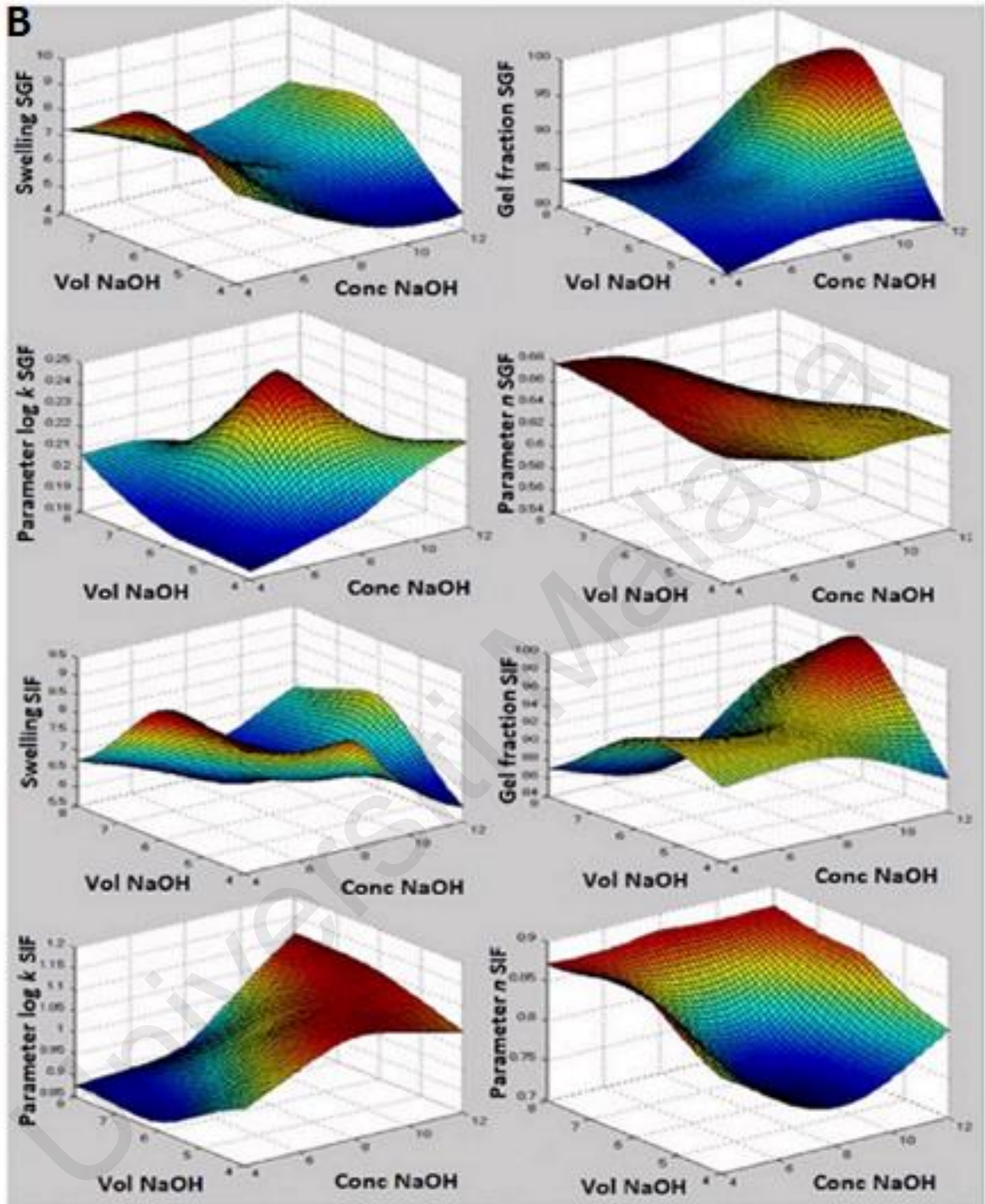


Figure 4.7, continued

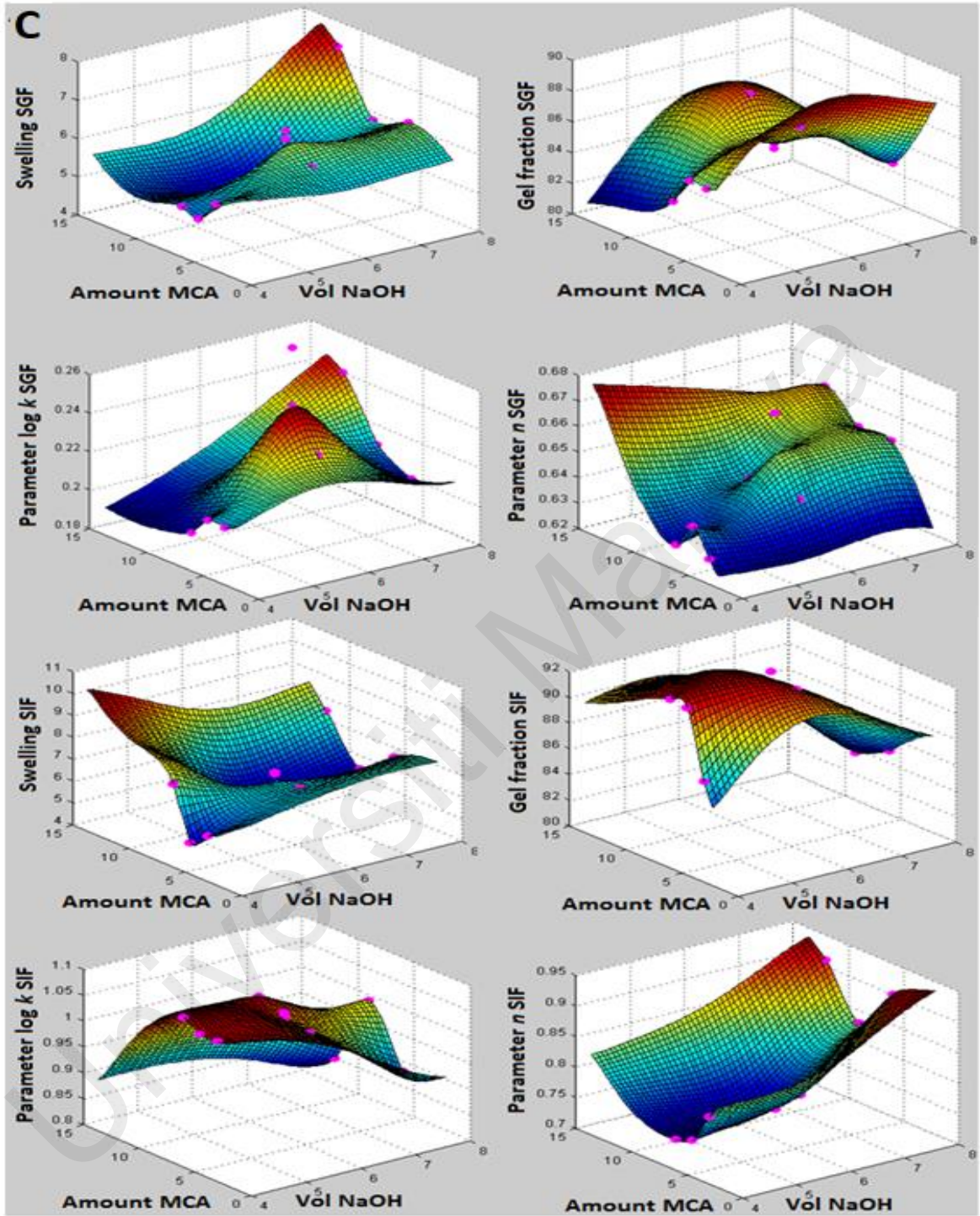


Figure 4.7, continued

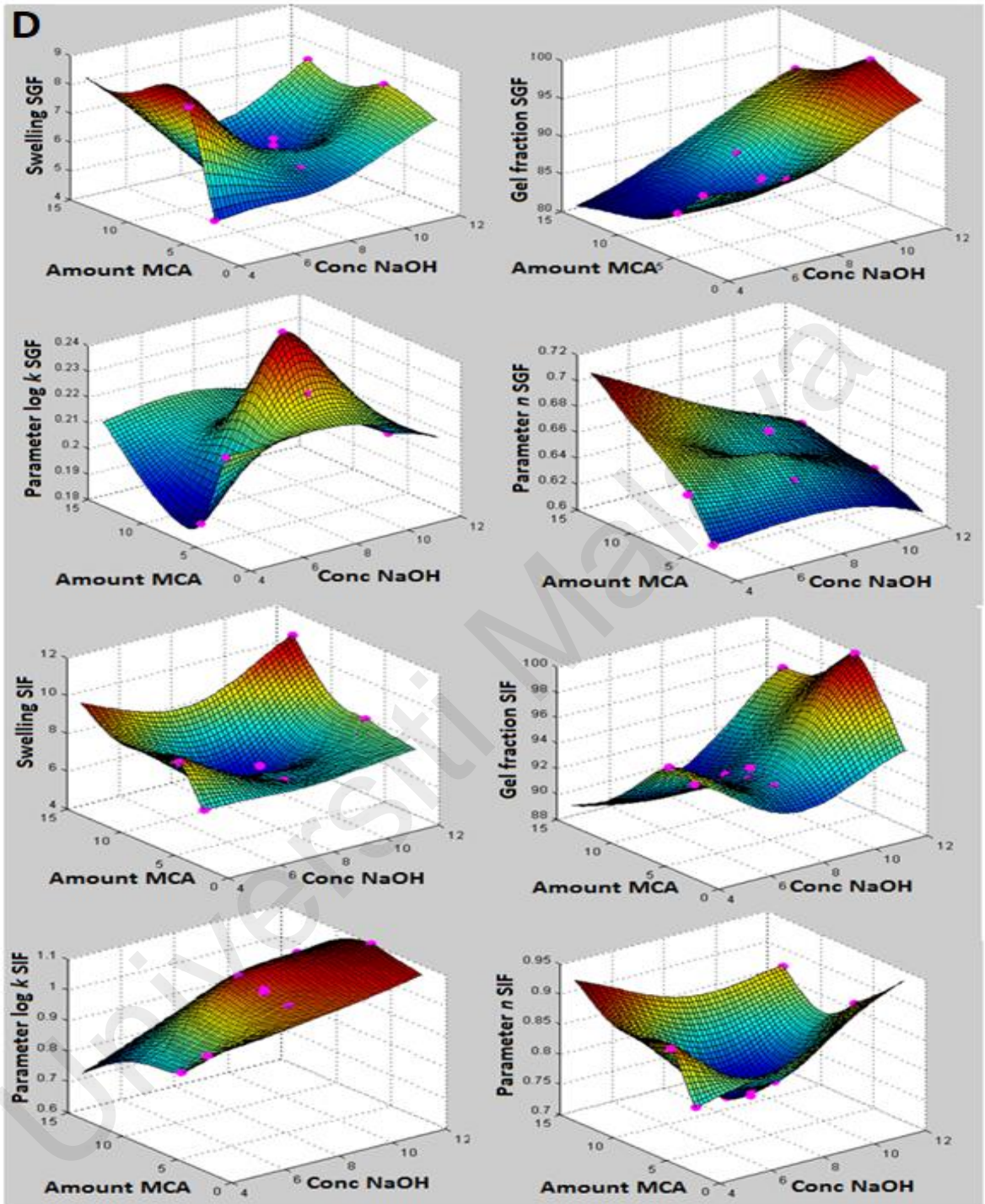
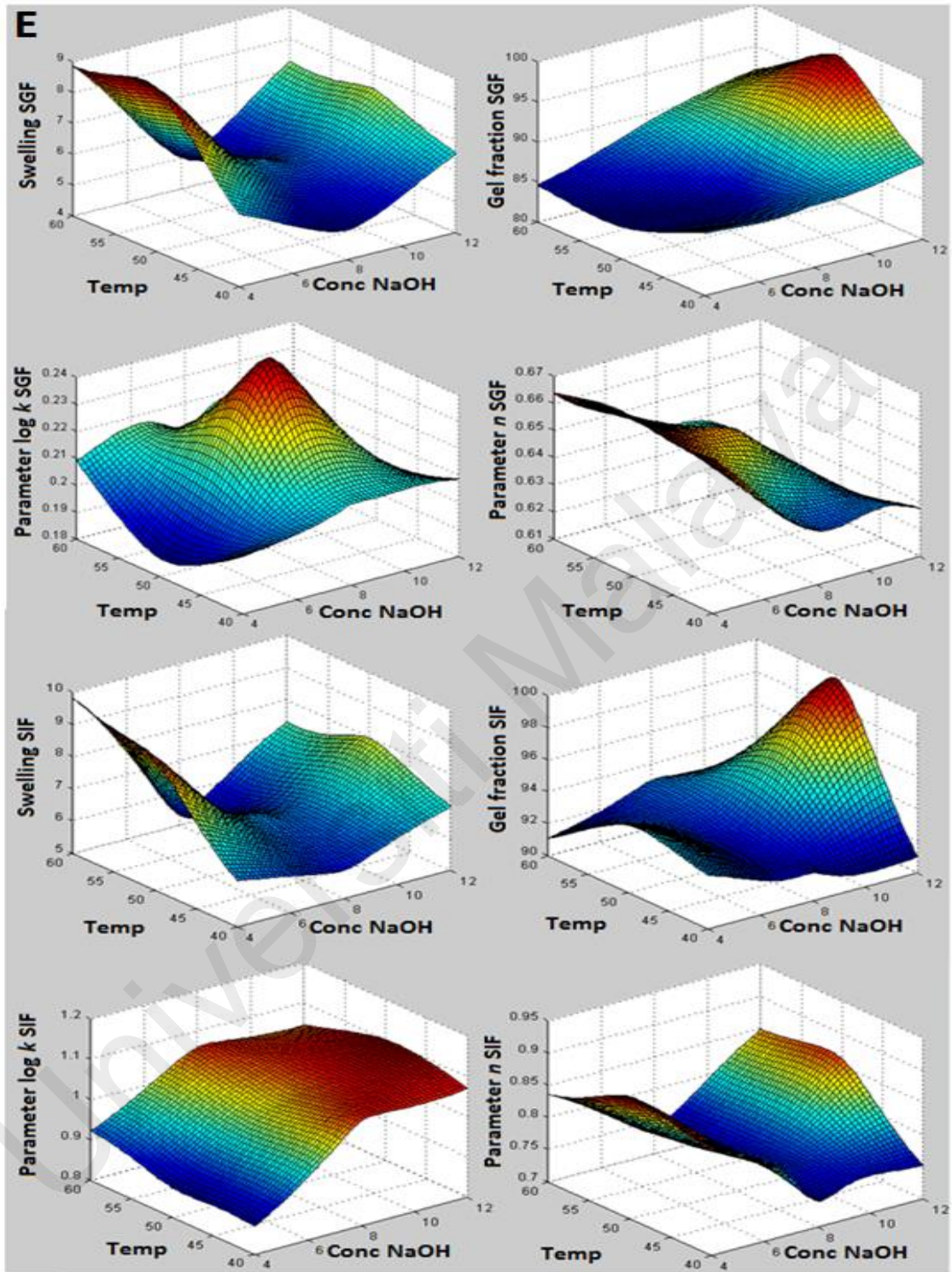


Figure 4.7, continued



4.5. Characterisation of the optimised insulin-entrapped CS/CMC*i* nanoparticles

The preparation of insulin-entrapped CS/CMC*i* nanoparticles was based on a 1.5:1 ratio of CS to optimise CMC*i* (DS 0.1749). In the pre-formulation of nanoparticles, an increase in the particle size was observed by increasing CS concentration. This resulted from a turbid suspension of nanoparticle which led to aggregation on further increase of CS concentration. The optimised nanoparticles showed high insulin entrapment efficiency, good loading and a homogenous nanoparticle size of approximately 613 ± 41 nm with a low polydispersity index (Table 4.6). Size of the nanoparticles is important in regulating the efficacy of a drug delivery system. A smaller size and higher surface-to-volume ratio can retain better contact with mucosal tissue and may provide better local drug concentration (Peppas & Huang, 2004). The optimised nanoparticles had a fairly good loading of $10.7 \pm 0.6\%$ and entrapment efficiency of $86.9 \pm 2.6\%$, compared to previously published studies of 9.8% and 72.8% (Sarmiento *et al.*, 2007) and 8.04% and 72.6% (Liu *et al.*, 2007). The zeta potential of optimised nanoparticles is positively attributed to higher concentration of CS in the formulation. The zeta potential value of $+52.5 \pm 0.5$ mV is likely to provide good dispersibility and reduce aggregation of the nanoparticles, and hence, more stable nanoparticles. These results are in accordance with other published studies (Grenha *et al.*, 2010; Cody *et al.*, 2012).

The mucosal tissue across the GIT acts as a barrier in the absorption of insulin (Rekha & Sharma, 2013). Mucoadhesive polymers may overcome the obstacle by extending the presence of insulin in the GIT, liberating insulin near the mucosal layer, assisting intimate contact of insulin with the mucosal layer of the intestinal wall. Hence, greater insulin concentration gradient across the intestinal wall facilitates the absorption of insulin (Ding *et al.*, 2012; Rekha & Sharma, 2013; Sheng *et al.*, 2016). The mucoadhesiveness of CS/CMC*i* nanoparticles is determined using the everted sac method in rats' small intestine. This method is a simple laboratory procedure in which incubated nanoparticles

bind to the mucosal part of the everted intestinal tissue, as depicted in Figure 3.1 (A, B). In a previous everted sac study, microspheres of poly(caprolactone) and poly(fumaric-co-sebacic anhydride) showed a mucoadhesion of $61.3 \pm 17.1\%$ (Santos *et al.*, 1999). A greater percentage of binding means better mucoadhesion of nanoparticles to the mucosal layer (Santos *et al.*, 1999; Alam *et al.*, 2012). The percent mucoadhesion for CS/CMC_i nanoparticles was $79.1 \pm 4.3\%$ compared to CS/C_i nanoparticles, which was $75.6 \pm 3.1\%$ (Table 4.6). A high percentage of mucoadhesion suggests that CS/CMC_i nanoparticles have good mucoadhesive property, which infers better drug permeation (Jain *et al.*, 2007).

Universiti Malaysia

Table 4.6: Comparative properties of optimised insulin-loaded nanoparticles formulated with native Ci and CMCI.

Formulation	^cZeta potential (mV)	^cSize (Wet nanoparticle) (nm)	^cPolydispersity	^cEntrapment efficiency (%)	^cLoading capacity (%)	^dMucoadhesion (%)
^a CS/native Ci (1.5:1)	+42.2 ± 1.8	600 ± 58	0.5 ± 0.04	80.3 ± 3.5	8.3 ± 0.8	79.1 ± 4.3
^b CS/CMCI (1.5:1)	+52.5 ± 0.5	613 ± 41	0.3 ± 0.01	86.9 ± 2.6	10.7 ± 0.6	75.6 ± 3.1

a: Chitosan (CS)/native *Iota*-carrageenan (Ci) nanoparticles having weight ratio 1.5:1

b: Chitosan (CS)/Carboxymethylated *iota*-carrageenan (CMCI) nanoparticles having a weight ratio of 1.5:1

c: The experimental values are expressed in mean ± SD; n = 3.

d: The experimental values are expressed in mean ± SD; n = 6.

The FT-IR spectra of CMCi (A), CS (B), insulin (C) and insulin-entrapped CS/CMCi nanoparticles (D) are shown in Figure 4.8. In CMCi, the basic characteristic peaks (stretching) at 806 cm^{-1} and 1263 cm^{-1} are attributed to the sulfate groups at C2 of 3, 6-anhydro- α -D-galactopyranose-2-sulfate and C4 of the β -D-galactopyranose-4-sulfate units, respectively (Raman *et al.*, 2015). The peaks at 855 cm^{-1} , 931 cm^{-1} and 1070 cm^{-1} correspond to functional groups β -D-galactopyranose-4-sulfate, 3,6-anhydro- α -D-galactopyranose-2-sulfate and the glycosidic linkage, respectively (Abad *et al.*, 2003). The peaks at 1428 cm^{-1} and 1608 cm^{-1} are characteristics of -COOH groups, and the peak at 1327 cm^{-1} is attributed to the $-\text{CH}_2$ group of the carboxymethyl unit as per Figure 4.8(A) (Fan *et al.*, 2011). The FT-IR spectrum of CS showed two peaks at 1653 cm^{-1} and 1597 cm^{-1} , attributed to amide I (ONH₂ group) and amide II (NH₂ bending), and a peak at 1080 cm^{-1} , which corresponds to the glycosidic linkage as per Figure 4.8(B) (Schiffman & Schauer, 2007). The FT-IR spectrum of insulin showed two characteristic protein peaks at 1656 cm^{-1} and 1539 cm^{-1} that correspond to amide I and amide II peaks resulting from association of C=O and C-N stretching with C-N-H bending vibrations, respectively (Figure 4.8(C)) (Sarmiento *et al.*, 2006a). The spectrum of the insulin-entrapped CS/CMCi nanoparticles showed the typical peaks of CMCi. However, the two insulin peaks shifted to 1632 cm^{-1} and 1535 cm^{-1} . This may be due to electrostatic interaction between sulfate groups in the CMCi and amino groups in the insulin during nanoparticle formation as per Figure 4.8(D).

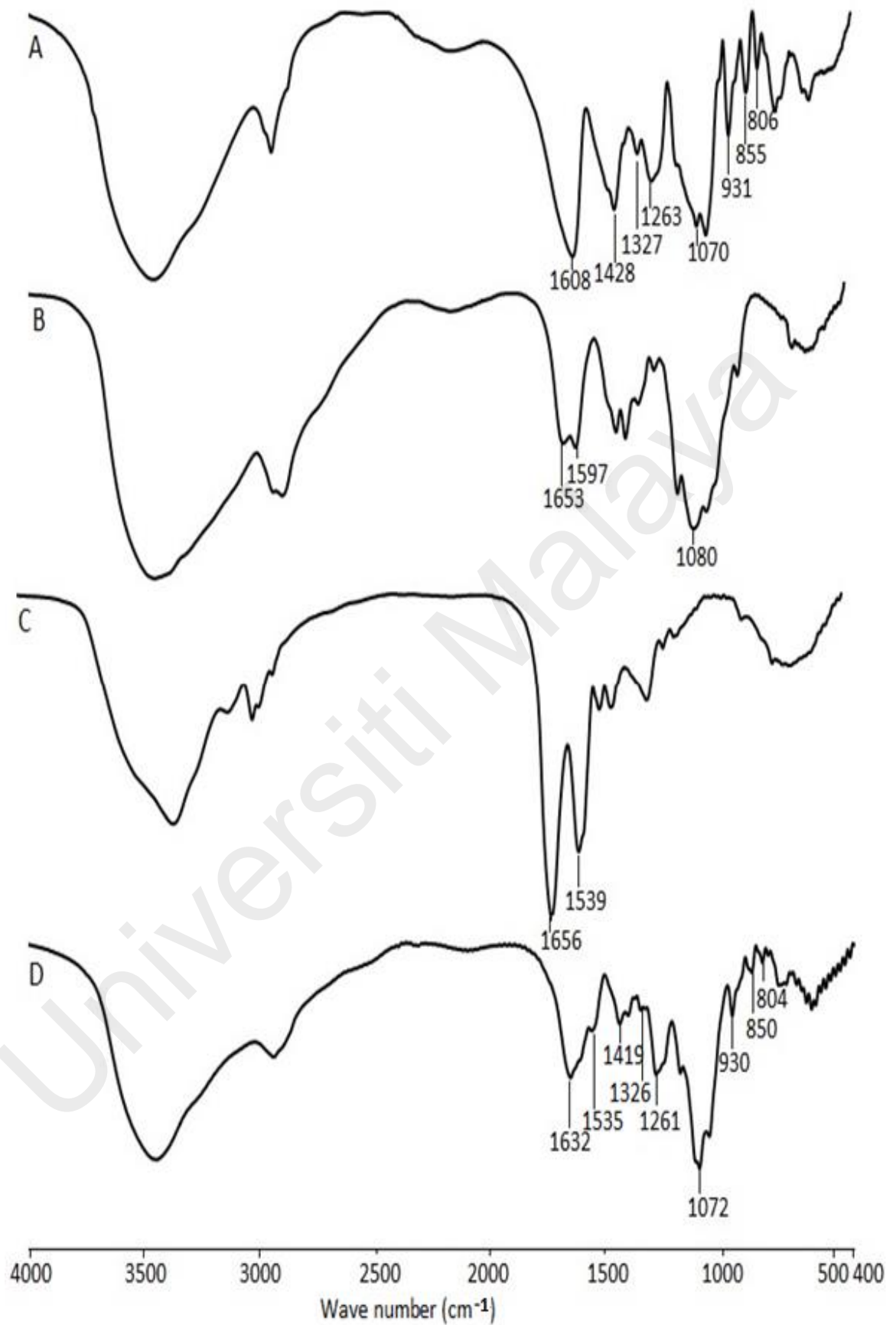


Figure 4.8: FTIR spectra of (A) carboxymethylated *iota*-carrageenan (CMCi), (B) chitosan (CS), (C) insulin, and (D) insulin-entrapped CS/CMCi nanoparticles.

The TEM and FESEM micrographs showed that the dried native CS/Ci nanoparticles were spherically intact (Figure 4.9(A)) with compact surfaces (Figure 4.9(C)). Conversely, the optimized nanoparticles exhibited a dense core (Figure 4.9(B)) with a more porous outer layer (Figure 4.9(D)). The variation in shape may be attributed to the difference in the pore size of nanoparticles. The TEM and FESEM micrographs showed fair correlation with the size of nanoparticles measured by zetasizer (wet nanoparticle diameter), that show slightly bigger particles for CS/CMCi nanoparticles compared to CS/Ci nanoparticles (Table 4.6). Furthermore, the average size of nanoparticles measured by zetasizer was higher (613 nm) than the size estimated in TEM (213 nm), due to higher swelling capability of CS/CMCi nanoparticles. The difference in size is due to the sample preparation techniques used, as freshly prepared sample suspension is used in the zetasizer and dried sample suspension is used in TEM (dry nanoparticles). Similar results were obtained in a previous study on magnetite chitosan/carrageenan nanoparticles (Long *et al.*, 2015).

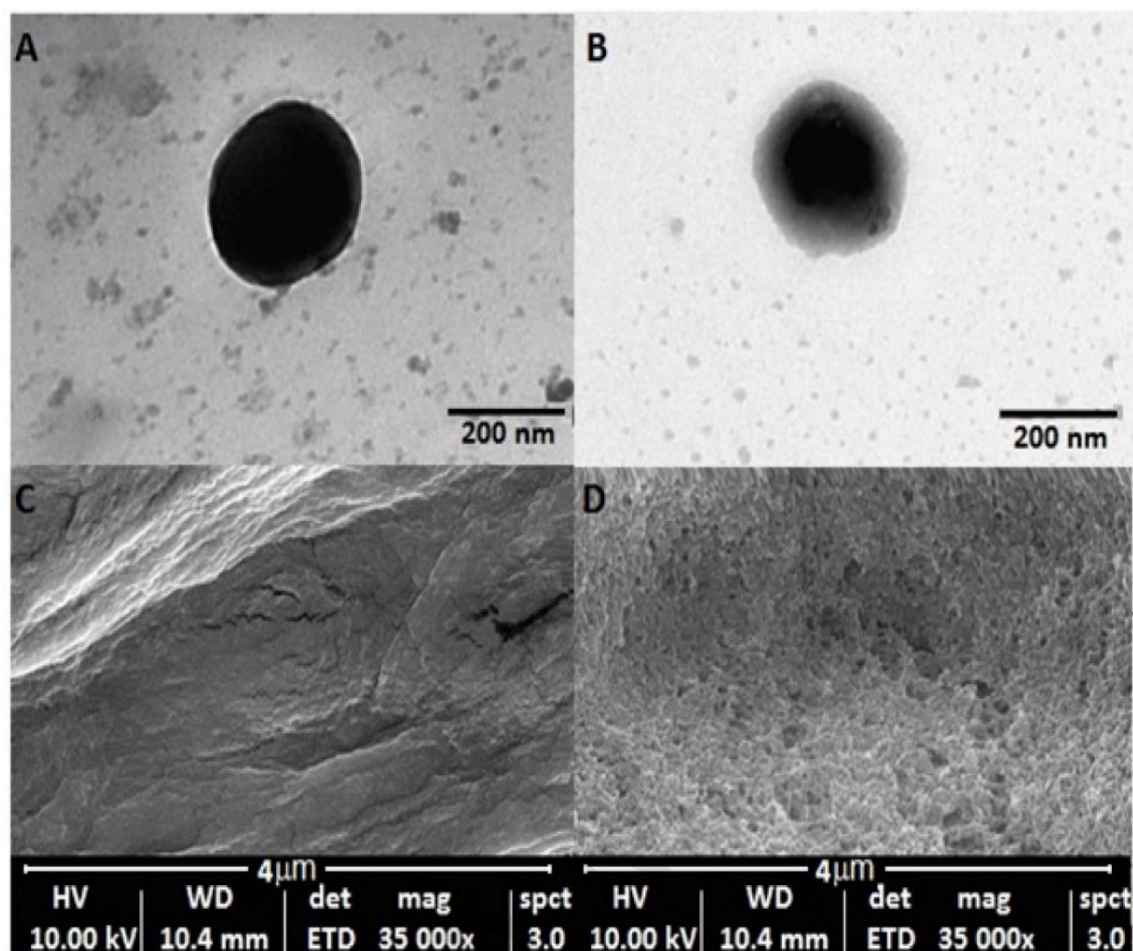


Figure 4.9: TEM micrographs of nanoparticles formulated from (A) native CS/Ci and (B) optimised CS/CMCi, and FESEM micrographs of nanoparticles made from (C) native CS/Ci and (D) optimised CS/CMCi.

4.6. *In vitro* studies of optimised insulin-entrapped CS/CMCi nanoparticles

4.6.1. Release kinetics, stability of released insulin against enzymatic degradation bioactivity of released insulin from CS/CMCi nanoparticles, storage stability and HPLC method validation

The *in vitro* release of insulin from optimised CS/CMCi nanoparticles under gastric- and intestine-simulated pH conditions was investigated (Figure 4.10(A)). In acidic SGF (pH 1.2), CMCi had a tightly enclosed network due to hydrogen bonding between the COOH groups. Furthermore, the NH₂ units of insulin and CS and the SO₄²⁻ unit of *iota*-carrageenan were oppositely charged and tightly bound and premature release of insulin

was limited (Leong *et al.*, 2011b). In SIF (pH 6.8), the network structure opened due to the electrostatic repulsion among the COO^- groups of CMCi. Furthermore, the ionic attraction between the NH_2 units of insulin and CS and the SO_4^{2-} unit of *iota*-carrageenan became weaker as the amino groups were no longer ionized, which led to significant swelling and allowed a larger amount of entrapped insulin to be released (Leong *et al.*, 2011b; Grenha *et al.*, 2010). The cumulative amount of insulin released in SIF was much higher ($86.64 \pm 2.20\%$) than that in SGF ($4.91 \pm 0.24\%$). This result is in line with other oral insulin formulations that have shown restricted release in SGF and higher release in SIF (Zhang *et al.*, 2011; Li *et al.*, 2012; Saboktakin *et al.*, 2015). Drug release from polymeric nanoparticle formulations is a complicated process, such as permeation of GIT fluids into the nanoparticles following swelling and diffusion and finally dissolution of the drug (Lopes *et al.*, 2016). Hence, to measure the release, the parameter n is calculated based on the Korsmeyer-Peppas model (Eq. 3.1), and had values of 0.62 in SGF and 0.90 in SIF, respectively. For spherical nanoparticles, a n value of 0.43 indicated a diffusion-controlled release and a value of 0.85 indicated a swelling-controlled release. An intermediate value indicates an anomalous release and is both diffusion- and swelling-controlled (Lin & Metters, 2006). Thus, the release of insulin from the optimised nanoparticles in SGF was both diffusion- and swelling-controlled, while in SIF, it was swelling-controlled. This may be attributed to protonation of the carboxylic acid groups in lower pH of SGF (pH 1.2), which led to the formation of strong hydrogen bonds between polymers, the release is both diffusion- and swelling-controlled. However, in SIF (pH 6.8), the degree of swelling increased due to deprotonation, which led to electrostatic repulsion between the carboxylate units and hence the release is swelling-controlled (Leong *et al.*, 2011b). The k value is the indicator of the structural and geometric characteristics of spherical nanoparticles, and higher in SIF (1.07) than in SGF (0.21). This difference may be attributed to the fact that in SIF, the polymer structure

swelled (as mentioned in section 4.3) leading to structural and geometrical changes, which led to insulin release (Korsmeyer & Peppas, 1983). After 2 h in SGF, the release of insulin from the optimised CS/CMCi nanoparticles was $4.91 \pm 0.24\%$ (mean \pm SD, $n = 3$), compared to $22.75 \pm 2.20\%$ ($p < 0.05$) for native CS/Ci nanoparticles. In SIF, the release of insulin from optimised CS/CMCi nanoparticles was $86.64 \pm 2.20\%$, compared to $70.18 \pm 1.18\%$ ($p < 0.05$) for native CS/Ci nanoparticles.

The bioavailability of oral insulin is strongly affected by enzymatic degradation in the stomach and intestinal lumen (Lundquist & Artursson, 2016). Hence, the ability of CS/CMCi nanoparticles to protect the entrapped insulin from GIT enzymes was evaluated by determining insulin release in SGF containing pepsin (pH 1.2) and SIF containing trypsin (pH 6.8) compared with the release profile of insulin in enzyme free SGF and SIF (Figure 4.10 (B)). There was no significant difference in cumulative amount of insulin release in SGF with pepsin ($5.01 \pm 0.12\%$) and SIF with trypsin ($79.56 \pm 5.93\%$) compared to enzyme free SGF ($4.91 \pm 0.24\%$) and SIF ($86.64 \pm 2.20\%$). Although CS/CMCi nanoparticles could protect insulin from GIT enzymes, the cumulative release was lower ($79.56 \pm 5.93\%$) compared to enzyme free media ($86.64 \pm 2.20\%$). This shows the ability of GIT enzymes to digest insulin, especially near the surface of the nanoparticles (Makhlof *et al.*, 2011).

Insulin is a fragile biomolecule with unstable bonds and responsive side chains, interruption of its complex structure can cause loss of bioactivity. Its bioactivity is dependent on the integrity of its 3D structure (Lopes *et al.*, 2015). To confirm the bioactivity of entrapped insulin from CS/CMCi nanoparticles in SIF (pH 6.8), the final aliquot taken at 12 h was evaluated using ELISA. The results were higher than HPLC results conducted in the *in vitro* release study, showing $93.52 \pm 6.62\%$ of insulin content

compared to HPLC analysis ($86.64 \pm 2.20\%$). The above suggest that CS/CMCi nanoparticles maintain the bioactivity of insulin during the formulation process.

All protein formulations including insulin should be stored properly in controlled temperature, as it is likely to degrade at high temperatures. Storage at room temperature may degrade and/or inactive insulin due to hydrolytic reactions (Vimalavathini & Gitanjali, 2009; Oliva *et al.*, 2000). Therefore, based on the amount of insulin released, insulin entrapped in optimised CS/CMCi nanoparticle should be stored at 25°C (room temperature), and between 4 and -20°C in the dark over 90 days. The level of insulin released was approximately 90% for freshly prepared nanoparticles kept at the above temperatures (Figure 4.10(C)). The remaining 10% of insulin remains entrapped in the nanoparticles and was not fully released, consistent with the findings shown in Figure 4.10(A). At room temperature, the level of insulin released was approximately 90% from freshly prepared nanoparticles throughout the first 7 days, but the amount decreased significantly over time ($p < 0.05$). This suggests that the entrapped insulin in the nanoparticles is stable at between 4 and -20°C, and stable after 7 days at elevated temperatures (25°C) compared to the control sample (pure insulin solution 1 mg/mL), which is stable up to 3 days at room temperature (data not mentioned in graph). Thus, the insulin-entrapped nanoparticles are best stored at low temperatures. Similar temperature effects on insulin stability have been observed for other human insulin formulations (Vimalavathini & Gitanjali, 2009).

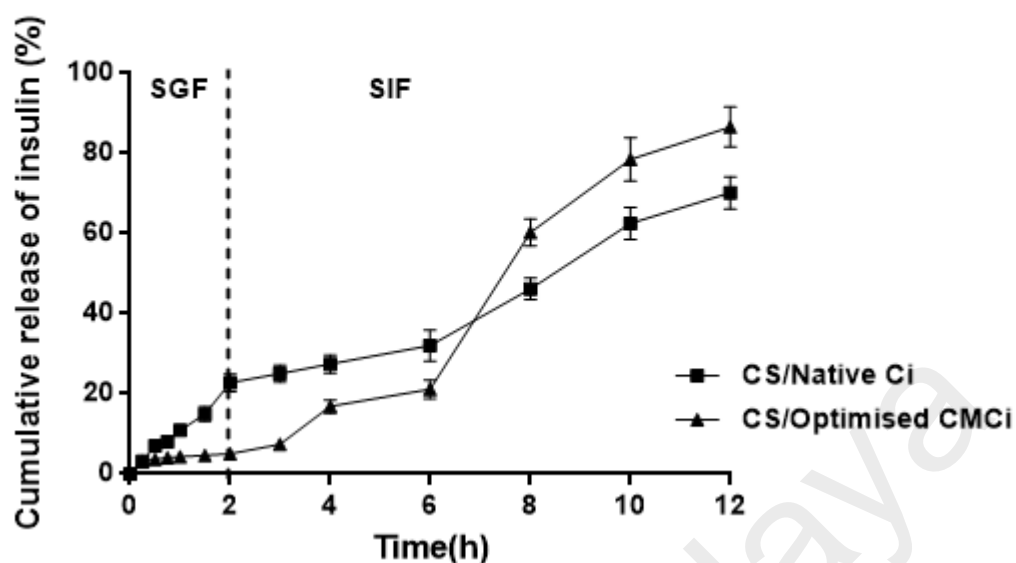
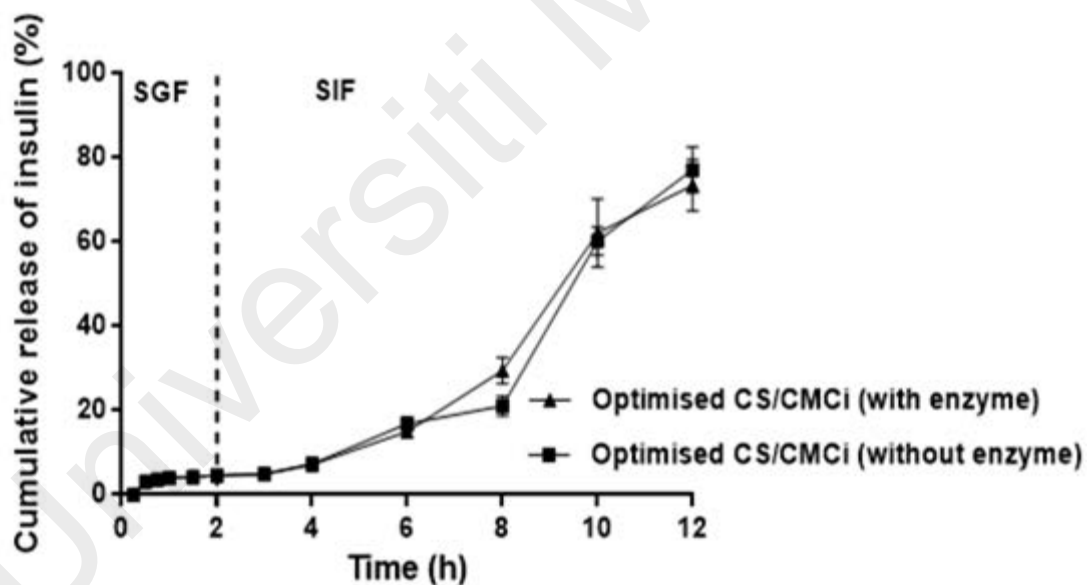
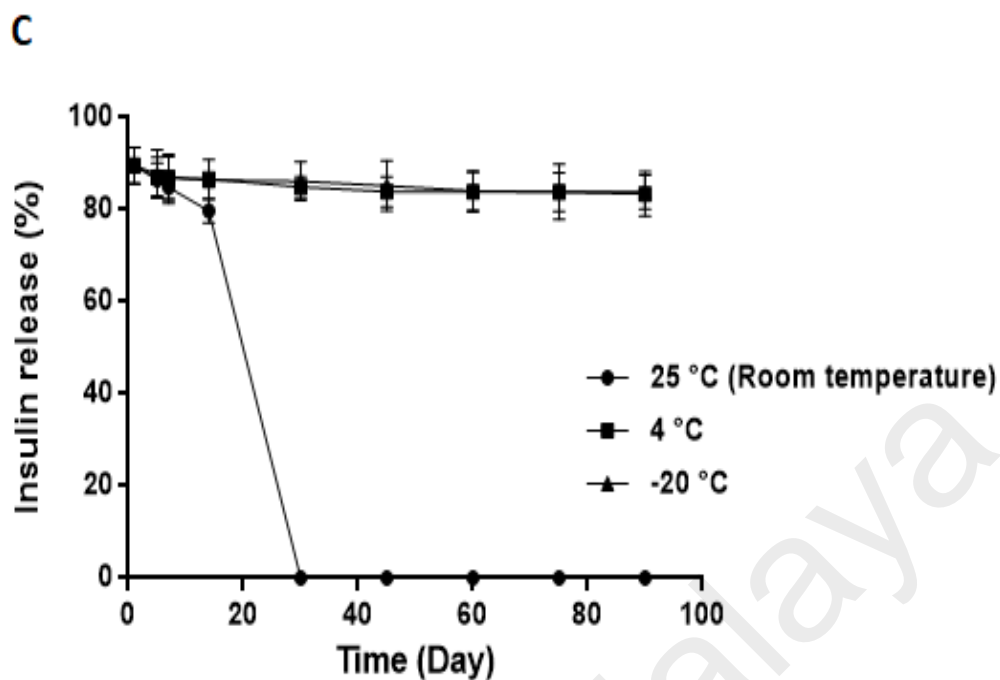
A**B**

Figure 4.10: (A) Release study of insulin from the optimised chitosan (CS)/carboxymethylated *iota*-carrageenan (CMCi) nanoparticles and native Ci/CS in simulated gastric fluid (SGF) (pH 1.2) and simulated intestinal fluid (SIF) (pH) 6.8 at 37°C. The results are presented as mean \pm SD (n = 3). (B) Release of insulin from the optimised CS/CMCi nanoparticles in SGF (pH 1.2) and SIF (pH) 6.8 at 37°C with enzymes (SGF with pepsin and SIF with trypsin) and without enzymes. The results are presented as the mean \pm SD (n = 3). (C) Insulin release (%) from the CS/CMCi nanoparticles stored at 25, 4 and -20°C over a period of 90 days compared to nanoparticles prepared at the starting point of experiment. The results are presented as the mean \pm SD (n = 3).

Figure 4.10, Continued



HPLC method for insulin analysis was used according to a previously described method (Leong *et al.*, 2011b). The insulin peak was detected at a retention time of 5.125 min (Figure 4.11(A)). The validation of the HPLC method showed good linearity ($R^2 = 0.9963$) (Figure 4.11(B)). The precision of the method, is determined by the coefficient of variance (CV) and accuracy being within the acceptable value of less than $\pm 15\%$ (U.S. Department of Health and Human Services Food and Drug Administration, 2001) (Table 4.7).

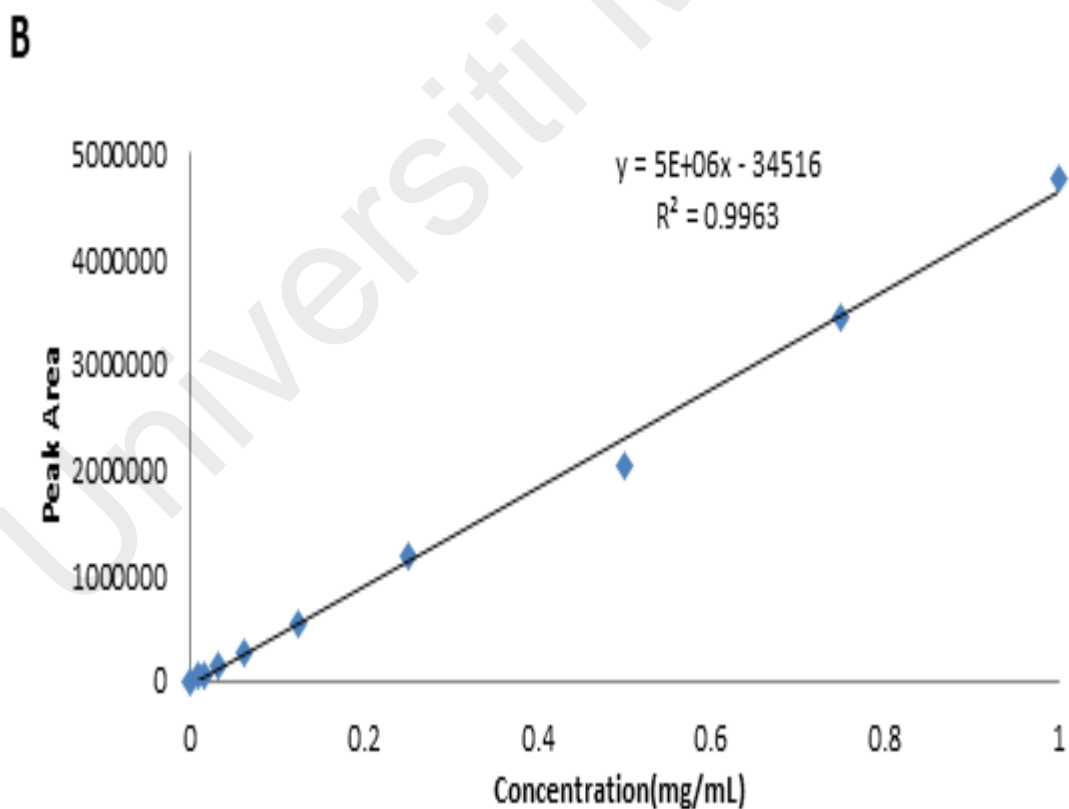
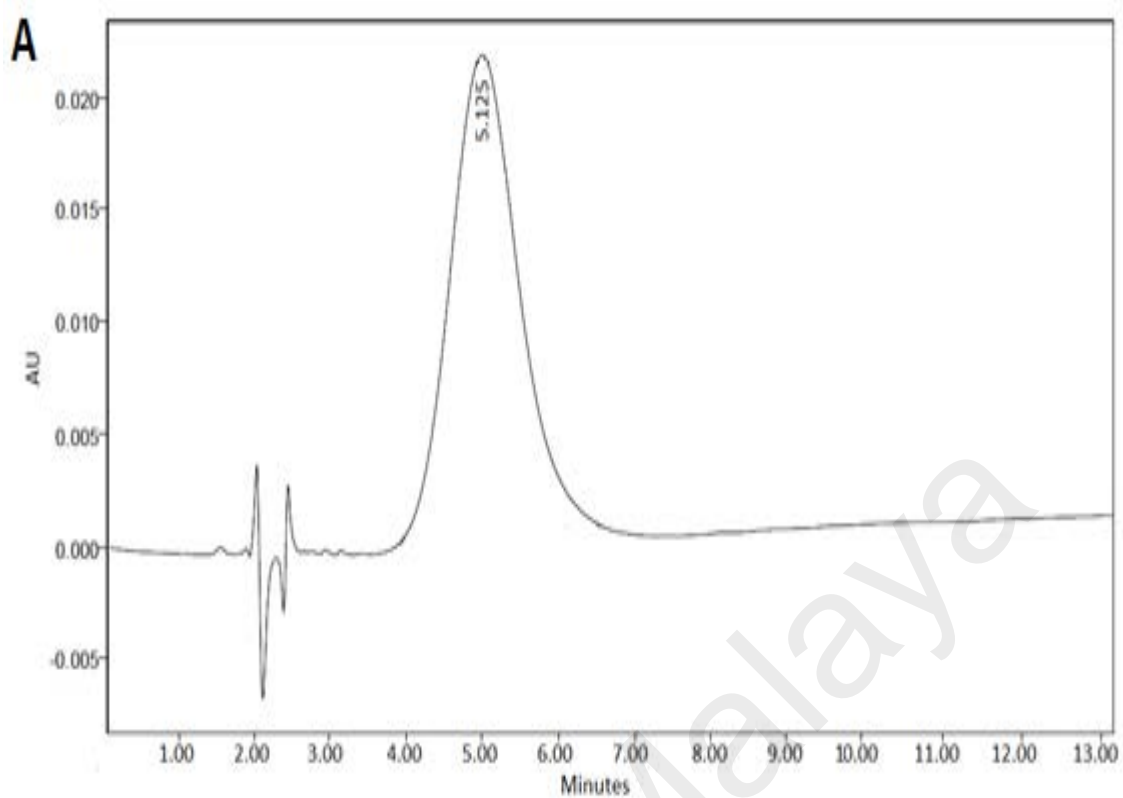


Figure 4.11: (A) Representative human recombinant insulin chromatogram (0.250 mg/mL). (B) Standard curve of human recombinant insulin (0.005–1.00 mg/mL).

Table 4.7: HPLC method validation of insulin.

Concentration ($\mu\text{g/mL}$)		Intraday ^a			Interday ^b		
		Mean \pm SD	CV (%) ^c	Accuracy (%) ^d	Mean \pm SD	CV (%) ^c	Accuracy (%) ^d
SGF	LOQ (3.00)	3.10 \pm 0.39	12.48	3.28	3.06 \pm 0.22	7.23	2.15
	Low (5.00)	4.58 \pm 0.31	6.76	-8.35	4.80 \pm 0.49	10.27	-3.91
	Medium (100.00)	96.00 \pm 6.27	6.53	-4.00	95.19 \pm 5.74	6.03	-4.81
	High (750.00)	742.82 \pm 16.76	2.26	-0.96	740.89 \pm 17.36	2.34	-1.21
SIF	LOQ (3.00)	2.90 \pm 0.21	7.23	-3.18	2.88 \pm 0.29	10.24	-3.99
	Low (5.00)	5.10 \pm 0.50	9.78	2.09	4.82 \pm 0.61	12.72	-3.42
	Medium (100.00)	97.51 \pm 8.31	8.52	-2.49	98.32 \pm 6.76	6.88	-1.68
	High (750.00)	741.12 \pm 13.67	1.84	-1.18	739.79 \pm 15.58	2.11	-1.36

LOQ: Limit of quantification.

a: Six replicate experiments were performed in the same day.

b: Experiments were performed for six days.

c: CV (%) calculated as (Standard deviation / Mean) \times 100%.

d: Accuracy calculated as (Concentration obtained - Actual concentration) / Actual concentration \times 100%.

4.7. Cytotoxicity study

The scientific community has raised concerns over the toxicity of polymeric nanoparticles. Therefore, it is essential to perform cytotoxicity study on new polymeric nanoparticles to ensure safety of the drug carrier (Grabowski *et al.*, 2013; Sandri *et al.*, 2010). Polymeric nanoparticles can improve bioavailability but may be toxic to cells. Increasing the nanoparticle's intestinal permeation may sometimes be harmful to intestinal mucosal cells. Caco-2 cells which morphologically and functionally mimic the intestinal tissue, are used to confirm the toxic effect of nanoparticles (Kean & Thanou, 2010; Kumari & Yadav, 2011). Hence, in this study, the principal objective of cytotoxicity assays is to investigate the viability of Caco-2 cells in the presence of CS/CMCi nanoparticles. Cytotoxicity is evaluated by determining both cell viability (MTS assay, Figure 4.12 A) and cell death (LDH assay, Figure 4.12 B). The MTS assay showed that CS/CMCi nanoparticles at 0.5–10 mg/mL had no discerning effect on its viability (Figure 4.12 A) with viability remaining more than 90%. CS/CMCi nanoparticles concentration of 20 mg/mL showed reduced cell viability from $81.7 \pm 3.5\%$ at Day 1 to $75.7 \pm 3.3\%$ at Day 3. Similarly, cell death increased from $7.2 \pm 1.1\%$ at Day 1 to $13.4 \pm 1.4\%$ at Day 3 (Figure 4.12 B), consistent with previously reported data using lectin functionalised carboxymethylated *kappa*-carrageenan (Leong *et al.*, 2011b). However, to increase the loading capacity of CMCi/CS nanoparticles requires less polymeric carrier to transport insulin across the intestinal epithelial tissue. Therefore, in the design of the polymeric insulin nanoparticles it is unlikely that concentration as high as 20 mg/mL is required.

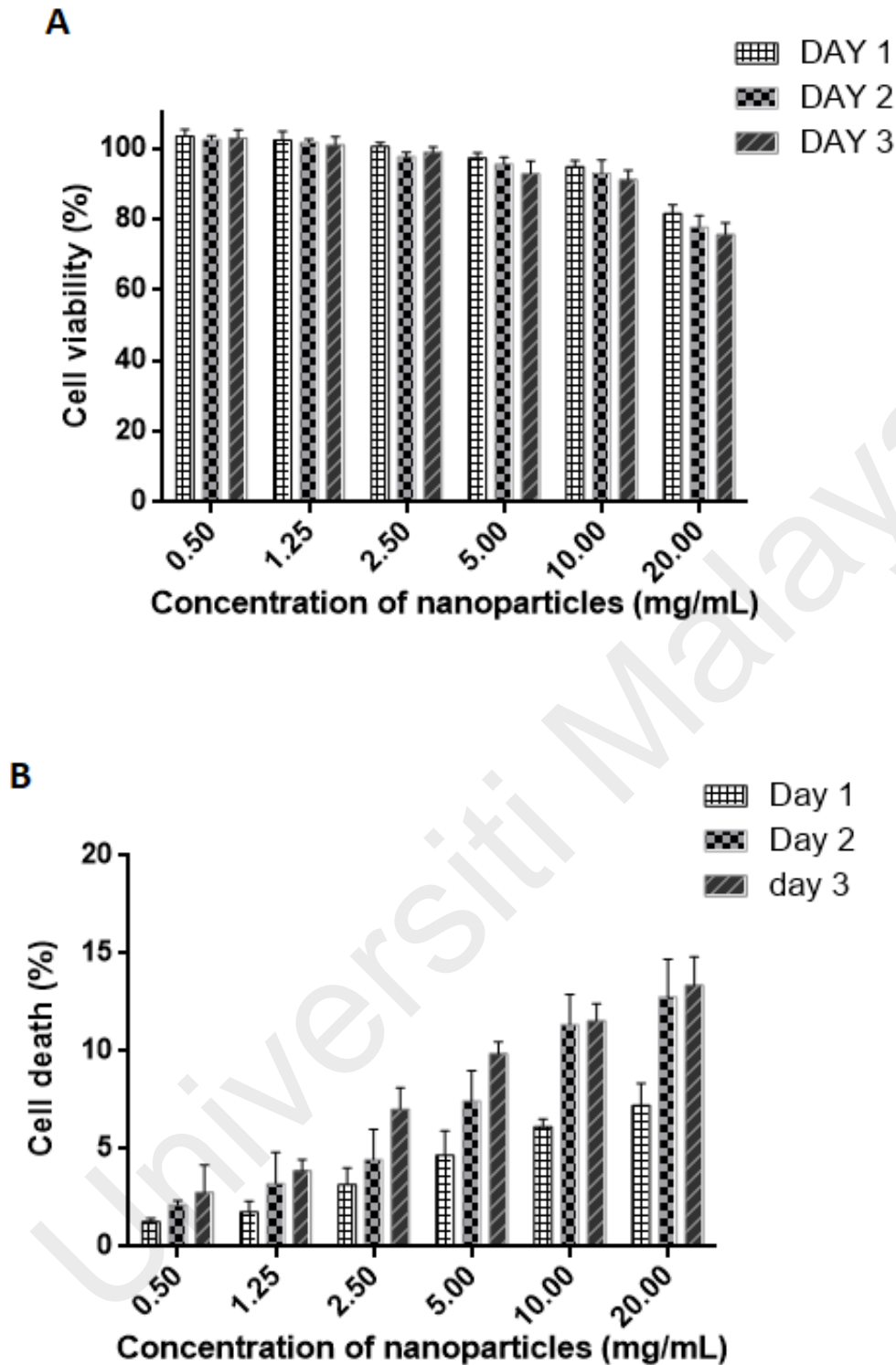


Figure 4.12: (A) Cell viability (%) of Caco-2 cells after incubation with CS/CMC nanoparticles at a concentration range of 0.5–20 mg/mL for 1, 2 or 3 days (MTS Assay). (B) Cell death (%) of Caco-2 cells after incubation with CS/CMC nanoparticles at a concentration range of 0.5–20 mg/mL for 1, 2 or 3 days (LDH Assay). The results are presented as the mean \pm SD (n = 6).

4.8. *In vitro* insulin membrane transport study

4.8.1. Parallel artificial membrane permeability assay (PAMPA)

The PAMPA assay is used to quickly estimate passive intestinal absorption of drugs (Koljonen *et al.*, 2008; Righeschi *et al.*, 2016). It is a simple alternative test to Caco-2 assay to study drug permeability (Kerns *et al.*, 2004). The study evaluated the ability of insulin from CS/CMC_i nanoparticles to diffuse from donor to acceptor compartment, through a PVDF membrane. The effective permeability (P_e) (cm/s) values (Eq.3.10) for insulin entrapped CS/CMC_i nanoparticles, insulin solution (control) along with the membrane integrity marker, lucifer yellow are listed in Table 4.8. Fluorescence intensity versus concentration (0.1–50 $\mu\text{g/mL}$) of the lucifer yellow was used to plot a standard curve for the calculation of lucifer yellow concentration (linearity, $R^2 = 0.998$) (Figure 4.13).

To achieve good membrane integrity the P_e (cm/s) value of lucifer yellow must be below 1×10^{-6} cm/s (Aungst *et al.*, 2000; Tirumalasetty & Eley, 2006). In this study, the P_e value of lucifer yellow was 0.06×10^{-6} cm/s, indicating that PAMPA membranes had good membrane integrity. Although a negligible amount of insulin solution was transported through the membranes (P_e , 0.13×10^{-6} cm/s), no permeation of insulin from the nanoparticles was observed. These results suggest that the insulin from the nanoparticles is unlikely to be transported passively through the intestinal membrane.

Table 4.8: The effective permeability (Pe) (cm/s) values and apparent permeability (Papp) coefficient values (cm/s) of the *in vitro* PAMPA and Caco-2 transport study.

Preparations	^a Pe × 10 ⁻⁶ (cm/s)	^a Papp × 10 ⁻⁶ (cm/s)
Insulin solution	0.13 ± 0.04 × 10 ⁻⁶	0.24 ± 0.02 × 10 ⁻⁶
Insulin entrapped CS/CMC <i>i</i> nanoparticles	Not detected	5.27 ± 0.23 × 10 ⁻⁶
Lucifer yellow	0.06 ± 0.01 × 10 ⁻⁶	-

a: The experimental values are expressed in mean ± SD; n = 3

-: No Papp coefficient value calculated for lucifer yellow in Caco-2 cells

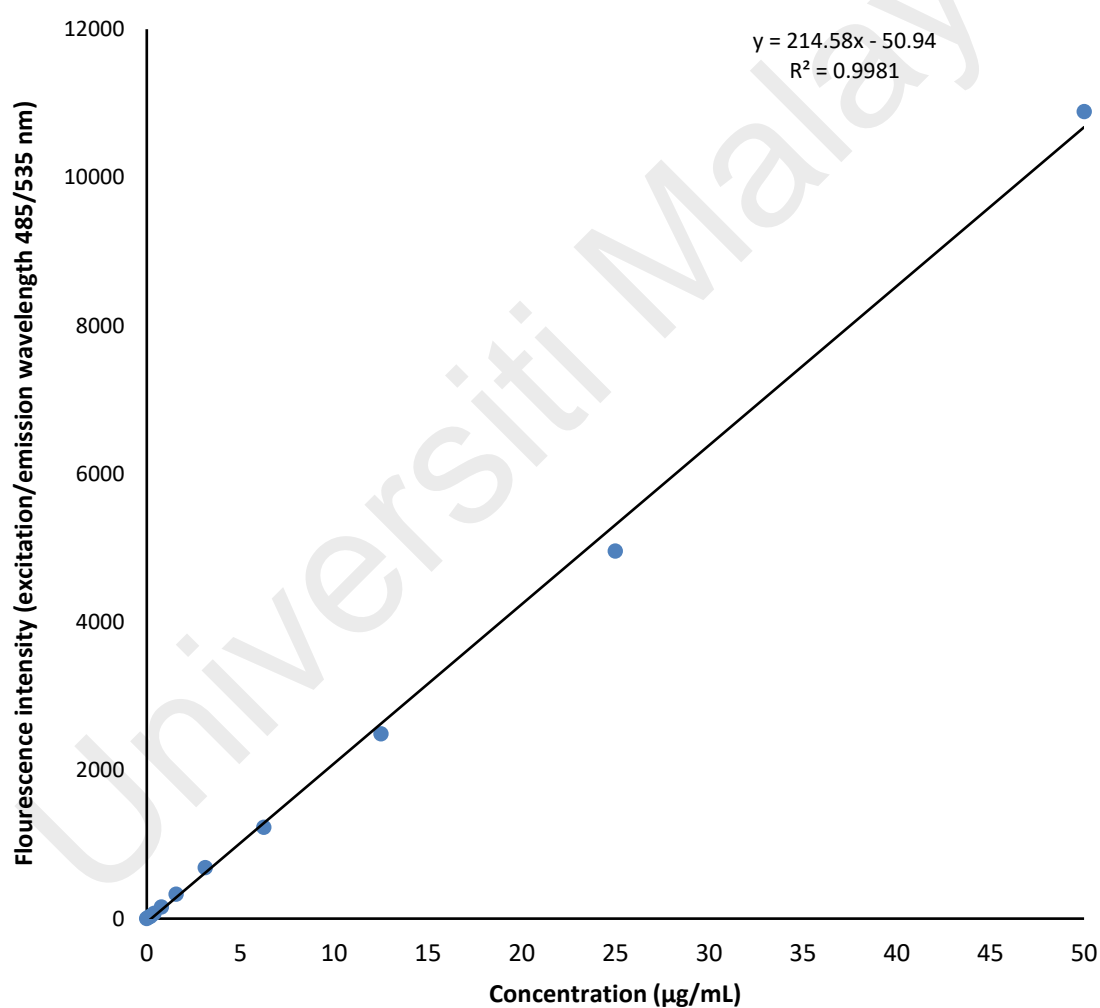


Figure 4.13: Standard curve of Lucifer yellow (0.01–50.00 µg/mL).

4.8.2. Transepithelial electrical resistance (TEER) measurement and transport of insulin by Caco-2 cells

Although PAMPA assay may predict the passive absorption of drugs, it does not account for active absorption (Kerns *et al.*, 2004). Meanwhile, Caco-2 cells possess segregated apical brush border epithelial tissue and TJs, which represent natural small-intestinal cells and appropriate for evaluating active transportation of drugs (Chenn *et al.*, 2016).

Transepithelial electrical resistance (TEER), measured in ohms, is used to evaluate the integrity of TJs in Caco-2 cell monolayer models used for transport study (Benson *et al.*, 2013). TJs presence in Caco-2 cells controls diffusion and permits the cell monolayers to form a permeable barrier, hence regulates the transport mechanism. The successful use of this model to estimate drug transport relies on the resemblance of this *in vitro* model with physiological *in vivo* barrier integrity (Srinivasan. *et al.*, 2015). In this study, the integrity of Caco-2 cell monolayer are observed by TEER ($\Omega \text{ cm}^2$) measurement and lucifer yellow rejection (%) test over a 21-day culture period (Table 4.9). At day 21, the TEER value was $648 \pm 8 \Omega \text{ cm}^2$ and the lucifer yellow rejection was $98.2 \pm 2.3\%$, confirming the confluency of Caco-2 cell monolayer for transport study (Niu *et al.*, 2014; Nkabinde *et al.*, 2012). Assessment of TEER of Caco-2 cells may also indicate the paracellular permeability of drug molecules (van der Merwe *et al.*, 2004). The opening of TJs leads to significant reduction of TEER value from paracellular transport of ions (Niu *et al.*, 2014). Figure 4.15 A shows a significant reduction in TEER value was observed for CS/CMCi nanoparticles compared to control ($p < 0.01$). However, after withdrawal of the nanoparticles (after 12 h), the TEER value gradually increased, showing restoration of the TJs. These results suggest that the nanoparticles may help in transitory and reversible opening of TJs between the Caco-2 cells (Figure 4.14). Different insulin entrapped chitosan coated nanoparticles have shown similar fluctuations in TEER value upon withdrawal in Caco-2 cells (Lin *et al.*, 2007).

Table 4.9: Caco-2 cell monolayer confluency measurement by TEER measurement and lucifer yellow rejection (%) test over a 21-day culture period.

Time (Days)	^{a,c} TEER ($\Omega \text{ cm}^2$)	^{b,c} Lucifer yellow rejection (%)
5	73 \pm 9	34.2 \pm 3.3
10	410 \pm 5	78.9 \pm 1.8
21	648 \pm 8	98.2 \pm 2.3

a: Calculated using Eq. 3.10.

b: Calculated using Eq. 3.11.

c: The experimental values are expressed in mean \pm SD; n = 3.

The cumulative amount of insulin from the nanoparticles that permeated through the Caco-2 cells is shown in Figure 4.15(B). The results show a significant amount of insulin from the nanoparticles permeated through the Caco-2 cells compared to the insulin solution ($p < 0.01$). The Papp coefficient values (cm/s) of the nanoparticles ($5.27 \pm 0.23 \times 10^{-6}$) was 22 times higher than insulin solution ($0.24 \pm 0.02 \times 10^{-6}$), attributed to the fact that insulin alone was unable to permeate across the intestine (as $P_{app} < 1 \times 10^{-6}$) (Niu *et al.*, 2014) (Table 4.8). However, the insulin entrapped CS/CMCi nanoparticles exhibited enhanced permeability across the paracellular pathway. From the results, the ability of CS/CMCi nanoparticles in assisting paracellular transport of insulin compared to insulin solution can be credited to the following. Mainly, the electrostatic interaction between positively charged chitosan and negatively charged cell surface caused the transitory opening of TJs (Lin *et al.*, 2007; Jin *et al.*, 2016). Additionally, the mucoadhesiveness of CS/CMCi nanoparticles (Table 4.6), support adherence of the nanoparticles to the mucosal surface, which extends insulin residence time on the surface. As a result, a greater insulin concentration gradient was created across the mucosal tissue, which assists insulin permeation. Similar results were obtained for other chitosan containing oral insulin formulations. Lin *et al.*, (2007), reported that CS coated nanoparticles helps transient and reversible opening of TJs between Caco-2 cells, which enhances paracellular permeability and increases insulin concentration across the intestinal epithelial cells. Liu *et al.*, (2016a) stated that *N*-trimethyl chitosan chloride coated poly(lactide-co-glycolide)-monomethoxy-

poly(polyethylene glycol) nanoparticles reversibly opens the TJs and helps insulin permeation through Caco-2 cells. The Papp coefficient values (cm/s) of the nanoparticles was 7.42×10^{-7} , 7 times higher than the insulin solution, showing better transport of insulin through Caco-2 cells. The insulin entrapped CS/CMC_i nanoparticles was 22 times higher compared to insulin solution, hence a better insulin transport. Figure 4.14 shows the schematic presentation of paracellular transport of insulin from insulin entrapped CS/CMC_i nanoparticles.

Universiti Malaya

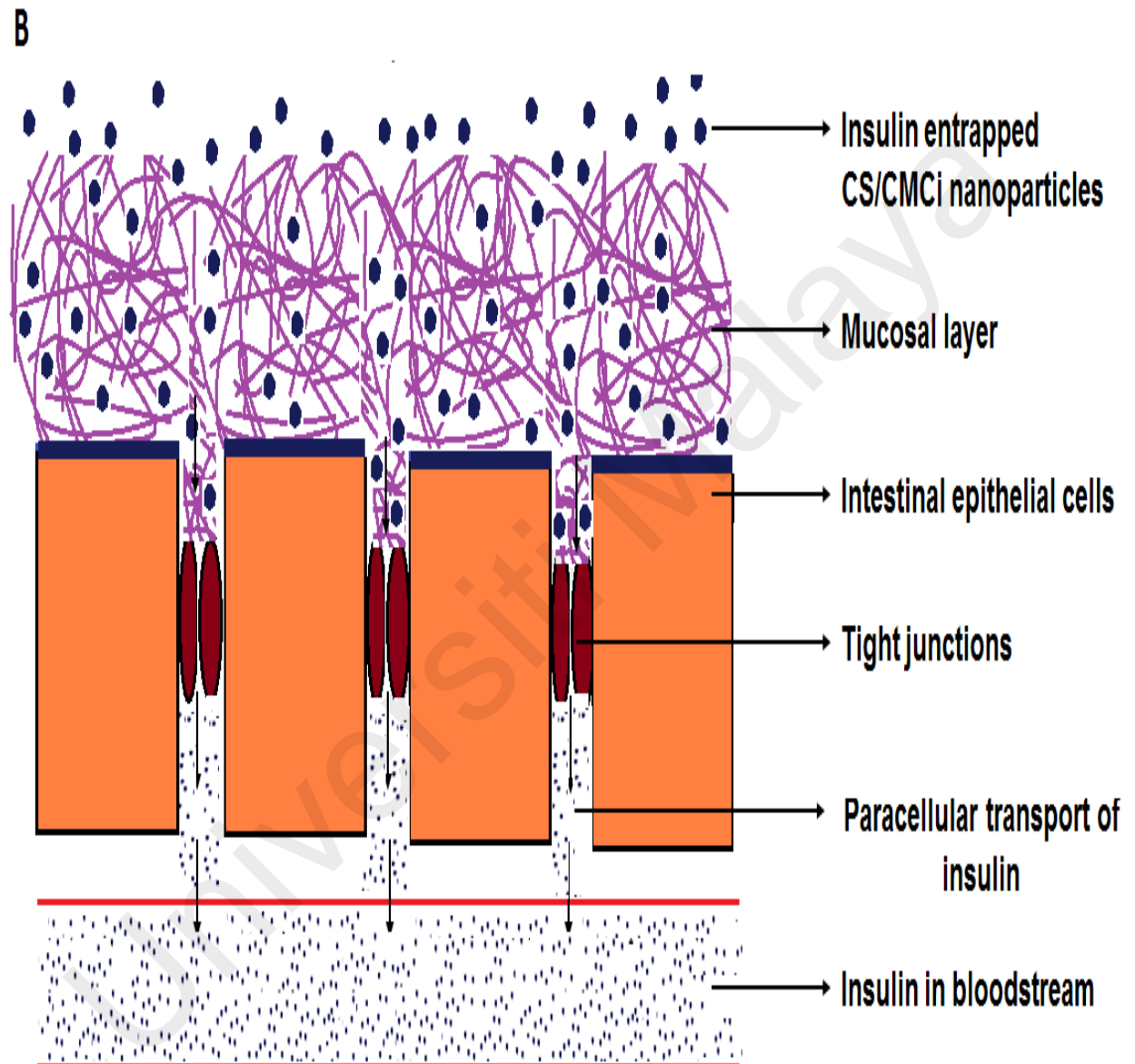
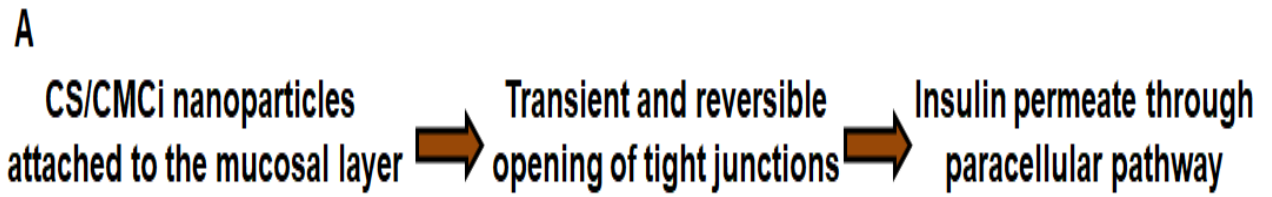


Figure 4.14: (A) Process of paracellular transport of insulin entrapped CS/CMC*i* nanoparticles. (B) Representative image of paracellular transport of insulin from insulin entrapped CS/CMC*i* nanoparticles.

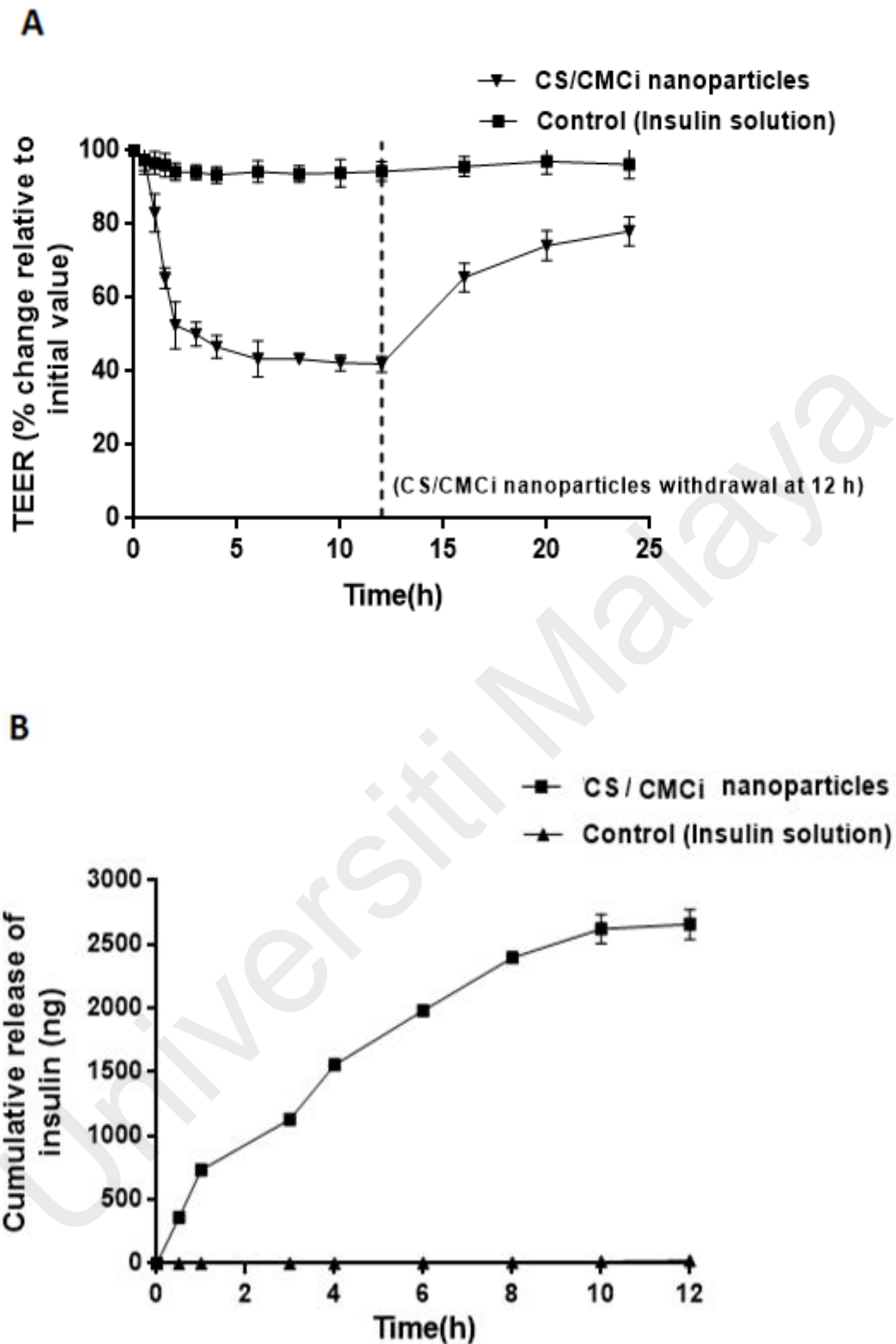


Figure 4.15: (A) TEER values of Caco-2 cells after incubation with 1.0 mg of insulin entrapped CS/CMC nanoparticles and control (insulin solution 0.2 mg/mL) (B) Cumulative amount of insulin permeated through Caco-2 cells after incubation with 1.0 mg of insulin entrapped CS/CMC nanoparticles and control (insulin solution 0.2 mg/mL). The results are presented as the mean \pm SD ($n = 3$).

4.9. *In vivo* hypoglycemic and bioavailability study

The results confirmed that the insulin entrapped nanoparticles were protected in the acidic environment of the stomach (Section 4.6), well attached to the intestinal epithelial tissue (Section 4.5), transiently pass through the TJs (Section 4.8), and biologically active in intestinal fluid (Section 4.6). Hence, the hypoglycemic effects of insulin nanoparticles in diabetic rats was measured in term of its bioavailability (Figure 4.16 (A and B)). The *in vivo* hypoglycemic data showed some relationships between *in vitro* bioactivity, mucoadhesiveness and cell studied. Predictably, the orally administered insulin solution (100 IU/kg) did not show significant hypoglycemic effects, due to degradation in the GIT and poor transportation across the intestinal epithelia. Similar results were obtained for empty nanoparticles and empty capsules. However, blood glucose levels decreased after 12 h of administration although no insulin was detected in the serum, possibly due to stress caused by hunger and blood sampling (Figure 4.16(A)) (Drenick *et al.*, 1964; Laffel, 1999). On the other hand, insulin entrapped CS/CMC_i nanoparticles controlled hyperglycemia likely due to insulin detected in the serum compared to the oral insulin solution (100 IU/kg). During this study, the blood glucose did not return to the initial level, which may be due to hunger and insulin. Similar hypoglycemic effects were reported in previous studies (Sonaje *et al.*, 2009; Jin *et al.*, 2012; Li *et al.*, 2013a). The correspondent serum insulin versus time plot is depicted in Figure 4.16 (B). No observable serum insulin was found in oral insulin solution (100 IU/kg), empty CS/CMC_i nanoparticles and empty capsules treated diabetic rats. Subcutaneous injection of insulin solution (2 IU/kg), showed a peak serum insulin concentration 1 h post-injection, whereas orally administered insulin nanoparticles (100 IU/kg) showed a peak concentration after 5 h and lasted up to 24–30 h. The subcutaneous injection of insulin may cause acute hypoglycemic trauma as well as patient discomfort, which are the disadvantages of the current route of administration (Soares *et al.*, 2012; Shah *et al.*, 2016). However, insulin entrapped CS/CMC_i nanoparticles showed

controlled hypoglycemic effect without the sudden hypoglycemic peak observed with subcutaneous insulin injection, indicating its appeal in basal insulin management of diabetes.

The pharmacokinetic data such as C_{max} , T_{max} and AUC_{0-36} of subcutaneous insulin injection (2 IU/kg) and insulin entrapped CS/CMC_i nanoparticles (25, 50 and 100 IU/kg) and the relative bioavailability (BA (%)) are shown in Table 4.10. The BA (%) for the various doses of insulin nanoparticles (25, 50 and 100 IU/kg) was between 13.6–16.1%. The highest BA (16.1%) achieved improved on previous lectin-functionalized microparticles (14.8%) with a similar dosage of 100 IU/kg (Leong *et al.*, 2011b). The CS/CMC_i nanoparticles at 25 and 50 IU/kg showed better BA (%) compared to previous studies. Sonaje *et al.*, (2009) reported that oral administration of insulin entrapped pH-responsive chitosan complexed poly-g-glutamic acid nanoparticles (insulin 30 IU/kg) showed a hypoglycemic effect for 10 h in diabetic rats with relative bioavailability of $15.1 \pm 0.9\%$. He *et al.* (2013), studied insulin (30 IU/kg) loaded microspheres formulated from arginine-based poly(ester amide) and l-lysine-/l-leucine-based poly(ester amide) with a pendant COOH groups. The microspheres successfully controlled blood glucose level for 10 h in diabetic rats with relative bioavailability of $5.89 \pm 1.84\%$. Ansari *et al.* (2016) showed that solid lipid nanoparticles of glyceryltrimyristate with soy lecithin and polyvinyl alcohol (insulin 30 IU/kg) exhibited relative bioavailability of 8.26% compared to oral insulin solution (insulin 30 IU/kg), which showed relative bioavailability of 1.7%.

It has been shown that intestinal absorption of drugs in animal models and humans are similar (Cao *et al.*, 2006). Thus, the intestinal absorption of insulin from CS/CMC_i nanoparticles in rats used in this study is expected to be similar if administered to humans. However, the correlation of oral bioavailability of drugs between rats and humans is rather weak (Cao *et al.*, 2006; Musther *et al.*, 2014). Nonetheless, it is expected that bioavailability of oral drugs is often higher in humans compared to rats. In spite of the potential inaccuracies (low correlation coefficient), the study tried to estimate insulin bioavailability using its data on rats combined with correlation analysis of oral drug bioavailability between rats and humans from

two previous studies ($F_{\text{human}} = 0.544 F_{\text{rat}} + 35.759$; $R^2 = 0.287$ (Musther *et al.*, 2014) and $F_{\text{human}} = 0.5918 F_{\text{rat}} + 37.358$; $R^2 = 0.2917$ (Cao *et al.*, 2006), where F_{human} is human oral bioavailability, F_{rat} is rat oral bioavailability and R^2 is coefficient of determination. The estimated insulin bioavailability of CS/CMC*i* nanoparticles in humans (insulin 100 IU/kg) were 44.7% and 46.9%, respectively. In another study, monosodium N-(4-chlorosalicyloyl)-4-aminobutyrate with insulin (300 IU) capsules, orally administered to 10 male type 2 diabetes patients showed a swift action with bioavailability of $26 \pm 28\%$ between 0–1 h that lasted less than 6 h (Kapitza *et al.*, 2010). Thus, it is conceivable that the bioavailability of the nanoparticles in humans is potentially 3 times higher than between 13.6–16.1% in rats.

In summary, our hypoglycemic results are promising, avoiding several obstacles with oral insulin delivery and showed extended blood glucose lowering effect lasting up to 24–30 h. This suggests that paracellular transport of insulin facilitated by chitosan allows a considerable quantity of insulin to permeate through the intestinal wall into systemic circulation. Moreover, the pH-responsive carboxymethylated *iota*-carrageenan also protects the entrapped insulin from enzymatic degradation. Hence, the combined effects improve the bioavailability of the administered insulin compared to previously reported study (Leong *et al.*, 2011b).

Table 4.10: Pharmacokinetic data of insulin in diabetic rats after subcutaneous injection of insulin solution or oral administration of insulin entrapped CS/CMCi nanoparticles.

Preparations (Insulin dose)	^{a,e} C _{max} (mIU/L)	^{b,e} T _{max} (h)	^{c,e} AUC _{0-36h}	^{d,e} BA (%)
Subcutaneous injection (2 IU/kg)	121.3 ± 13.5	1	222.5 ± 53.3	100
CS/CMCi nanoparticles (25 IU/kg)	45.6 ± 8.5 ^f	3	432.3 ± 63.2 ^f	15.5 ± 2.5 ^f
CS/CMCi nanoparticles (50 IU/kg)	64.6 ± 15.0 ^f	3	754.3 ± 60.9 ^f	13.6 ± 1.2 ^f
CS/CMCi nanoparticles (100 IU/kg)	175.1 ± 23.7 ^f	5	1789.4 ± 158.6 ^f	16.1 ± 1.6 ^f

a: C_{max} is the maximum serum insulin concentration.

b: T_{max} is the time taken to reach maximum concentration.

c: AUC_{0-36h} is the area under the serum insulin concentration time curve (0-36h).

d: BA (%) is the relative bioavailability calculated using Eq. 3.14.

e: The experimental values are expressed in mean ± SD; n = 6.

f: $p < 0.05$ compared to subcutaneous injection (2 IU/kg).

Universiti Malaysia

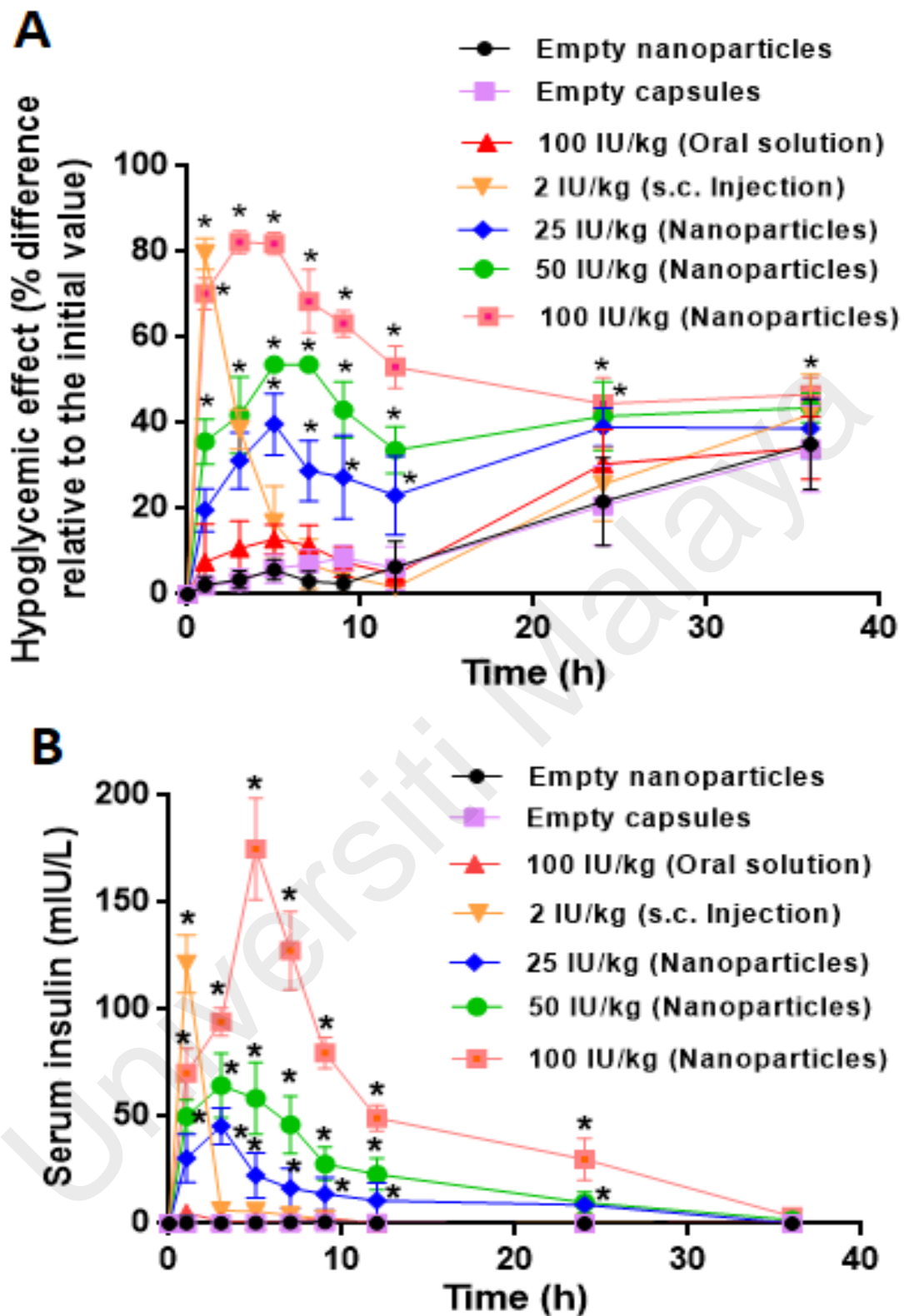


Figure 4.16: (A) Blood glucose levels in diabetic SD rats after subcutaneous or oral administration of various preparations. (B) Serum insulin levels in diabetic SD rats after subcutaneous or oral administration of various preparations. The results are presented as the mean \pm SD ($n = 6$). * $p < 0.05$ compared to empty nanoparticles, empty capsules or oral insulin solution (100 IU/kg).

CHAPTER 5: CONCLUSION, LACUNAE AND FUTURE

5.1. Conclusion

We have successfully synthesised carboxymethylated *iota*-carrageenan using a four-factor and three level Box-Behnken design. The NMR and FT-IR spectra confirm the carboxymethylation of *iota*-carrageenan. The RSM^{MSI} model successfully optimised the preparation of insulin-containing CS/CMC_i nanoparticles. The experimental values of CS/CMC_i nanoparticles prepared under optimum conditions were similar to the predicted values (% error below ± 10). The drug loading content and entrapment efficiency were $10.7 \pm 0.6\%$ and $86.9 \pm 2.6\%$, respectively. The corresponding TEM and FESEM images showed that the optimised nanoparticles had a spherical, dense core with a porous outer layer and a particle size of approximately 313 nm (dry particles). In wet conditions, the mean particle size was 613 nm. A high percentage of mucoadhesion ($79.1 \pm 4.3\%$), suggests that the nanoparticles have good mucoadhesive property, leading to better drug permeation. The drug-release behaviour of the nanoparticles exhibited diffusion- and swelling-controlled release in SGF and swelling-controlled release in SIF. The insulin entrapped in the nanoparticles was released at a low level (approximately 5%) in SGF and at a high level (approximately 86%) in SIF. More importantly, the insulin retained its bioactivity and stability in simulated enzymatic environment of the GIT with pepsin and trypsin. The nanoparticles were also stable for up to 3 months stored between 4 and -20°C and for up to 7 days at room temperature. The nanoparticles were compatible with Caco-2 cells as cell death and cell viability were within the limits observed in a 3 day study. The nanoparticles showed a paracellular transport across the Caco-2 cell monolayers and apparent permeability coefficients (P_{app}) 22 times higher than control insulin solution, suggesting the transient and reversible opening of tight junctions (TJs). The *in vivo* study on diabetic SD rats showed extended blood glucose lowering effect and prolonged insulin detection up to 24–30 h. Moreover, the relative bioavailability of insulin was about 16.1% over

36 h (insulin 100 IU/kg). The results suggest that CS/CMC_i nanoparticles may be employed as an oral insulin delivery system, and the extended glycemic control makes it specifically convenient for basal insulin therapy.

Universiti Malaya

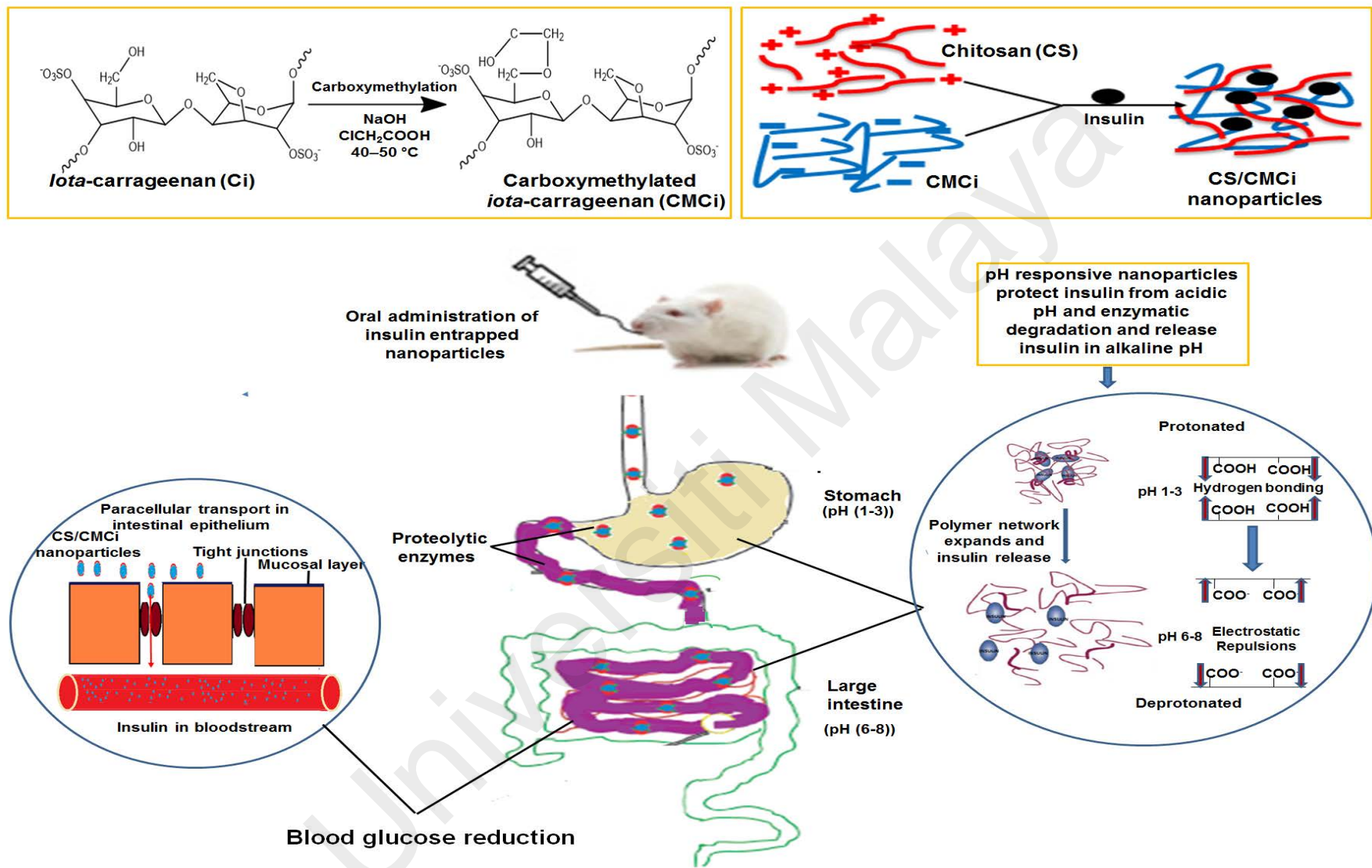


Figure 5.1: Summary of insulin entrapped CS/CMCi nanoparticles study.

5.2. Lacunae and future works

This study primarily focused on the formulation of pH responsive CS/CMC_i nanoparticles and their application to improve bioavailability of oral insulin. The main goal of this nanoparticulate polymeric carrier is to protect insulin from the harsh acidic environment of the stomach and proteolytic enzymes, enhance transport across the mucosal barrier and improve oral bioavailability. However, the size of the nanoparticles is one limitation. The TEM and FESEM images showed that the optimized nanoparticles had a spherical, dense core with a porous outer layer and a particle size of approximately 313 nm (dry particles). In wet conditions, the mean particle size was 613 nm. Ultrasonication can be used to break the nanoparticle aggregates, hence reducing its size (Kim *et al.*, 2013). However, ultrasonication may degrade insulin by changing its secondary structure and bioactivity (Lopes *et al.*, 2015; Santos *et al.*, 2013). Hence, a mild polyelectrolyte complexation method is used to avoid deleterious organic solvents or harsh mechanical force to formulate the nanoparticles (Grenha *et al.*, 2010).

Study on the effect of particle size and swelling on the cellular uptake revealed that as the nanoparticle swells more drug released from the nanoparticle, which results in a concentration gradient, hence improve the cellular uptake (Zheng *et al.*, 2016). In the future, cellular uptake of insulin entrapped in the CS/CMC_i nanoparticles can be investigated using fluorescent labelled insulin and be observed using an epifluorescence optics equipped microscope. Additionally, the opening of TJs can be visualised by staining with tetramethylrhodamine B isothiocyanate–phalloidin and observing this using a confocal laser scanning microscope (Niu *et al.*, 2014).

An *in vivo* imaging system can be used to observe luminescence images of nanoparticles given to rats using oral gavage. Since the CS/CMC_i nanoparticles are intended to adhere to intestinal mucosa and exhibit drug release, it would be interesting to observe the nanoparticles using *in vivo* imaging. Briefly, fluorescein labelled nanoparticles can be given by oral gavage

to live Wistar rats. The animals may subsequently cut open in the abdomen to expose the GIT and the *in vivo* luminescence imaging can be performed with luminescence imaging system (Niu *et al.*, 2014).

It has been estimated that CS/CMC_i nanoparticles are stable upto 90 days when stored at 4 and -20°C . Hence, further study on improving the storage stability of insulin nanoparticles can be carried out by using various stabilizing agents such as poloxamers, celluloses, soluplus etc.

Universiti Malaya

REFERENCES

- Abad, L. V., Relleve, L. S., Aranilla, C. T. and Rosa, A. M. D. (2003). Properties of radiation synthesised PVP-kappa carrageenan hydrogel blends. *Radiation Physics and Chemistry*, 68: 901–908.
- Agarwal, V., Reddy, I. K. and Khan, M. (2000). Oral delivery of proteins: effect of chicken and duck ovomucoid on the stability of insulin in the presence of a-chymotrypsin and trypsin. *Pharmacy and Pharmacology Communications*, 6: 223–227.
- Agrawal, A. K., Harde, H., Thanki, K. and Jain, S. (2014). Improved stability and antidiabetic potential of insulin containing folic acid functionalized polymer stabilized multilayered liposomes following oral administration. *Biomacromolecules*, 15(1): 350–360.
- Agu, R. U., Ugwoke, M. I., Armand, M., Kinget, R. and Verbeke, N. (2001). The lung as a route for systemic delivery of therapeutic proteins and peptides. *Respiratory Research*, 2(4): 198–209.
- Ahmad, N., Mohd Amin, M. C., Ismail, I. and Buang, F. (2016). Enhancement of oral insulin bioavailability: *in vitro* and *in vivo* assessment of nanoporous stimuli-responsive hydrogel microparticles. *Expert Opinion on Drug Delivery*, 13(5): 621–632.
- Alai, M. S., Lin, W. J. and Pingale, S. S. (2015). Application of polymeric nanoparticles and micelles in insulin oral delivery. *Journal of Food and Drug Analysis*, 23(3): 351–358.
- Alam, M. A., Al-Jenoobi, F. I. and Al-Mohizea, A. M. (2012). Everted gut sac model as a tool in pharmaceutical research: limitations and applications. *Journal of Pharmacy and Pharmacology*, 64(3): 326–336.
- Amin, A., Shah, T., Patel, J. and Gajjar, A. (2008). Non-invasive insulin: Annual update on non-invasive insulin delivery technology. *Drug Delivery Technology*, 8(3): 43–48.
- Amini, M. and Parvaresh, E. (2009). Prevalence of macro- and microvascular complications among patients with type 2 diabetes in Iran: A systematic review. *Diabetes Research and Clinical Practice*, 83(1): 18–25.
- Andrews, S., Lee, J. W., Choi, S. O. and Prausnitz, M. R. (2011). Transdermal insulin delivery using microdermabrasion. *Pharmaceutical Research*, 28(9): 2110–2118.
- Ansari, M. J., Anwer, M. K., Jamil, S., Al-Shdefat, R., Ali, B. E., Ahmad, M. M. and Ansari, M. N. (2016). Enhanced oral bioavailability of insulin-loaded solid lipid nanoparticles:

pharmacokinetic bioavailability of insulin-loaded solid lipid nanoparticles in diabetic rats. *Drug Delivery*, 23(6): 1972–1979.

Aungst, B. J. (2000). Intestinal permeation enhancers. *Journal of Pharmaceutical Sciences*, 89(4): 429–442.

Aungst, B. J., Nguyen, N. H., Bulgarelli, J. P. and Oates-Lenz, K. (2000). The influence of donor and reservoir additives on Caco-2: permeability and secretory transport of HIV protease inhibitors and other lipophilic compounds. *Pharmaceutical Research*, 17(10): 1175–1180.

Bailey, C. J. and Barnett, A. H. (2007). Why is Exubera being withdrawn? *British Medical Journal*, 335: 1156.

Banerjee, A., Lee, J. H. and Mitragotri, S. (2016). Intestinal mucoadhesive devices for oral delivery of insulin. *Bioengineering and Translational Medicine*, 1: 338–346.

Benson, K., Cramer, S. and Galla, H. J. (2013). Impedance-based cell monitoring: barrier properties and beyond. *Fluids and Barriers of CNS*, 10(1): 5.

Bernkop-Schnürch, A. (1998). The use of inhibitory agents to overcome the enzymatic barrier to perorally administered therapeutic peptides and proteins. *Journal of Controlled Release*, 52(1–2): 1–16.

Bernstein, G. (2008). Delivery of insulin to the buccal mucosa utilizing the RapidMist system. *Expert Opinion on Drug Delivery*, 5(9): 1047–1055.

Bhattarai, N., Gunn, J. and Zhang, M. (2010). Chitosan-based hydrogels for controlled, localized drug delivery. *Advanced Drug Delivery Reviews*, 62(1): 83–99.

Campo, V. L., Kawano, D. F., da Silva, D. B. and Carvalho, I. (2009). Carrageenans: Biological properties, chemical modifications and structural analysis-A review. *Carbohydrate Polymers*, 77(2): 167–180.

Cao, X., Gibbs, S. T., Fang, L., Miller, H. A., Landowski, C. P., Shin, H. ... Sun, D. (2006). Why is it challenging to predict intestinal drug absorption and oral bioavailability in human using rat? *Pharmaceutical Research*, 23(8): 1675–1686.

Chaplin, S. and Bain, S. (2016). Properties of GLP-1 agonists and their use in type 2 diabetes. *Prescriber*, 27(1): 43–46.

- Charoo, N. A., Rahman, Z., Repka, M. A. and Murthy, S. N. (2010). Electroporation: An avenue for transdermal drug delivery. *Current Drug Delivery*, 7: 125–136.
- Chaturvedi, K., Ganguly, K., Nadagouda, M. N. and Aminabhavi, T. M. (2013). Polymeric hydrogels for oral insulin delivery. *Journal of Controlled Release*, 165: 129–138.
- Chaubey, P., Mishra, B., Mudavath, S. L., Patel, R. R., Chaurasia, S. ... Monteiro, M. (2018). Mannose-conjugated curcumin-chitosan nanoparticles: Efficacy and toxicity assessments against *Leishmania donovani*. *International Journal of Biological Macromolecules*, 111: 109–120.
- Chen, L., Magliano, D. J. and Zimmet, P. Z. (2011a). The worldwide epidemiology of type 2 diabetes mellitus-present and future perspectives. *Nature Reviews Endocrinology*, 8(4): 228–236.
- Chen, M. C., Sonaje, K., Chen, K. J. and Sung, H. W. (2011b). A review of the prospects for polymeric nanoparticle platform in oral insulin delivery. *Biomaterials*, 32: 9826–9838.
- Cheng, L., Bulmer, C. and Margaritis, A. (2015). Characterisation of novel composite alginate chitosan-carrageenan nanoparticles for encapsulation of BSA as a model drug delivery system. *Current Drug Delivery*, 12: 351–357.
- Chenn, L., Lu, X., Liang, X., Hong, D., Guan, Z., Guan, Y. and Zhu, W. (2016). Mechanistic studies of the transport of peimine in the Caco-2 cell model. *Acta Pharmaceutica Sinica B*, 6(2): 125–131.
- Cody, B., Argyrios, M. and Anargyros, X. (2012). Encapsulation and controlled release of recombinant human erythropoietin from chitosan-carrageenan nanoparticles. *Current Drug Delivery*, 9(11): 527–537.
- Cosson, E., Carbillon, L. and Valensi, P. (2017). High fasting plasma glucose during early pregnancy: A review about early gestational diabetes mellitus. *Journal of Diabetes Research*, 2017: 1–12.
- Damgé, C., Maincent, P. and Ubrich, N. (2007). Oral delivery of insulin associated to polymeric nanoparticles in diabetic rats. *Journal of Controlled Release*, 117: 163–170.
- De Meyts, P. (2004). Insulin and its receptor: Structure, function and evolution. *Bioessays*, 26(12): 1351–1362.

- Degim, Z., Unal, N., Essiz, D. and Abbasoglu, U. (2004). The effect of various liposome formulations on insulin penetration across Caco-2 cell monolayer. *Life Sciences*, 75(23): 2819–2827.
- Ding, J., He, R., Zhou, G., Tang, C. and Yin, C. (2012). Multilayered mucoadhesive hydrogel films based on thiolated hyaluronic acid and polyvinylalcohol for insulin delivery. *Acta Biomaterialia*, 8(10): 3643–3651.
- Diop, M., Auberval, N., Viciglio, A., Langlos, A., Bietiger, W., Mura, C. ... Sigrist, S. (2015). Design, characterisation, and bioefficiency of insulin–chitosan nanoparticles after stabilisation by freeze-drying or cross-linking. *International Journal of Pharmaceutics*, 491(1–2): 402–408.
- Dipiro, J. T., Talbert, R. L., Yee, G. C., Matzke, G. R., Wells, B. G. and Posey, L. M. (2011). *Pharmacotherapy, A Pathophysiologic Approach* (8th ed.). United States of America: Mc-Graw Hill, 1255–1299.
- Drenick, E. J., Swendseid, M. E., Bland, W. H. and Tuttle, S. G. (1964). Prolonged starvation as treatment for severe obesity. *The Journal of the American Medical Association*, 187(2): 100–105.
- Dollo, G., LeCorre, P., Gue'rin, A., Chevanne, F., Burgot, J. L. and Leverage, R. (2003). Spray dried redispersible oil-in-water emulsion to improve oral bioavailability of poorly soluble drugs. *European Journal of Pharmaceutical Sciences*, 19(4): 273–280.
- Duan, X. and Mao, S. (2010). New strategies to improve the intranasal absorption of insulin. *Drug Discovery Today*, 15(11–12): 416–427.
- Dudhani, A. R. and Kosaraju, S. L. (2010). Bioadhesive chitosan nanoparticles: Preparation and characterisation. *Carbohydrate Polymers*, 81: 243–251.
- Elomaa, M., Asplund, T., Soininen, P., Laatikainen, R., Peltonen, S., Hyvarinen, S. and Urtili, A. (2004). Determination of the degree of substitution of acetylated starch by hydrolysis, ¹HNMR and TGA/IR. *Carbohydrate Polymers*, 57: 261–267.
- Erdoğan, M., Hizal, G., Tunca, Ü., Hayrabetyan, D. and Pekcan, Ö. (2002). Molecular weight effect on swelling of polymer gels in homopolymer solutions: a fluorescence study. *Polymer*, 43(6): 1925–1931.
- Fan, L., Wang, L., Gao, S., Wu, P., Li, M., Xie, W., Liu, S. and Wang, W. (2011). Synthesis, characterisation and properties of carboxymethyl *kappa* carrageenan. *Carbohydrate Polymers*, 86: 1167–1174.

- Farag, R. K. and Mohamed, R. R. (2013). Synthesis and characterisation of carboxymethyl chitosan nanogels for swelling studies and antimicrobial activity. *Molecules*, 18: 190–203.
- Farrar, D., Tuffnell, D. J., West, J. and West, H. M. (2016). Continuous subcutaneous insulin infusion versus multiple daily injections of insulin for pregnant women with diabetes. *Cochrane Database of Systematic Reviews*, 6: 1–56.
- Fennell, D. (2009). Oral insulin conditionally approved by FDA. Available from: <https://www.diabetesselfmanagement.com/blog/oral-insulin-conditionally-approved-by-fda/> [Last accessed on 2018 Feb 23].
- Fernández-Urrusuno, R., Calvo, P., Remuñán-López, C., Vila-Jato, J. L. and Alonso, M. J. (1999). Enhancement of nasal absorption of insulin using chitosan nanoparticles. *Pharmaceutical Research*, 16(10): 1576–1581.
- Fonte, P., Araújo, F., Reis, S. and Sarmiento, B. (2013). Oral insulin delivery: How far are we? *Journal of Diabetes Science and Technology*, 7(2): 520–531.
- Fonte, P., Araújo, F., Silva, C., Pereira, C., Reis, S., Santos, H. A. and Sarmiento, B. (2015). Polymer-based nanoparticles for oral insulin delivery: Revisited approaches. *Biotechnology Advances*, 33: 1342–1354.
- Foss, A. C., Goto, T., Morishita, M. and Peppas, N. A. (2004). Development of acrylic-based copolymers for oral insulin delivery. *European Journal of Pharmaceutics and Biopharmaceutics*, 57(2): 163–169.
- Goldberg, M. and Gomez-Orellana, I. (2003). Challenges for the oral delivery of macromolecules. *Nature Reviews Drug Discovery*, 2(4): 289–295.
- Grabowski, N., Hillaireau, H., Vergnaud, J., Santiago, L. A., Kerdine-Romer, S., Pallardy, M. ... Fattal, E. (2013). Toxicity of surface-modified PLGA nanoparticles toward lung alveolar epithelial cells. *International Journal of Pharmaceutics*, 454(2): 686–694.
- Gradel, A. K. J., Porsgaard, T., Lykkesfeldt, J., Seested, T., Gram-Nielsen, S., Kristensen, N. R. ... Refsgaard, H. H. F. (2018). Factors Affecting the Absorption of Subcutaneously Administered Insulin: Effect on Variability. *Journal of Diabetes Research*, 2018: 1–17.

- Grenha, A., Gomes, M. E., Rodrigues, M., Santo, V. E., Mano, J. F., Neves, N. M. and Reis, R. L. (2010). Development of new chitosan/carrageenan nanoparticles for drug delivery applications. *Journal of Biomedical Materials Research, A*, 92(4): 1265–1272.
- Gupta, N. V. and Shivakumar, H. V. (2012). Investigation of swelling behavior and mechanical properties of a pH-sensitive superporous hydrogel composite. *Iranian Journal of Pharmaceutical Research*, 11(2): 481–493.
- Hamidi, M., Azadi, A. and Rafiei, P. (2008). Hydrogel nanoparticles in drug delivery. *Advanced Drug Delivery Reviews*, 60(15): 1638–1649.
- Han, L., Zhao, Y., Yin, L., Li, R., Liang, Y., Huang, H. ... Feng, M. (2012). Insulin-loaded pH-sensitive hyaluronic acid nanoparticles enhance transcellular delivery. *AAPS PharmSciTech*, 13(3): 836–845.
- He, P., Liu, H., Tang, Z., Deng, M., Yang, Y., Pang, X. and Chen, X. (2013). Poly(ester amide) blend microspheres for oral insulin delivery. *International Journal of Pharmaceutics*, 455(1–2): 259–266.
- Heinemann, L. and Jacques, Y. (2009). Oral insulin and buccal insulin: A critical reappraisal. *Journal of Diabetes Science and Technology*, 3(3): 568–584.
- Heinze, T. H., Pfeiffer, K. and Lazik, W. (2001). Starch derivatives with high degree of functionalization. III. Influence of reaction conditions and starting materials on molecular structure of carboxymethyl starch. *Journal of Applied Polymer Science*, 81(8): 2036–2044.
- Henkin, R. I. (2010). Inhaled insulin—Intrapulmonary, intranasal, and other routes of administration: Mechanisms of action. *Nutrition*, 26(1): 33–39.
- Heurtault, B., Saulnier, P., Pech, B., Proust, J. E. and Benoit, J. P. (2003). Physico-chemical stability of colloidal lipid particles. *Biomaterials*, 24(23): 4283–4300.
- Hosny, E. A. (1999). Relative hypoglycaemia of rectal insulin suppositories containing deoxycholic acid, sodium taurocholate, polycarbophol, and their combinations in diabetic rabbits. *Drug Development and Industrial Pharmacy*, 25(6): 745–752.
- Houlden, R., Capes, S., Clement, M. and Miller, D. (2013). In-hospital management of diabetes. *Canadian Journal of Diabetes*, 37: S77–S81.

- Hu, Y., Mei, Z. and Hu, X. (2015). pH-sensitive interpenetrating network hydrogels based on pachyman and its carboxymethylated derivatives for oral drug delivery. *Journal of Polymer Research*, 22(98): 1–10.
- Hyllested-Winge, J., Sparre, T. and Pedersen, L. K. (2016). NovoPen Echo[®] insulin delivery device. *Medical Devices: Evidence and Research*, 9: 11–18.
- Ichikawa, H. and Peppas, N. A. (2003). Novel complexation hydrogels for oral peptide delivery: *in vitro* evaluation of their cytocompatibility and insulin-transport enhancing effects using Caco-2 cell monolayers. *Journal of Biomedical Materials Research A*, 67(2): 609–617.
- Illum, L. (2003). Nasal drug delivery-possibilities, problems and solutions. *Journal of Controlled Release*, 87(1–3): 187–198.
- Jain, S. K, Jain, N. K., Gupta, Y., Jain, A., Jain, D and Chaurasia, M. (2007). Mucoadhesive chitosan microspheres for non-invasive and improved nasal delivery of insulin. *Indian Journal of pharmaceutical Sciences*, 69(4): 498–504.
- Jain, S. and Saraf, S. (2010). Type 2 diabetes mellitus-its global prevalence and therapeutic strategies. *Diabetes and Metabolic syndrome: Clinical Research and Reviews*, 4(1): 48–56.
- Jin, X., Zhang, S. B., Li, S. M., Liang, K. and Jia, Z. Y. (2016). Influence of chitosan nanoparticles as the absorption enhancers on salvianolic acid B *in vitro* and *in vivo* evaluation. *Pharmacognosy Magazine*, 12(45): 57–63.
- Jin, Y., Song, Y., Zhu, X., Zhou, D., Chen, C., Zhang, Z. and Huang, Y. (2012). Goblet cell-targeting nanoparticles for oral insulin delivery and the influence of mucus on insulin transport. *Biomaterials*, 33(5): 1573–1582.
- Kajimoto, K., Yamamoto, M., Watanabe, M., Kigasawa, K., Kanamura, K., Harashima, H. and Kogure, K. (2011). Noninvasive and persistent transfollicular drug delivery system using a combination of liposomes and iontophoresis. *International Journal of Pharmaceutics*, 403(1–2): 57–65.
- Kanikkannan, N. (2002). Iontophoresis-based transdermal delivery systems. *BioDrugs*, 16(5): 339–347.
- Kapitza, C., Zijlstra, E., Heinemann, L., Castelli, M. C., Riley, G. and Heise, T. (2010). Oral insulin: a comparison with subcutaneous regular human insulin in patients with type 2 diabetes. *Diabetes Care*, 33(6): 1288–1290.

- Kean, T. and Thanou, M. (2010). Biodegradation, biodistribution and toxicity of chitosan. *Advanced Drug Delivery Reviews*, 62(1): 3–11.
- Kerns, E. H., Di, L., Petusky, S., Farris, M., Ley, R. and Jupp, P. (2004). Combined application of parallel artificial membrane permeability assay and Caco-2 permeability assays in drug discovery. *Journal of Pharmaceutical Sciences*, 93(6): 1440–1453.
- Khafagy, E. S., Morishita, M., Onuki, Y. and Takayama, K. (2007). Current challenges in non-invasive insulin delivery systems: A comparative review. *Advanced Drug Delivery Reviews*, 59(15): 1521–1546.
- Kim, H. Y., Han, J. A., Kweon, D. K., Park, J. D. and Lim, S. T. (2013). Effect of ultrasonic treatments on nanoparticle preparation of acid-hydrolyzed waxy maize starch. *Carbohydrate Polymers*, 93(2): 582–588.
- Klein, S. (2010). The use of bio relevant dissolution media to forecast the *in vivo* performance of a drug. *AAPS PharmSciTech*, 12(3): 397–406.
- Koljonen, M., Rousu, K., Cierny, J., Kaukonen, A. M. and Hirvonen, J. (2008). Transport evaluation of salicylic acid and structurally related compounds across Caco-2 cell monolayers and artificial PAMPA membranes. *European Journal of Pharmaceutical Sciences*, 70(2): 531–538.
- Korsmeyer, R. W. and Peppas, N. A. (1983). Macromolecular and modeling aspects of swelling controlled systems. In: T.J. Roseman and S.Z. Mansdorf (Eds.), *Controlled Release Delivery Systems*, Marcel Dekker, New York, pp. 77–90.
- Kugler, A. J., Fabbio, K. L., Pham, D. Q. and Nadeau, D. A. (2015). Inhaled technosphere insulin: A novel delivery system and formulation for the treatment of types 1 and 2 diabetes mellitus. *Pharmacotherapy*, 35(3): 298–314.
- Kumari, A. and Yadav, S. K. (2011). Cellular interactions of therapeutically delivered nanoparticles. *Expert Opinion on Drug Delivery*, 8(2): 141–151.
- Laffel, L. (1999). Ketone bodies: a review of physiology, pathophysiology and application of monitoring to diabetes. *Diabetes Metabolism Research and Reviews*, 15(6): 412–426.
- Lassmann-Vague, V. and Raccach, D. (2006). Alternative route of insulin delivery. *Diabetes and Metabolism*, 32(5–C2): 513–522.

- Leary, A. C., Dowling, M., Cussen, K., O'Brien, J. and Stote, R. M. (2008). Pharmacokinetics and pharmacodynamics of intranasal insulin spray (Nasulin™) administered to healthy male volunteers: Influence of the nasal cycle. *Journal of Diabetes Science and Technology*, 2(6): 1054–1060.
- Lee, S., Lee, J., Lee, D. Y., Kim, S. K., Lee, Y. and Byun, Y. (2005). A new drug carrier, N α -deoxycholyl-L-lysyl-methylester, for enhancing insulin absorption in the intestine. *Diabetologia*, 48: 405–411.
- Lee, Y. C. and Yalkowsky, S. H. (1999). Ocular devices for the controlled systemic delivery of insulin: *In vitro* and *in vivo* dissolution. *International Journal of Pharmaceutics*, 181(1): 71–77.
- Leong, K. H., Chung, L. Y., Noordin, M. I., Mohamad, K., Nishikawa, M., Onuki, Y., Morishita, M. and Takayama, K. (2011a). Carboxymethylation of *kappa*-carrageenan for intestinal targeted delivery of bioactive macromolecules. *Carbohydrate Polymers*, 83: 1507–1515.
- Leong, K. H., Chung, L. Y., Noordin, M. I., Onuki, Y., Morishita, M. and Takayama, K. (2011b). Lectin functionalized Carboxymethylated *kappa*-carrageenan microparticle for oral insulin delivery. *Carbohydrate Polymers*, 86: 555–565.
- Li, C., Hein, S. and Wang, K. (2012). Chitosan-carrageenan polyelectrolyte complex for the delivery of protein drugs. *ISRN Biomaterials*, 2013: 1–6.
- Li, X., Gao, S., Zhu, C., Zhu, Q., Gan, Y., Rantanen, J. ... Yang, M. (2013a). Intestinal mucosa permeability following oral insulin delivery using core shell corona nanolipoparticles. *Biomaterials*, 34(37): 9678–9687.
- Li, X., Qi, J., Xie, Y., Zhang, X., Hu, S., Xu, Y., Lu, Y. and Wu, W. (2013b). Nanoemulsions coated with alginate/chitosan as oral insulin delivery systems: preparation, characterisation, and hypoglycemic effect in rats. *International Journal of Nanomedicine*, 8: 23–32.
- Lin, C. C. and Metters, A. T. (2006). Hydrogels in controlled release formulations: Network design and mathematical modelling. *Advanced Drug Delivery Reviews*, 58(12–13): 1379–1408.
- Lin, Y. H., Chen, C. T., Liang, H. F., Kulkarni, A. R., Lee, P. W., Chen, C. H. and Sung, H. W. (2007). Novel nanoparticles for oral insulin delivery via the paracellular pathway. *Nanotechnology*, 18(10): 1–11.

- Liu, C., Shan, W., Liu, M., Zhu, X., Xu, J., Xu, Y. and Huang, Y. (2016a). A novel ligand conjugated nanoparticles for oral insulin delivery. *Drug Delivery*, 23(6): 2015–2025.
- Liu, J., Werner, U., Funke, M., Besenius, M., Saaby, L., Fanø, M. ... Müllertz, A. (2019). SEDDS for intestinal absorption of insulin: Application of Caco-2 and Caco-2/HT29 co-culture monolayers and intra-jejunal instillation in rats. *International Journal of Pharmaceutics*, 560: 377–384.
- Liu, J., Zhang, S. M., Chen, P. P., Cheng, L., Zhou, W., Tang, W. X., Chen, W. Z. and Ke, C. M. (2007). Controlled release of insulin from PLGA nanoparticles embedded within PVA hydrogels. *Journal of Materials Science: Materials in Medicine*, 18(11): 2205–2210.
- Liu, L., Yao, W., Rao, Y., Lu, X. and Gao, J. (2017). pH-responsive carriers for oral drug delivery: challenges and opportunities of current platforms. *Drug Delivery*, 24(1): 569–581.
- Liu, L., Zhou, C., Xia, X. and Liu, Y. (2016b). Self-assembled lecithin/chitosan nanoparticles for oral insulin delivery: preparation and functional evaluation. *International Journal of Nanomedicine*, 11: 761–769.
- Long, J., Yu, X., Xu, E., Wu, Z., Xu, X., Jin, Z. and Jiao, A. (2015). In situ synthesis of new magnetite chitosan/carrageenan nanocomposites by electrostatic interactions for protein delivery applications. *Carbohydrate Polymers*, 131: 98–107.
- Lopes, M. A., Abraham-Vieira, B., Oliveira, C., Fonte, P., Souza, A. M., Lira, T. ... Ribeiro, A. J. (2015). Probing insulin bioactivity in oral nanoparticles produced by ultrasonication-assisted emulsification/internal gelation. *International Journal of Nanomedicine*, 10: 5865–5880.
- Lopes, M., Derenne, A., Pereira, C., Veiga, F., Seiça, R., Sarmentod, B. and Ribeiro, A. (2016). Impact of the *in vitro* gastrointestinal passage of biopolymer-based nanoparticles on insulin absorption. *RCS Advances*, 6(24): 20155–20165.
- Luijf, Y. M. and DeVries, J. H. (2010). Dosing accuracy of insulin pens versus conventional syringes and vials. *Diabetes Technology and Therapeutics*, 12(S1): 73–77.
- Lundquist, P. and Artursson, P. (2016). Oral absorption of peptides and nanoparticles across the human intestine: Opportunities, limitations and studies in human tissues. *Advanced Drug Delivery Reviews*, 106(B): 256–276.

- Luo, Y. Y., Xiong, X. Y., Tian, Y., Li, Z. L., Gong, Y. C. and Li, Y. P. (2016). A review of biodegradable polymeric systems for oral insulin delivery. *Drug Delivery*, 23(6): 1882–1891.
- Luzio, S. D., Dunseath, G., Lockett, A., Broke-Smith, T. P., New, R. R. and Owens, D. R. (2010). The glucose lowering effect of an oral insulin (Capsulin) during an isoglycaemic clamp study in persons with type 2 diabetes. *Diabetes, Obesity and Metabolism*, 12(1): 82–87.
- Ma, O., Lavertu, M., Sun, J., Nguyen, S., Buschmann, M. D., Winnik, F. M. and Hoemann, C. D. (2008). Precise derivatization of structurally distinct chitosans with rhodamine B isothiocyanate. *Carbohydrate Polymers*, 72(4): 616–624.
- Ma, Z. and Lim, L. Y. (2003). Uptake of chitosan and associated insulin in Caco-2 cell monolayers: A comparison between chitosan molecules and chitosan nanoparticles. *Pharmaceutical Research*, 20(11): 1812–1819.
- Makhlof, A., Tozuka, Y. and Takeuchi, H. (2011). Design and evaluation of novel pH-sensitive chitosan nanoparticles for oral insulin delivery. *European Journal of Pharmaceutical Sciences*, 42(5): 445–451.
- Malakar, J., Sen, S. O., Nayak, A. K. and Sen, K. K. (2012). Formulation, optimization and evaluation of transferosomal gel for transdermal insulin delivery. *Saudi Pharmaceutical Journal*, 20(4): 355–363.
- Manoharan, C. and Singh, J. (2015). Addition of zinc improves the physical stability of insulin in the primary emulsification step of the Poly(lactide-co-glycolide) microsphere preparation process. *Polymers*, 7(5): 836–850.
- Marschütz, M. K. and Bernkop-Schnürch, A. (2000). Oral peptide drug delivery: polymer-inhibitor conjugates protecting insulin from enzymatic degradation *in vitro*. *Biomaterials*, 21(14): 1499–1507.
- McGibbon, A., Richardson, C., Hernandez, C. and Dornan, J. (2013). Pharmacotherapy in type 1 diabetes. *Canadian Journal of Diabetes*, 37: S56-S60.
- Miller-Chou, B. A. and Koenig, J. L. (2003). A review of polymer dissolution. *Progress in Polymer Science*, 28(8): 1223–1270.
- Ministry of Health, Malaysia (2009). Management of type 2 diabetes mellitus (MOH/P/PAK/184.09(GU)), 1–73.

- Morishita, M. and Peppas, N. A. (2006). Is the oral route possible for peptide and protein drug delivery? *Drug Discovery Today*, 11(19–20): 905–910.
- Morishita, M., Goto, T., Nakamura, K., Lowman, A. M., Takayama, K. and Peppas, N. A. (2006). Novel oral insulin delivery system based on complexation polymer hydrogels: single and multiple administration studies in type 1 and 2 diabetic rats. *Journal of Controlled Release*, 110(3): 587–599.
- Mukhopadhyay, P., Mishra, R., Rana, D. and Kundu, P. P. (2012). Strategies for effective oral insulin delivery with modified chitosan nanoparticles: A review. *Progress in Polymer Science*, 37(11): 1457–1475.
- Mukhopadhyay, P., Sarkar, K., Chakraborty, M., Bhattacharya, S., Mishra, R. and Kundu, P. P. (2013). Oral insulin delivery by self-assembled chitosan nanoparticles: *In vitro* and *in vivo* studies in diabetic animal model. *Materials Science and Engineering, C*, 33(1): 376–382.
- Musther, H., Olivares-Morales, A., Hatley, O. J., Liu, B. and Hodjegan, A. R. (2014). Animal versus human oral drug bioavailability: Do they correlate? *European Journal of Pharmaceutical Sciences*, 57: 280–291.
- Nadvorny, D., Soares-Sobrinho, J. L., de La Roca Soares, M. F., Ribeiro, A. J., Veiga, F. and Seabra, G. M. (2018). Molecular dynamics simulations reveal the influence of dextran sulfate in nanoparticle formation with calcium alginate to encapsulate insulin. *Journal of Biomolecular Structure and Dynamics*, 36(5): 1255–1260.
- Neumiller, J. J., Campbell, R. K. and Wood, L. D. (2010). A review of inhaled technosphere insulin. *Annals of Pharmacotherapy*, 44(7–8): 1231–1239.
- Nguyen, T. M., Lee, S. and Lee, S. B. (2014). Conductive polymer nanotube patch for fast and controlled ex vivo transdermal drug delivery. *Nanomedicine (Lond)*, 9(15): 2263–2272.
- Niu, M., Lu, Y., Hovgaard, L. and Wu, W. (2011). Liposomes containing glycocholate as potential oral insulin delivery systems: preparation, *in vitro* characterisation, and improved protection against enzymatic degradation. *International Journal of Nanomedicine*, 6: 1155–1166.
- Niu, M., Lu, Y., Hovgaard, L., Guan, P., Tan, Y., Lian, R., Qi, J. and Wu, W. (2012). Hypoglycemic activity and oral bioavailability of insulin-loaded liposomes containing bile salts in rats: The effect of cholate type, particle size and administered dose. *European Journal of Pharmaceutics and Biopharmaceutics*, 81(2): 265–272.

- Niu, M., Tan, Y., Guan, P., Hovgaard, L., Lu, Y., Qi, J. ... Wu, W. (2014). Enhanced oral absorption of insulin-loaded liposomes containing bile salts: A mechanistic study. *International Journal of Pharmaceutics*, 460(1–2): 119–130.
- Nkabinde, L. A., Shoba-Zikhali, L. N., Semete-Makokotlela, B., Kalombo, L., Swai, H. S., Hayeshi, R. ... Hamman, J. H. (2012). Permeation of PLGA nanoparticles across different *in vitro* models. *Current Drug Delivery*, 9(6): 617–627.
- Ogurtsova, K., da Rocha Fernandes, J. D., Huang, Y., Linnenkamp, U., Guariguata, L., Cho, N. H. ... Makaroff, L. E. (2017). IDF Diabetes Atlas: Global estimates for the prevalence of diabetes for 2015 and 2040. *Diabetes Research and Clinical Practice*, 128: 40–50.
- Oliva, A., Fariña, J. and Llabrés, M. (2000). Development of two high performance liquid chromatographic methods for the analysis and characterisation of insulin and its degradation products in pharmaceutical preparations. *Journal of Chromatography B: Biomedical Sciences and Application*, 749(1): 25–34.
- Onuki, Y., Nishikawa, M., Morishita, M. and Takayama, K. (2008). Development of photo cross linked polyacrylic acid hydrogel as an adhesive for dermatological patches: Involvement of formulation factors in physical properties and pharmacological effects. *International Journal of Pharmaceutics*, 349(1–2): 47–52.
- Oramed completes patient recruitment of phase IIb HBA1C trial for oral insulin capsule ORMD-0801. (2019, June 27). Retrieved from <https://www.prnewswire.com/il/news-release/oramed-completes-patient-recruitment-of-phase-iib-hba1c-trial-for-oral-insulin-capsule-ormd-0801-300853994.html>.
- Pan, Y., Li, Y. J., Zhao, H. Y., Zheng, J. M., Xu, H., Wei, G. ... Cui, F. D. (2002). Bioadhesive polysaccharide in protein delivery system: chitosan nanoparticles improve the intestinal absorption of insulin *in vivo*. *International Journal of Pharmaceutics*, 249(1–2): 139–147.
- Park, K., Know, I. C. and Park, K. (2011). Oral protein delivery: Current status and future prospect. *Reactive and Functional Polymers*, 71(3): 280–287.
- Parsonage, E. E., Peppas, N. A. and Lee, P. I. (1987). Properties of positive resists. II. Dissolution characteristics of irradiated poly (methyl methacrylate) and poly(methyl methacrylate-comaleic anhydride). *Journal of Vacuum Science and Technology B*, 5(2): 538–545.
- Peppas, N. A. (2004). Devices based on intelligent biopolymers for oral protein delivery. *International Journal of Pharmaceutics*, 277(1–2): 11–17.

- Peppas, N. A. and Huang, Y. (2004). Nanoscale technology of mucoadhesive interactions. *Advanced Drug Delivery Reviews*, 56(11): 1675–1687.
- Petzold, K., Schwikal, K. and Heinze, T. (2006). Carboxymethyl xylan-synthesis and detailed structure characterisation. *Carbohydrate Polymers*, 64(2): 292–298.
- Phillips, J., Russel-Jones, D. L., Wright, J., Brackenridge, A., New, R. and Bansal, G. (2004). Early evaluation of a novel oral insulin delivery system in healthy volunteers. *Diabetes*, 53(suppl 2): A113.
- Prajapati, V. D., Maheriya, P. M., Jani, G. K. and Solanki, H. K. (2014). Carrageenan: A natural seaweed polysaccharide and its applications. *Carbohydrate Polymers*, 105: 97–112.
- Prausnitz, M. R. and Langer, R. (2008). Transdermal drug delivery. *Nature Biotechnology*, 26(11): 1261–1268.
- Presas, E., McCartney, F., Sultan, E., Hunger, C., Nellen, S., Alvarez, C. V. ... O'Driscoll, C. M. (2018). Physicochemical, pharmacokinetic and pharmacodynamic analyses of amphiphilic cyclodextrin-based nanoparticles designed to enhance intestinal delivery of insulin. *Journal of Controlled Release*, 286: 402–414.
- Quianzon, C. C. and Cheikh, I. (2012). History of insulin. *Journal of Community Hospital Internal Medicine Perspectives*, 2(2): 1–3.
- Raman, M., Devi, V. and Doble, M. (2015). Biocompatible ι -carrageenan- γ -maghemite nanocomposite for biomedical applications – synthesis, characterisation and in vitro anticancer efficacy. *Journal of Nanobiotechnology*, 13(1): 1–13.
- Rao, R. and Nanda, S. (2009). Sonophoresis: Recent advancements and future trends. *Journal of Pharmacy and Pharmacology*, 61(6): 689–705.
- Reis, C. P., Ribeiro, A. J., Veiga, F., Neufeld, R. J. and Damgé, C. (2008). Polyelectrolyte biomaterial interactions provide nanoparticulate carrier for oral insulin delivery. *Drug Delivery*, 15(2): 127–139.
- Rekha, M. R. and Sharma, C. P. (2009). Synthesis and evaluation of lauryl succinyl chitosan particles towards oral insulin delivery and absorption. *Journal of Controlled Release*, 135(2): 144–151.

- Rekha, M. R. and Sharma, C. P. (2013). Oral delivery of therapeutic protein/peptide for diabetes-Future perspectives. *International Journal of Pharmaceutics*, 440(1): 48–62.
- Richardson, P. C. and Boss, A. H. (2007). Technosphere insulin technology. *Diabetes Technology and Therapeutics*, 9(Suppl 1): 65–72.
- Rieux, A., Fievez, V., Garinot, M., Schneider, Y. J. and Pr at, V. (2006). Nanoparticles as potential oral delivery systems of protein and vaccines: A mechanistic approach. *Journal of Controlled Release*, 116(1): 1–27.
- Righeschi, C., Bergonzi, M. C., Isacchi, B., Bazzicalupi, C., Gratteri, P. and Bilia, A. R. (2016). Enhanced curcumin permeability by SLN formulation: the PAMPA approach. *LWT – Food Science and Technology*, 66: 475–483.
- Rodrigues, S., Cordeiro, C., Seijo, B., Remu n n-L pez, C. and Grenha, A. (2015). Hybrid nanosystems based on natural polymers as protein carriers for respiratory delivery: Stability and toxicological evaluation. *Carbohydrate Polymers*, 123: 369–380.
- Rodrigues, S., da Costa, A. M. and Grenha, A. (2012). Chitosan/carrageenan nanoparticles: Effect of cross-linking with TPP and charge ratio. *Carbohydrate Polymers*, 89(1): 282–289.
- Rubeaan, K.A., Rafiullah, M. and Jayavanth, S. (2016). Oral insulin delivery systems using chitosan-based formulation: a review. *Expert Opinion on Drug Delivery*, 13(2): 223–237.
- Saboktakin, M. R., Maharramovand, A. and Ramazanov, M. (2015). pH sensitive chitosan-based supramolecular gel for oral drug delivery of insulin. *Journal of Molecular and Genetic Medicine*, 9(2):1–4.
- Saboo, B. D. and Talaviya, P. A. (2012). Continuous subcutaneous insulin infusion: practical issues. *Indian Journal of Endocrinology and Metabolism*, 16(2): S259–S262.
- Sandri, G., Bonferoni, M. C., Rossi, S., Ferrari, F., Boselli, C. and Caramella, C. (2010). Insulin-loaded nanoparticles based on N-trimethyl chitosan: *In vitro* (Caco-2 model) and *ex vivo* (excised rat jejunum, duodenum, and ileum) evaluation of penetration enhancement properties. *AAPS PharmSciTech*, 11(1): 362–371.
- Sankalia, M. G., Mashru, R. C., Sankalia, J. M. and Sutariya, V. B. (2006). Stability improvement of alpha-amylase entrapped in kappa-carrageenan beads: Physicochemical characterisation and optimization using composite index. *International Journal of Pharmaceutics*, 312(1–2): 1–14.

- Santos, A. C., Cunha, J., Veiga, F., Cordeiro-da-Silva, A. and Ribeiro, A. J. (2013). Ultrasonication of insulin-loaded microgel particles produced by internal gelation: impact on particle's size and insulin bioactivity. *Carbohydrate Polymers*, 98(2): 1397–1408.
- Santos, C. A., Jacob, J. S., Hertzog, B. A., Freedman, B. D., Press, D. L., Harnpicharnchai, P. and Mathiowitz, E. (1999). Correlation of two bioadhesion assays: The everted sac technique and the CAHN microbalance. *Journal of Controlled Release*, 61(1–2): 113–122.
- Sarmiento, B., Ferreira, D., Veiga, F. and Ribeiro, A. (2006a). Characterisation of insulin-loaded alginate nanoparticles produced by ionotropic pre-gelation through DSC and FTIR studies. *Carbohydrate Polymers*, 66(1): 1–7.
- Sarmiento, B., Ribeiro, A., Veiga, F. and Ferreira, D. (2006b). Development and characterisation of new insulin containing polysaccharide nanoparticles. *Colloids and Surfaces B: Biointerfaces*, 53(2): 193–202.
- Sarmiento, B., Ribeiro, A., Veiga, F., Sampaio, P., Neufeld, R. and Ferreira, D. (2007). Alginate/Chitosan nanoparticles are effective for oral insulin delivery. *Pharmaceutical Research*, 24(12): 2198–2206.
- Sayani, A. P. and Chien, Y. W. (1996). Systemic delivery of peptides and proteins across absorptive mucosae. *Critical Reviews in Therapeutic Drug Carrier Systems*, 13(1–2): 85–184.
- Schiffman, J. D. and Schauer, C. L. (2007). Cross-linking chitosan nanofibers. *Biomacromolecules*, 8(2): 594–601.
- Sgorla, D., Lechanteur, A., Almeida, A., Sousa, F., Melo, E. ... Sarmiento, B. (2018). Development and characterisation of lipid-polymeric nanoparticles for oral insulin delivery. *Expert Opinion on Drug Delivery*, 15(3): 213–222.
- Shah, R. B., Patel, M., Maahs, D. M. and Shah, V. N. (2016). Insulin delivery methods: Past, present and future. *International Journal of Pharmaceutical Investigation*, 6(1): 1–9.
- Shaikh, R., Singh, T. R. R., Garland, M. J., Woolfson, A. D. and Donnelly, R. F. (2011). Mucoadhesive drug delivery systems. *Journal of Pharmacy and Bioallied Sciences*, 3(1): 89–100.
- Sharpe, L. A., Daily, A. M., Horava, S. D. and Peppas, N. A. (2014). Therapeutic applications of hydrogels in oral drug delivery. *Expert Opinion on Drug Delivery*, 11(6): 901–915.

- Sheng, J., He, H., Han, L., Qin, J., Chen, S., Ru, G., Li, R., Yang, P., Wang, J. and Yang, V. C. (2016). Enhancing insulin oral absorption by using mucoadhesive nanoparticles loaded with LMWP-linked insulin conjugates. *Journal of Controlled Release*, 233: 181–190.
- Sinha, V. R. and Trehan, A. (2003). Biodegradable microspheres for protein delivery. *Journal of Controlled Release*, 90(3): 261–280.
- Skyler, J. S. (2010). Continuous subcutaneous insulin infusion-An historical perspective. *Diabetes Technology and Therapeutics*, 12: S5–9.
- Soares, S., Costa, A. and Sarmiento, B. (2012). Novel non-invasive methods of insulin delivery. *Expert Opinion on Drug Delivery*, 9(12): 1539–1558.
- Sonaje, K., Lin, Y. H., Juang, J. H., Wey, S. P., Chen, C. T. and Sung, H. W. (2009). *In vivo* evaluation of safety and efficacy of self-assembled nanoparticles for oral insulin delivery. *Biomaterials*, 30(12): 2329–2339.
- Srinivasan, B., Kolli, A. R., Esch, M. B., Abaci, H. E., Shuler, M. L. and Hickman, J. J. (2015). TEER measurement techniques for in vitro barrier model systems. *Journal of Laboratory Automation*, 20(2): 107–126.
- Srivastava, A., Yadav, T., Sharma, S., Nayak, A., Kumari, A. and Mishra, N. (2016). Polymers in drug delivery. *Journal of Biosciences and Medicines*, 4(1): 69–84.
- Swenson, E. S., Milisen, W. B. and Curatolo, W. (1994). Intestinal permeability enhancement: efficacy, acute local toxicity, and reversibility. *Pharmaceutical Research*, 11(8): 1132–1142.
- Takayama, K., Obata, Y., Morishita, M. and Nagai, T. (2004). Multivariate spline interpolation as a novel method to optimise pharmaceutical formulations. *Pharmazie*, 59(5): 392–395.
- Takeuchi, H., Sasaki, H., Niwa, T., Hino, T., Kawashima, Y. and Uesugi, K. (1992). Design of redispersible dry emulsion as an advanced dosage form of oily drug (vitamin E nicotinate) by spray-drying technique. *Drug Development and Industrial Pharmacy*, 18(9): 919–937.
- Thompson, D., Berger, H., Feig, D., Gagnon, R., Kader, T., Keely, E. ... Vinokuroff, C. (2013). Diabetes and pregnancy. *Canadian Journal of Diabetes*, 37: S168–S183.
- Tirumalasetty, P. P. and Eley, J. G. (2006). Permeability enhancing effects of the alkylglycoside, octylglucoside on insulin permeation across epithelial membrane *in vitro*. *Journal of Pharmaceutical Sciences*, 9(1): 32–39.

- Tomoda, K., Asahiyama, M., Ohtsuki, E., Nakajima, T., Terada, H., Kanebako, M. ... Makino, K. (2009). Preparation and properties of carrageenan microspheres containing allopurinol and local anesthetic agents for the treatment of oral mucositis. *Colloids and Surface B: Biointerfaces*, 71(1): 27–35.
- Toorisaka, E., Hashida, M., Kamiya, N., Ono, H., Kokazu, Y. and Goto, M. (2005). An enteric-coated dry emulsion formulation for oral insulin delivery. *Journal of Controlled Release*, 107(1): 91–96.
- Toorisaka, E., Ono, H., Arimori, K., Kamiya, N. and Goto, M. (2003). Hypoglycemic effect of surfactant-coated insulin solubilised in a novel solid-in-oil-in-water (S/O/W) emulsion. *International Journal of Pharmaceutics*, 252(1–2): 271–274.
- U.S. Department of Health and Human Services Food and Drug Administration, USFDA (2001). *Bioanalytical Method Validation*, 1–28.
- van de Velde, F. and Rollema, H. S. (2006). High resolution NMR of carrageenans. In G. A. Webb (Ed.), *Modern Magnetic Resonance* (pp. 1605–1610). Netherlands: Springer.
- van der Merwe, S. M., Verhoef, J. C., Verheijden, J. H., Kotzé, A. F. and Junginger, H. E. (2004). Trimethylated chitosan as polymeric absorption enhancer for improved peroral delivery of peptide drugs. *European Journal of Pharmaceutics and Biopharmaceutics*, 58(2): 225–235.
- Vimalavathini, R. and Gitanjali, B. (2009). Effect of temperature on the potency and pharmacological action of insulin. *Indian Journal of Medical Research*, 130(2): 166–169.
- Vllasaliu, D., Exposito-Harris, R., Heras, A., Casettari, L., Garnett, M., Illum, L. and Stolnik, S. (2010). Tight junction modulation by chitosan nanoparticles: Comparison with chitosan solution. *International Journal of Pharmaceutics*, 400(1–2): 183–193.
- Wende, F. J., Gohil, S., Mojarradi, H., Gerfaud, T., Nord, L. I., Karlsson, A. ... Sandström, C. (2016). Determination of substitution positions in hyaluronic acid hydrogels using NMR and MS based methods. *Carbohydrate Polymers*, 136: 1348–1357.
- Whitelaw, D. C., Kelly, C. A., Ironmonger, W., Cunliffe, C. M., New, R. and Phillips, J. N. (2005). Absorption of orally ingested insulin in human type 1 diabetic subjects: proof of concept study. *Diabetes*, 54(suppl 1): 5-LB.
- Woitiski, C. B., Neufeld, R. J., Veiga, F., Carvalho, R. A. and Figueiredo, I. V. (2010). Pharmacological effect of orally delivered insulin facilitated by multilayered stable nanoparticles. *European Journal of Pharmaceutical Sciences*, 41(3–4): 556–563.

- Woitiski, C. B., Sarmiento, B., Carvalho, R. A., Neufeld, R. J. and Veiga, F. (2011). Facilitated nanoscale delivery of insulin across intestinal membrane models. *International Journal of Pharmaceutics*, 412(1–2): 123–231.
- Wong, C. Y., Martinez, J. and Dass, C. R. (2016). Oral delivery of insulin for treatment of diabetes: status quo, challenges and opportunities. *Journal of Pharmacy and Pharmacology*, 68(9): 1093–1108.
- Wu, Y., Ding, Y., Tanaka, Y. and Zhang, W. (2014). Risk factors contributing to type 2 diabetes and recent advances in the treatment and prevention. *International Journal of Medical Sciences*, 11(11): 1185–1200.
- Xie, Z., Chang, C. and Zhou, Z. (2014). Molecular mechanisms in autoimmune type 1 diabetes: a critical review. *Clinical Reviews in Allergy and Immunology*, 47(2): 174–192.
- Xuan, B., McClellan, D. A., Moore, R. and Chiou, G. C. Y. (2005). Alternative delivery of insulin via eye drops. *Diabetes Technology and Therapeutics*, 7(5): 695–698.
- Yang, J., Chen, J., Pan, D., Wan, Y. and Wang, Z. (2013). pH-sensitive interpenetrating network hydrogels based on chitosan derivatives and alginate for oral drug delivery. *Carbohydrate Polymers*, 92(1): 719–725.
- Yin, L., Ding, J., He, C., Cui, L., Tang, C. and Yin, C. (2009). Drug permeability and mucoadhesion properties of thiolated trimethyl chitosan nanoparticles in oral insulin delivery. *Biomaterials*, 30(29): 5691–5700.
- Yu, J. and Chien, Y. W. (1997). Pulmonary drug delivery: physiologic and mechanistic aspects. *Critical Reviews in Therapeutic Drug Carrier Systems*, 14(4): 395–453.
- Zaccardi, F., Webb, D. R., Yates, T. and Davies, M. J. (2016). Pathophysiology of type 1 and type 2 diabetes mellitus: a 90-year perspective. *Postgraduate Medical Journal*, 92(1084): 63–69.
- Zhang, J., Liang, X., Zhang, Y. and Shang, Q. (2016). Fabrication and evaluation of a novel polymeric hydrogel of carboxymethyl chitosan-g-polyacrylic acid (CMC-g-PAA) for oral insulin delivery. *RCS Advances*, 6(58): 52858–52867.
- Zhang, N., Ping, Q. N., Huang, G. H. and Xu, W. F. (2005). Investigation of lectin-modified insulin liposomes as carriers for oral administration. *International Journal of Pharmaceutics*, 294(1–2): 247–259.

- Zhang, N., Ping, Q., Huang, G., Xu, W., Cheng, Y. and Han, X. (2006). Lectin-modified solid lipid nanoparticles as carriers for oral administration of insulin. *International Journal of Pharmaceutics*, 327(1–2): 153–159.
- Zhang, X., Qi, J., Lu, Y., He, W., Li, X. and Wu, W. (2014). Biotinylated liposomes as potential carriers for the oral delivery of insulin. *Nanomedicine: Nanotechnology, Biology and Medicine*, 10(1): 167–176.
- Zhang, Y., Wei, W., Lv, P., Wang, L. and Ma, G. (2011). Preparation and evaluation of alginate–chitosan microspheres for oral delivery of insulin. *European Journal of Pharmaceutics and Biopharmaceutics*, 77(1): 11–19.
- Zhao, Y. Z., Li, X., Lu, C. T., Xu, Y. Y., Lv, H. F., Dai, D. D. ... Zhang, M. (2012). Experiment on the feasibility of using modified gelatin nanoparticles as insulin pulmonary administration system for diabetes therapy. *Acta Diabetologica*, 49(4): 315–325.
- Zheng, M. and Yu, J. (2016). The effect of particle shape and size on cellular uptake. *Drug Delivery and Translational Research*, 6(1): 67–72.
- Zijlstra, E., Heinemann, L. and Plum-Mörschel, L. (2014). Oral insulin reloaded: a structured approach. *Journal of Diabetes Science and Technology*, 8(3): 458–465.

LIST OF PUBLICATIONS AND PAPERS PRESENTED

A) Publication

- 1) P. Sahoo, K.H. Leong, S. Nyamathulla, Y. Onuki, K. Takayama, L.Y. Chung, **Optimization of pH-responsive carboxymethylated iota-carrageenan/chitosan nanoparticles for oral insulin delivery using response surface methodology**, *Reactive and Functional Polymer*. 119 (2017) 145–155.

- 2) P. Sahoo, K.H. Leong, S. Nyamathulla, Y. Onuki, K. Takayama, L.Y. Chung, **Chitosan complexed carboxymethylated iota-carrageenan oral insulin particles: Stability, permeability and *in vivo* evaluation**, (Article in press) *Materials Today Communication*. <https://doi.org/10.1016/j.mtcomm.2019.100557>.

Abstract

We previously reported that insulin-entrapped chitosan complexed carboxymethylated *iota*-carrageenan (CS/CMCi) nanoparticles exhibit pH-responsive swelling behavior. However, the particles' stability in the enzymatic gastrointestinal environment, their drug permeability mechanism, and related *in vivo* studies have not been discussed to date. In this study, we investigated the stability, muco-adhesiveness, transport mechanism and *in vivo* assessment of the particles. The particles retained their bioactivity and displayed a generally stable behavior in the simulated enzymatic environment of the gastrointestinal tract with high muco-adhesiveness ($79.1 \pm 4.3\%$). The results of cellular membrane permeability experiments further suggested that insulin from the insulin-entrapped particles was transported across the Caco-2 cell monolayers mainly *via* the paracellular pathway. This activity was inferred by the trans-epithelial electrical resistance (TEER) and the apparent permeability coefficient (P_{app}) of the

insulin-entrapped particles (22-fold greater than control insulin solution), suggesting that the opening of tight junctions (TJs) of Caco-2 cells was involved in the process. The particles did not exhibit significant cytotoxicity at 0.5–10.0 mg/mL based on 3-(4,5-dimethylthiazol-2-yl)-5-(3-carboxymethoxyphenyl)-2-(4-sulfophenyl)-2H-tetrazolium, inner salts (MTS) and lactate dehydrogenase (LDH) assays. Additionally, an *in vivo* study with diabetic Sprague Dawley (SD) rats revealed an extended blood glucose-lowering effect for up to 36 h (C_{\max} : 175.1 ± 23.7 mIU/L, T_{\max} : 5 h, AUC: 1789.4 ± 158.6). The estimated bioavailability of insulin from CS/CMCi particles in humans was 44.7–46.9%, which may be increased three fold compared with rats. Thus, the above results support the effectiveness of chitosan-complexed carboxymethylated *iota*-carrageenan nanoparticles as an oral insulin delivery system for extended glycemic control in basal insulin therapy.

B) Research Presentation

Poster presentation at The Malaysian Local Chapter of the Controlled Release Society Inc. (MyCRS): Academia Networking Day & Annual General Meeting, a pre-conference event held in conjunction with the 7th Asian Conference on colloid & Interface Science (ACCIS). High Impact Research Building, University of Malaya, 50603, Kuala Lumpur, Malaysia, 8th August 2017.

Development and optimization of pH responsive carboxymethylated *iota*-carrageenan/chitosan nanoparticles for oral insulin delivery

(Best poster of the MyCRS poster presentation competition).

Pratyusa Sahoo¹, Kok Hoong Leong¹, Shaik Nyamathulla¹, Yoshinori Onuki², Kozo Takayama³, Lip Yong Chung¹

¹Department of Pharmacy, Faculty of Medicine, University of Malaya, Malaysia

²Department of Pharmaceutical Technology, Graduate School of Medical and Pharmaceutical Science, University of Toyama, Japan

³Department of Pharmaceutics, Faculty of Pharmaceutical Sciences, Hoshi University, Japan

Universiti Malaya